CORRECTED VERSION*

PCT

WORLD INTELLECTUAL PROPERTY ORGANIZATION
International Bureau

INTERNATIONAL APPLICATION PUBLISHED UNDER THE PATENT COOPERATION TREATY (PCT)

(51) International Patent Classification 6 :
C08J 9/00, C08G 79/00, 79/10, 79/12

A1

(11) International Publication Number: WO 99/37705

(43) International Publication Date: 29 July 1999 (29.07.99)

(21) International Application Number: PCT/US98/26201

(22) International Filing Date: 9 December 1998 (09.12.98)

(30) Priority Data:

60/069,143	9 December 1997 (09.12.97)	US
60/097,012	18 August 1998 (18.08.98)	US

(71) Applicant *(for all designated States except US)*: THE REGENTS OF THE UNIVERSITY OF CALIFORNIA [US/US]; 12th floor, 1111 Franklin Street, Oakland, CA 94607-5200 (US).

(72) Inventors; and

(75) Inventors/Applicants *(for US only)*: STUCKY, Galen, D. [US/US]; 973 W. Campus Route Lane, Goleta, CA 93117 (US). CHMELKA, Bradley, F. [US/US]; 933 W. Campus Lane, Goleta, CA 93117 (US). ZHAO, Dongyuan [US/US]; 6763 Abrego, Isla Vista, CA 93117 (US). MELOSH, Nick [US/US]; 8240 E. Calle Potreto, Tucson, AZ 85750 (US). HUO, Qisheng [US/US]; 239-1 Palmdale Drive, Williamsville, NY 14221 (US). FENG, Jianglin [US/US]; Apartment 7, 410 Seymour Road, Charlottesville, VA 22903 (US). YANG, Peidong [US/US]; University of California, Chemistry Dept., Santa Barbara, CA 93117 (US). PINE, David [US/US]; 1037 St. Mary's Place, Santa Barbara, CA 93111 (US). MARGOLESE, David [US/US]; 636 Romero Canyon Road, Montecito, CA 93106 (US). LUKENS, Wayne, Jr. [US/US]; P.O. Box 354, Summerland, CA 93067 (US). FREDRICKSON, Glenn, H. [US/US]; 311 Alston Road, Santa Barbara, CA 93108 (US). SCHMIDT-WINKEL, Patrick [US/US]; Linfield Place #A, Goleta, CA 93117 (US).

(74) Agent: BERLINER, Robert; Fulbright & Jaworski L.L.P., 29th floor, 865 S. Figueroa Street, Los Angeles, CA 90017-2576 (US).

(81) Designated States: AL, AM, AT, AU, AZ, BA, BB, BG, BR, BY, CA, CH, CN, CU, CZ, DE, DK, EE, ES, FI, GB, GD, GE, GH, GM, HR, HU, ID, IL, IN, IS, JP, KE, KG, KP, KR, KZ, LC, LK, LR, LS, LT, LU, LV, MD, MG, MK, MN, MW, MX, NO, NZ, PL, PT, RO, RU, SD, SE, SG, SI, SK, SL, TJ, TM, TR, TT, UA, UG, US, UZ, VN, YU, ZW, ARIPO patent (GH, GM, KE, LS, MW, SD, SZ, UG, ZW), Eurasian patent (AM, AZ, BY, KG, KZ, MD, RU, TJ, TM), European patent (AT, BE, CH, CY, DE, DK, ES, FI, FR, GB, GR, IE, IT, LU, MC, NL, PT, SE), OAPI patent (BF, BJ, CF, CG, CI, CM, GA, GN, GW, ML, MR, NE, SN, TD, TG).

Published

With international search report.

Before the expiration of the time limit for amending the claims and to be republished in the event of the receipt of amendments.

(54) Title: BLOCK POLYMER PROCESSING FOR MESOSTRUCTURED INORGANIC OXIDE MATERIALS

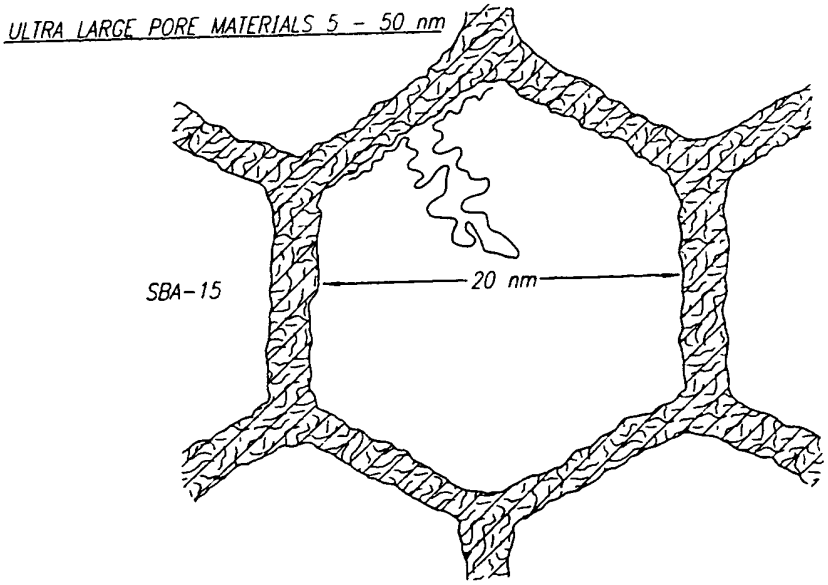

(57) Abstract

Highly mesoscopically ordered, hydrothermally stable and ultra large pore size metal oxide-block copolymer composite or mesoporous films, fibers, and monoliths are formed using amphiphilic block copolymers which act as structure directing agents for the metal oxide in a self-assembling system.

*(Referred to in PCT Gazette No. 09/2000, Section II)

FOR THE PURPOSES OF INFORMATION ONLY

Codes used to identify States party to the PCT on the front pages of pamphlets publishing international applications under the PCT.

AL	Albania	**ES**	Spain	**LS**	Lesotho	**SI**	Slovenia
AM	Armenia	**FI**	Finland	**LT**	Lithuania	**SK**	Slovakia
AT	Austria	**FR**	France	**LU**	Luxembourg	**SN**	Senegal
AU	Australia	**GA**	Gabon	**LV**	Latvia	**SZ**	Swaziland
AZ	Azerbaijan	**GB**	United Kingdom	**MC**	Monaco	**TD**	Chad
BA	Bosnia and Herzegovina	**GE**	Georgia	**MD**	Republic of Moldova	**TG**	Togo
BB	Barbados	**GH**	Ghana	**MG**	Madagascar	**TJ**	Tajikistan
BE	Belgium	**GN**	Guinea	**MK**	The former Yugoslav Republic of Macedonia	**TM**	Turkmenistan
BF	Burkina Faso	**GR**	Greece			**TR**	Turkey
BG	Bulgaria	**HU**	Hungary	**ML**	Mali	**TT**	Trinidad and Tobago
BJ	Benin	**IE**	Ireland	**MN**	Mongolia	**UA**	Ukraine
BR	Brazil	**IL**	Israel	**MR**	Mauritania	**UG**	Uganda
BY	Belarus	**IS**	Iceland	**MW**	Malawi	**US**	United States of America
CA	Canada	**IT**	Italy	**MX**	Mexico	**UZ**	Uzbekistan
CF	Central African Republic	**JP**	Japan	**NE**	Niger	**VN**	Viet Nam
CG	Congo	**KE**	Kenya	**NL**	Netherlands	**YU**	Yugoslavia
CH	Switzerland	**KG**	Kyrgyzstan	**NO**	Norway	**ZW**	Zimbabwe
CI	Côte d'Ivoire	**KP**	Democratic People's Republic of Korea	**NZ**	New Zealand		
CM	Cameroon			**PL**	Poland		
CN	China	**KR**	Republic of Korea	**PT**	Portugal		
CU	Cuba	**KZ**	Kazakstan	**RO**	Romania		
CZ	Czech Republic	**LC**	Saint Lucia	**RU**	Russian Federation		
DE	Germany	**LI**	Liechtenstein	**SD**	Sudan		
DK	Denmark	**LK**	Sri Lanka	**SE**	Sweden		
EE	Estonia	**LR**	Liberia	**SG**	Singapore		

Block Polymer Processing for Mesostructured Inorganic Oxide Materials

CROSS REFERENCE TO RELATED APPLICATIONS

This application claims the benefit of Provisional Patent Application Nos. 60/069,143, filed December 9, 1997, and 60/097,012, filed August 18, 1998.

STATEMENT REGARDING FEDERALLY FUNDED RESEARCH OR DEVELOPMENT

This invention was made with Government support under Grant Nos. DMR 9257064, DMR 9520971 and DMR 9632716 from the National Science Foundation, and Grant No. DAAH-04-96-1-0443 from the United States Army Research Office.

BACKGROUND OF THE INVENTION

Large pore size molecular sieves are in high demand for reactions or separations involving large molecules and have been sought after for several decades. Due to their low cost, ease of handling, and high resistance to photoinduced corrosion, many uses have been proposed for mesoporous metal oxide materials, such as SiO_2, particularly in the fields of catalysis, molecular separations, fuel cells, adsorbents, patterned-device development, optoelectronic devices, and chemical and biological sensors. One such application for these materials is the catalysis and separation of molecules that are too large to fit in the smaller 3-5 Å pores of crystalline molecular sieves, providing facile separation of biomolecules such as enzymes and/or proteins. Such technology would greatly speed processing of biological specimens, eliminating the need for time

consuming ultracentrifugation procedures for separating proteins. Other applications include supported-enzyme biosensors with high selectivity and antigen expression capabilities. Another application, for mesoporous TiO_2, is photocatalytic water splitting, which is extremely important for environmentally friendly energy generation. There is also tremendous interest in using mesoporous ZrO_2, $Si_{1-x}Al_xO_y$, $Si_{1-x}Ti_xO_y$, as acidic catalysts. Mesoporous WO_3 can be used as the support for ruthenium, which currently holds the world record for photocatalytic conversion of CH_4 to CH_3OH and H_2. Mesoporous materials with semiconducting frameworks, such as SnO_2 and WO_3, can be also used in the construction of fuel cells.

Mesoporous materials in the form of monoliths and films have a broad variety of applications, particularly as thermally stable low dielectric coatings, non-linear optical media for optical computing and self-switching circuits, and as host matrices for electrically- active species (e.g. conducting and lasing polymers and light emitting diodes). Such materials are of vital interest to the semiconductor and communications industries for coating chips, as well as to develop optical computing technology which will require optically transparent, thermally stable films as waveguides and optical switches.

These applications, however, are significantly hindered by the fact that, until this invention, mesoscopically ordered metal oxides could only be produced with pore sizes in the range (15 ~ 100 Å), and with relatively poor thermal stability. Many applications of mesoporous metal oxides require both mesoscopic ordering and framework crystallinity. However, these applications have been significantly hindered by the fact that, until this invention, mesoscopically ordered metal oxides generally have relative thin and fragile channel walls.

Since mesoporous molecular sieves, such as the M41S family of materials, were discovered in 1992, surfactant-templated synthetic

procedures have been extended to include a wide variety of compositions and conditions for exploiting the structure-directing functions of electrostatic and hydrogen-bonding interactions associated with amphiphilic molecules. For example, MCM-41 materials prepared by use of cationic cetyltrimethylammonium surfactants commonly have *d*(100) spacings of about 40 Å with uniform pore sizes of 20 - 30 Å. Cosolvent organic molecules, such as trimethylbenzene (TMB), have been used to expand the pore size of MCM-41 up to 100 Å, but unfortunately the resulting products possess less resolved XRD diffraction patterns. This is particularly the case concerning materials with pore sizes near the high-end of this range (ca. 100 Å) for which a single broad diffraction peak is often observed. Pinnavaia and coworkers, *infra*, have used nonionic surfactants in neutral aqueous media (S^0I^0 synthesis at pH = 7) to synthesize worm-like disordered mesoporous silica with somewhat larger pore sizes of 20 - 58 Å (the nomenclature S^0I^0 or S^+I^- are shorthand notations for describing mesophase synthesis conditions in which the nominal charges associated with the surfactant species S and inorganic species I are indicated). Extended thermal treatment during synthesis gives expanded pore sizes up to 50 Å; see D. Khushalani, A. Kuperman, G. A. Ozin, *Adv. Mater.* **7**, 842 (1995).

The preparation of films and monolithic silicates using acidic sol-gel processing methods is an active research field, and has been studied for several decades. Many studies have focused on creating a variety of hybrid organic-silicate materials, such as Wojcik and Klein's polyvinyl acetate toughening of TEOS monoliths (Wojcik, Klein; SPIE, *Passive Materials for Optical Elements II*, **2018**, 160-166 (1993)) or Lebeau et al's organ ic-inorgan ic optical coatings (B. Lebeau, Brasselet, Zyss, C. Sanchez; *Chem Mater.*, **9**, 1012-1020 (1997)). The majority of these studies use the organic phase to provide toughness or optical properties to the homogeneous (non-mesostructured) monolithic composite, and not

as a structure-directing agent to produce mesoscopically ordered materials. Attard and coworkers have reported the creation of monoliths with ~40 Å pore size, which were synthesized with low molecular weight nonionic surfactants, but did not comment on their thermal stability or transparency; see G. S. Attard; J. C. Glyde; C. G. G61tner, C. G. *Nature* **378**, 366 (1995). Dabadie et al. have produced mesoporous films with hexagonal or lamellar structure and pore sizes up to 34 Å using cationic surfactant species as structure-directing species; see Dabadie, Ayral, Guizard, Cot, Lacan; *J. Mater Chem.*, **6**, 1789-1794, (1996). However, large pore size (>50 Å) monoliths or films have not been reported, and, prior to our invention, the use of block copolymers as structure-directing agents has not been previously explored.(after our invention,Templin et al. reported using amphiphilic block copolymers as the structure-directing agents, aluminosilicate mesostructures with large ordering lengths (>15 nm); see Templin, M., Franck, A., Chesne, A. D., Leist, H., Zhang, Y., Ulrich, R., Schädler, V., Wiesner, U. Science **278**, 1795 (December 5, 1997)). For an overview of advanced hybrid organic-silica composites, see Novak's review article, B. Novak; *Adv. Mater.*, **5**, 422-433 (1993).

While the use of low-molecular weight surfactant species have produced mesostructurally ordered inorganic-organic composites, the resulting materials have been in the form of powders, thin films, or opaque monoliths. Extension of prior art surfactant templating procedures to the formation of nonsilica mesoporous oxides has met with only limited success, although these mesoporous metal oxides hold more promise in applications that involve electron transport and transfer or magnetic interactions. The following mesoporous inorganic oxides have been synthesized with small mesopore sizes (< 4 nm) over the past few years:

MnO_2 (Tian, Z., Tong, W., Wang, J., Duan, N., Krishnan, V. V., Suib, S. L. *Science*.

Al_2O_3 (Bagshaw, S. A., Pinnavaia, T. J. *Angew. Chem. Int. Ed. Engl.* **35**, 1102 (1996)),

TiO_2 (Antonelli, D. M., Ying, J. Y. *Angew. Chem. Int. Ed. Engl.* **34**, 2014 (1995)),

Nb_2O_5 (Antonelli, D. M., Ying, J. Y. *Chem. Mater.* **8**, 874 (1996)),

Ta_2O_5 (Antonelli, D. M., Ying, J. Y. *Chem. Mater.* **8**, 874 (1996)),

ZrO_2 (Ciesla, U., Schacht, S., Stucky, G. D., Unger, K. K., Schüth, F. *Angew. Chem. Int. Ed. Engl.* **35**, 541 (1996)),

HfO_2 (Liu, P., Liu, J., Sayari, A. *Chem. Commun.* 557 (1997)), and

reduced Pt (Attard, G. S., Barlett P. N., Coleman N. R. B., Elliott J. M., Owen, J. R., Wang, J. H. Science, **278**, 838 (1997)).

However these often have only thermally unstable mesostructures; see Ulagappan, N., Rao, C. N. R. *Chem Commun.* 1685 (1996), and Braun, P. V., Osenar, P., Stupp, S. I. *Nature* **380**, 325 (1996).

Stucky and co-workers first extended the surfactant templating strategy to the synthesis of non-silica-based mesostructures, mainly metal oxides. Both positively and negatively charged surfactants were used in the presence of water-soluble inorganic species. It was found that the charge density matching between the surfactant and the inorganic species is very important for the formation of the organic-inorganic mesophases. Unfortunately, most of these non-silica mesostructures are not thermally stable. Pinnavaia and co-workers, *supra*, used nonionic surfactants to synthesize mesoporous alumina in neutral aqueous media and suggested that the wormhole-disordered mesoporous materials are assembled by hydrogen-bonding interaction of inorganic source with the surfactants. Antonelli and Ying, *supra,* prepared stable mesoporous titanium oxide with phosphorus in a framework using a modified sol-gel method, in which an organometallic precursor was hydrolyzed in the presence of alkylphosphate surfactants. Mesoporous zirconium oxides were prepared using long-chain quaternary ammonium, primary amines,

and amphoteric cocamidopropyl betaine as the structure-directing agents; see Kim, A., Bruinsma, P., Chen, Y., Wang, L., Liu, J. *Chem. Commun.* 161 (1997); Pacheco, G., Zhao, E., Garcia, A., Sklyaro, A., Fripiat, J. J. *Chem. Commun.* 491 (1997); and Pacheco G., Zhao, E., Garcia, A., Skylyarov, A., Fripiat, J. J. J. Mater. Chem. **8**, 219 (1998).

A scaffolding process was also developed by Knowles *et al.* for the preparation of mesoporous ZrO_2 (Knowles J. A., Hudson M. J. J. *Chem. Soc., Chem. Commun.* 2083 (1995)). Porous HfO_2 has been synthesized using cetyltrimethyllammonium bromine as the structure-directing agent; see Liu, P., Liu. J., Sayari, A. *Chem. Commun.* 557 (1997). Suib et al, *supra,* prepared mixed-valent semiconducting mesoporous maganese oxide with hexagonal and cubic structures and showed that these materials are catalytically very active. A ligand-assisted templating approach has been successfully used by Ying and co-workers, *supra*, for the synthesis of Nb_2O_5 and Ta_2O_5. Covalent bond interaction between inorganic metal species and surfactant was utilized in this process to assemble the mesostructure. More recently, the surfactant templating strategy has been successfully extended to platinum by Attard, Barlett et al, *supra*.

For all these mesoporous non-silica oxides (except Pinnavaia's alumina work, in which copolymers were used to produce mesoporous alumina in neutral aqueous conditions), low-molecular-weight surfactants were used for the assembly of the mesostructures, and the resulting mesoporous materials generally had small mesopore sizes (<4 nm), and thin (1-3 nm) and fragile frameworks. The channel walls of these mesoporous metal oxides were exclusively amorphous. There have been claims, based solely on the X-ray diffraction data, of mesoporous ZrO_2 and MnO_2 with crystalline frameworks; see Bagshaw and Pinnavaia, *supra*, and Huang, Y., McCarthy, T. J., Sachtler, W. M. *Appl. Catal. A* **148**, 135 (1996). However, the reported X-ray diffraction patterns cannot

exclude the possibility of phase separation between the mesoporous and crystalline materials, and therefore their evidence has been inconclusive. In addition, most of the syntheses were carried out in aqueous solution using metal alkyoxides as inorganic precursors. The large proportion of water makes the hydrolysis and condensation of the reactive metal alkyoxides and the subsequent mesostructure assembly extremely difficult to control.

For an overview of the non-silica mesoporous materials prior to this invention, see the Sayari and Liu review article, Sayari, A., Liu, P. *Microporous Mater.* **12**, 149 (1997).

There has also been a need for porous inorganic materials with structure function on different length scales, for use in areas as diverse as large-molecule catalysis, biomolecule separation, the formation of semiconductor nanostructure, the development of medical implants and the morphogenesis of skeletal forms. The use of organic templates to control the structure of inorganic solid has proven very successful for designing porous materials with pore size ranging from angstroms to micrometers. For example, microporous aluminosilicate and aluminophosphate zeolite-type structures have been templated by organic moleculars such as amines. Larger mesoporous (20 ~ 300 Å) materials have been obtained by using long-chain surfactant as structure-directing-agents. Recent reports illustrate that techniques such as surfactant emulsion or latex sphere templating have been used to create TiO_2, ZrO_2, SiO_2 structures with pore sizes ranging from 100 nm to 1 μm. Recently, Nakanishi used a process that combined phase separation, solvent exchange with sol-gel chemistry to prepare macroscopic silica structures with random meso and macro-porous structure; see K. Nakanishi, *J. Porous Mater.* **4**, 67 (1997). Mann and coworkers used bacterial threads as the templates to synthesize ordered macrostructures in silica-

surfactant mesophases; see Davis, S. L. Burkett, N. H. Mendelson, S. Mann, *Nature*, **385**, 420 (1997)

Researchers have commented on the assembly of inorganic composites directed by protein or organic surfactants, but little on the effect of inorganic salts on the self-assembly of macroscopic silica or calcium carbonate structures with diatom, coral morphologies; see Davis, S. L. Burkett, N. H. Mendelson, S. Mann, *Nature*, **385**, 420 (1997); A. M. Belcher, X. H. Wu, R. J. Christensen, P. K. Hansma, G. D. Stucky, *Nature*, **381**, 56 (1996); and X. Y. Shen, A. M. Belcher, P. K. Hansma, G. D. Stucky, et al., *Bio. Chem.*, **272**, 32472 (1997).

BRIEF SUMMARY OF THE INVENTION

The present invention overcomes the drawbacks of prior efforts to prepare mesoporous materials and mesoscopic structures, and provides heretofore unattainable materials having very desirable and widely useful properties. These materials are prepared by using amphiphilic block copolymer species to act as structure-directing agents for metal oxides in self-assembling systems. Aqueous metal cations partition within the hydrophilic regions of the self-assembled system and associate with the hydrophilic polymer blocks. Subsequent polymerization of the metalate precursor species under strongly acidic conditions (e.g., pH 1), produces a densely cross linked, mesoscopically ordered metal oxide network. Mesoscopic order is imparted by cooperative self-assembly of the inorganic and amphiphilic species interacting across their hydrophilic-hydrophobic interface.

By slowly evaporating the aqueous solvent, the composite mesostructures can be formed into transparent, crack-free films, fibers or

monoliths, having two-dimensional hexagonal (p6mm), cubic (*Im3m*), or lamellar

mesostructures, depending on choice of the block copolymers. Heating to remove the organic template yields a mesoporous product that is thermally stable in boiling water. Calcination yields mesoporous structures with high BET surface areas. Unlike traditional sol-gel films and monoliths, the mesoscopically ordered silicates described in this invention can be produced with high degrees of order in the 100-200 Å length scale range, extremely large surface areas, low dielectric constants, large anisotropy, can incorporate very large host molecules, and yet still retain thermal stability and the transparency of fully densified silicates.

In accordance with a further embodiment of this invention, inorganic oxide membranes are synthesized with three-dimension (3-d) meso-macro structures using simultaneous multiphase assembly. Self-assembly of polymerized inorganic oxide species/amphiphilic block copolymers and the concurrent assembly of highly ordered mesoporous inorganic oxide frameworks are carried out at the interface of a third phase consisting of droplet of strong electrolyte inorganic salts/water solution. The result is a 2-d or 3-d macroporous/mesoporous membranes which, with silica, are coral-like, and can be as large as 4 cm x 4 cm with a thickness that can be adjusted between 10 μm to several millimeters. The macropore size (0.5 ~ 100 μm) can be controlled by varying the electrolyte strength of inorganic salts and evaporation rate of the solvents. Higher electrolyte strength of inorganic salts and faster evaporation result in a thicker inorganic oxide a framework and larger macropore size. The mesoscopic structure, either 2-d hexagonal (*p6mm*, pore size 40 ~ 90 Å) or 3-d cubic array, can be controlled by amphiphilic block copolymer templates. The resulting membranes are thermally stable and have large surface areas up to 1000 m^2/g, and pore volume up to 1.1 cm^3/g. Most

importantly, these meso-macroporous coral-like planes provide excellent access to the mesopore surfaces for catalytic, sorption, catalysis, separation, and sensor arrays, applications.

BRIEF DESCRIPTION OF THE DRAWINGS

Figure 1 shows a size comparison between two prior art porous inorganic materials, Faujasite and MCM-41, and SBA-15, prepared in accordance with this invention.

Figure 2 shows powder X-ray diffraction (XRD) patterns of as-synthesized and calcined mesoporous silica (SBA-15) prepared using the amphiphilic polyoxyalkylene block copolymer $PEO_{20}PPO_{70}PEO_{20}$.

Figure 3 shows scanning electron micrographs (SEM's) (a, b) of as-synthesized SBA-15 and transmission electron micrographs (TEM's) (c, d) with different orientations of calcined hexagonal mesoporous silica SBA-15 prepared using the block copolymer $PEO_{20}PPO_{70}PEO_{20}$.

Figure 4 shows nitrogen adsorption-desorption isotherm plots (top) and pore size distribution curves (bottom) measured using the adsorption branch of the isotherm for calcined mesoporous silica SBA-15 prepared using the block copolymer $PEO_{20}PPO_{70}PEO_{20}$ (a, b) without and (c, d) with TMB as an organic additive.

Figure 5 shows transmission electron micrographs with different pore sizes and silica wall thicknesses for calcined hexagonal mesoporous silica SBA-15 prepared using the block copolymer $PEO_{20}PPO_{70}PEO_{20}$. (a) pore size of
47 Å, silica wall thickness of 60 Å; (b) pore size of 89 Å, silica wall thickness of 30 Å; (c) pore size of 200 Å; (d) pore size of 260 Å.

Figure 6 shows powder X-ray diffraction (XRD) patterns of as-synthesized and calcined mesoporous silica SBA-15.

Figure 7 shows variation of the *d*(100) spacing (solid) and pore size (open) for mesoporous hexagonal SBA-15 calcined at 500°C for 6 h in air (circles) and for mesoporous MCM-41 (squares) as functions of the TMB/ amphiphile (copolymer or surfactant) ratio (g/g).

Figure 8 shows ^{29}Si MAS NMR spectra of as-synthesized silica-copolymer mesophase materials; (a) SBA-11 prepared by using Brij $C_{16}EO_{10}$ surfactant; (b) SBA-15 prepared using $PEO_{20}PPO_{70}PEO_{20}$ block copolymer.

Figure 9 shows thermogravimetric analysis (TGA) and differential thermal analysis (DTA) traces for the as-synthesized SBA-15 prepared by using the block copolymer $PEO_{20}PPO_{70}PEO_{20}$.

Figure 10 shows powder X-ray diffraction (XRD) patterns of (a), as-synthesized and, (b) calcined MCM-41 silica prepared using the cationic surfactant $C_{16}H_{33}N(CH_3)_3Br$; and (c), calcined MCM-41 after heating in boiling water for 6 h; Calcined SBA-15 (d, e) prepared by using the block copolymer $PEO_{20}PPO_{70}PEO_{20}$ after heating in boiling water for (d), 6 h; (e), 24 h.

Figure 11 shows photographs of transparent SBA-15 silica-copolymer monoliths incorporating (a) 27 wt% and (b) 34 wt% of the PEO-PPO-PEO structure-directing copolymer Pluronic F127.

Figure 12 shows a 200-keV TEM image of a 38 wt% SBA-15 silica-copolymer monolith prepared with Pluronic F127.

Figure 13 shows (a) a photograph of a transparent 50-μm-thick SBA-15 silicacopolymer film prepared with Pluronic P104. (b) an X-ray diffraction pattern of this film showing well resolved peaks that are indexable as (100), (110), (200), and (210) reflections associated with *p6mm* hexagonal symmetry in which the one-dimensional axes of the aggregates fie horizontally in the plane of the film.

Figure 14 shows the predicted variation of optical dielectric constant and refractive index as a function of silica porosity.

Figure 15 shows low-angle and wide-angle X-ray diffraction (XRD) patterns of (a, c), as-made zirconium/$EO_{20}PO_{70}EO_{20}$ composite mesostructure and (b, d) calcined mesoporous ZrO_2. The XRD patterns were obtained with a Scintag PADX diffractometer using Cu Kα radiation.

Figure 16 shows TEM micrographs of 2-dimensional hexagonal mesoporous ZrO_2. (a) and (b) are recorded along the [110] and [001] zone axes, respectively. Inset in (b) is the selected-area electron diffraction pattern obtained on the image area. The images were recorded with a 200 kV JEOL transmission electron microscope. All samples were calcined at 400 °C for 5 hr to remove the block copolymer surfactant species.

Figure 17 shows TEM micrographs of 2-dimensional hexagonal mesoporous TiO_2. (a) and (b) are recorded along the [110] and [001] zone axes, respectively. Inset in (a) is the selected-area electron diffraction pattern obtained on the image area.

Figure 18 shows TEM micrographs of 2-dimensional hexagonal mesoporous SnO_2. (a) and (b) are recorded along the [110] and [001]

zone axes, respectively. Inset in (a) is selected-area electron diffraction pattern obtained on the image area.

Figure 19 shows TEM micrographs of 2-dimensional hexagonal mesoporous WO_3. (a) and (b) are recorded along the [110] and [001] zone axes, respectively.

Figure 20 shows TEM micrograph of 2-dimensional hexagonal mesoporous Nb_2O_5, recorded along the [001] zone axis. Inset is selected-area electron diffraction pattern obtained on the image area.

Figure 21 shows TEM micrograph of 2-dimensional hexagonal mesoporous Ta_2O_5 recorded along the [001] zone axis.

Figure 22 shows TEM micrographs of disordered hexagonal mesoporous Al_2O_3.

Figure 23 shows TEM micrograph of 2-dimensional hexagonal mesoporous HfO_2 recorded along the [110] zone axis.

Figure 24 shows TEM micrographs of 2-dimensional hexagonal mesoporous $SiTiO_4$ recorded along the [001] zone axis.

Figure 25 shows TEM micrographs of 2-dimensional hexagonal mesoporous $SiAlO_{3.5}$. (a) and (b) are recorded along the [110] and [001] zone axes, respectively.

Figure 26 shows TEM micrograph of 2-dimensional hexagonal mesoporous $ZrTiO_4$ recorded along the [001] zone axes.

Figure 27 shows (a) Bright field TEM image of a thin slice of the mesoporous TiO_2 sample. (b) Dark field image obtained on the same area of the same TiO_2 sample. The bright spots in the image correspond to TiO_2 nanocrystals.

Figure 28 shows (a) Bright field TEM image of a thin slice of the mesoporous ZrO_2 sample. (b) Dark field image obtained on the same area of the same ZrO_2 sample. The bright spots in the image correspond to ZrO_2 nanocrystals.

Figure 29 shows nitrogen adsorption-desorption isotherms and pore size distribution plots (inset) calculated using BJH model from the adsorption branch isotherm for calcined ZrO_2. The isotherms were measured using a Micromeritics ASAP 2000 system. The samples were outgassed overnight at 200 °C before the analyses.

Figure 30 shows nitrogen adsorption-desorption isotherms (a) and pore size distribution plots (b) calculated using BJH model from the adsorption branch isotherm for calcined TiO_2. Inset in (b) is the EDX spectrum obtained on the mesoporous samples.

Figure 31 shows nitrogen adsorption-desorption isotherms and pore size distribution plots (lower inset) calculated using BJH model from the adsorption branch isotherm for calcined Nb_2O_5. EDX spectrum obtained on the mesoporous samples is shown in the upper inset.

Figure 32 shows nitrogen adsorption-desorption isotherms and pore size distribution plots (lower inset) calculated using BJH model from the adsorption branch isotherm for calcined Ta_2O_5. EDX spectrum obtained on the mesoporous samples is shown in the upper inset.

Figure 33 shows nitrogen adsorption-desorption isotherms and pore size distribution plots (inset) calculated using BJH model from the adsorption branch isotherm for calcined Al_2O_3.

Figure 34 shows nitrogen adsorption-desorption isotherms and pore size distribution plots (inset) calculated using BJH model from the adsorption branch isotherm for calcined WO_3.

Figure 35 shows nitrogen adsorption-desorption isotherms (a) and pore size distribution plots (b) calculated using BJH model from the adsorption branch isotherm for calcined $SiTiO_4$.

Figure 36 shows nitrogen adsorption-desorption isotherms (a) and pore size distribution plots (b) calculated using BJH model from the adsorption branch isotherm for calcined $ZrTiO_4$.

Figure 37 shows low-angle and wide-angle X-ray diffraction (XRD) patterns of (a, c), as-made titanium/$EO_{20}BO_{75}$ composite cubic mesostructure and (b, d) calcined mesoporous TiO_2.

Figure 38 shows TEM micrograph of cubic mesoporous TiO_2.

Figure 39 shows TEM micrograph of cubic mesoporous ZrO_2.

Figure 40 shows SEM image of calcined mesoporous Al_2O_3 monolithic thick film. The image was recorded on JEOL 6300FX microscope.

Figure 41 shows scanning electron micrographs (SEM) of (a, b) as-synthesized meso-macro silica membranes prepared by using P123 block copolymer ($EO_{20}PO_{70}EO_{20}$) in NaCl solution after washing out NaCl with

de-ionic water; (c), small macropore size silica membrane prepared by adding a little amount ethylene glycol in P123 block copolymer and NaCl solution; (d), silica membrane prepared with fast evaporation by using P123 block copolymer in NaCl solution. (e), silica membrane with grape vine morphology prepared with high concentration of NaCl; (f), inorganic salt NaCl crystals co-grown with the silica membrane.

Figure 42 shows scanning electron micrographs (SEM) of (a, b, c) as-synthesized meso-macro silica membranes prepared by using P123 block copolymer ($EO_{20}PO_{70}EO_{20}$) in (a), KCl; (b), NH_4Cl; (c), $NaNO_3$ solution after washing out inorganic salts with de-ionic water. (d), large macropore size silica membrane prepared by using P65 block copolymer ($EO_{26}PO_{39}EO_{26}$) in NaCl solution.

Figure 43 shows SEM images of as-synthesized silica membranes after washed with water prepared by (a), using F127 block copolymer ($EO_{106}PO_{70}EO_{106}$) in NaCl solution; (b, c, d), using P123 block copolymer in (b), $MgSO_4$ solution; (c), $MgCl_2$ solution; (d), Na_2SO_4 solution.

Figure 44 shows powder X-ray diffraction (XRD) patterns of as-synthesized and calcined mesomacro silica membranes prepared using the amphiphilic polyoxyalkylene block copolymer (a), P123, $EO_{20}PO_{70}EO_{20}$; (b), P103, $EO_{17}PO_{85}EO_{17}$; (c); P65, $EO_{26}PO_{39}EO_{26}$. The chemical composition of the reaction mixture was 1 g coploymer : 0.017 mol NaCl: 0.01 mol TEOS : 4 x 10^{-5} mol HCl: 0.72 mol H_2O: 0.33 mol EltOH.

Figure 45 shows transmission electron micrographs (TEM) (a, b) of calcined silica membrane prepared using the block copolymer P 123 in NaCl solution recorded in (a), (100); (b), (110) zone axes; (c, d) of

calcined silica membrane prepared by adding a little amount of ethylene glycol. TEM were taken on a 2000 JEOL electron microscope operating at 200 kV.

Figure 46 shows thermogravimetric analysis (TGA) and differential thermal analysis (DTA) traces for the as-synthesized meso-macroporous silica membranes prepared by using the block copolymer P123 ($EO_{20}PO_{70}EO_{20}$) in NaCl solution, (top), after removal NaCl by washing with water; (bottom), without removal NaCl.

Figure 47 shows nitrogen adsorption-desorption isotherm plots (a) and pore size distribution curves (b) for meso-macro silica membranes prepared using block copolymer P123 in NaCl solution without removal inorganic salt NaCl.

Figure 48 shows nitrogen adsorption-desorption isotherm plots (top) and pore size distribution curves (bottom) for calcined meso-macro silica membranes prepared in NaCl solution using different block copolymers.

Figure 49 shows nitrogen adsorption-desorption isotherm plots (a) and pore size distribution curves (b) for calcined meso-macro silica membranes prepared using block copolymer F127 in NaCl solution.

Figure 50 shows nitrogen adsorption-de sorption isotherm plots (a) and pore size distribution curves (b) for calcined meso-macro silica membranes prepared using non-ionic oligomeric surfactant Brij 76 ($C_{18}H_{37}EO_{10}OH$) in NaCl solution.

Figure 51 shows SEM images of (a)-(d), as-synthesized silica membranes prepared by using P123 block copolymer in LiCl solution without washing

recorded at different region, (a), top region; (b) middle region; (c), same (b) with large magnification; (d), bottom region of the membrane. (e)-(h) as-synthesized silica membranes prepared by using P123 block copolymer in $NiSO_4$ solution without washing recorded at different region, (a), top region; (b) same (a) with large magnification; (c) bottom region of the membrane; (d), disk-like $NiSO_4$ crystal.

Figure 52 shows the change of the compositions of the reaction mixture functioned with evaporation time. Change of the concentration in liquid phase of ethanol (open circle); water (solid circle); LiCl (open square); SiO_2 (solid square); Intensity ratio for (100) diffraction of silica-block copolymer mesophase (open triangle) and for (110) diffraction of LiCl crystal (solid triangle) at d spacing of 3.59 Å determined by XRD in solid phase.

Figure 53 shows a schematic diagram of the simple procedure used to prepare coral-like meso-macro silica membranes.

Figure 54 shows progressively higher magnifications of a section of a meso-macro silica membrane made in accordance with this invention..

DETAILED DESCRIPTION OF THE INVENTION

This invention provides a simple and general procedure for the syntheses of ordered large-pore (up to 14 nm) mesoporous metal oxides, including TiO_2, ZrO_2, Nb_2O_5, Ta_2O_5, Al_2O_3, SiO_2, WO_3, SnO_2, HfO_2 and mixed oxides $SiAlO_{3.5}$, $SiAlO_{5.5}$, Al_2TiO_5, $ZrTlO_4$, $SiTiO_4$. Commercially available, low-cost, non-toxic, and biodegradable amphiphilic poly(alkylene oxide) block copolymers can be used as the structure-directing agents in non-aqueous solutions for organizing the network

forming metal species. Preferably the block copolymer is a triblock copolymer in which a hydrophilic poly(alkylene oxide) such as poly(ethylene oxide (EO_x) is linearly covalent with the opposite ends of a hydrophobic poly(alkylene oxide) such as polypropylene) oxide (PO_y) or a diblock polymer in which , for example, poly(ethylene oxide) is linearly covalent with poly(butylene oxide) (BO_Y). This can variously be designated as follows:

poly(ethylene oxide)-poly(propylene oxide)-poly(polyethylene oxide)

$HO(CH_2CH_2O)_x(CH_2CH(CH_3)O)_y(CH_2CH_2O)_xH$

PEO-PPO-PEO

$EO_x\ PO_y\ EO_x$

or

poly(ethylene oxide)-poly(butylene oxide)-poly(polyethylene oxide)

$HO(CH_2CH_2O)_x(CH_2CH(CH_3CH_2)O)_yH$

PEO-PBO-PEO

$EO_x\ BO_y\ EO_x$

where x is 5 or greater and y is 30 or greater, with no theoretical upper limit to either value subject to practical considerations. Alternatively , for particular applications, one can use a reverse triblock copolymer or a star block amphiphilic poly(alkylene oxide block copolymer, for example, a star di-block copolymer or a reversed star di-block copolymer. Inexpensive inorganic salts rather than alkoxides or organic metal complexes are used as precursors. Both two-dimensional hexagonal (*p6mm*) and cubic (*Im3m*) mesostructures can be obtained, as well as lamellar mesostructures, depending on the choice of the block copolymers. Calcination at 400 °C yields mesoporous structures with high BET surface area (100 - 850 m^2/g), porosity of 40 - 65%, large *d* spacings (60 - 200 Å), pore sizes of 30 - 140 Å, and wall thickness of 30 - 90 Å.

These novel mesoporous metal oxides are believed to be formed through a mechanism that combines block copolymer self-assembly with chelating complexation of the inorganic metal species. A unique aspect of these thermally stable mesoporous oxides is their robust inorganic framework and thick channel walls, within which a high density of nanocrystallites can be nucleated during calcination without disrupting the mesoscopic ordering. In addition, variations of this simple sol-gel process yield mesoporous oxides with technologically important forms including thin films, monoliths and fibers. The nanocrystalline framework, periodic large-pore structures, and high versatility of the inexpensive synthetic methodology make these mesoporous materials an excellent choice for applications including catalysis, molecular separations, fuel cells, adsorbents, optoelectronic devices, and chemical and biological sensors. For example, due to its low cost, ease of handling, and high resistance to photoinduced corrosion, one application for mesoporous TiO_2 is photocatalytic water splitting, which is extremely important for environmentally friendly energy generation. There is also tremendous interest in using mesoporous ZrO_2, $Si_{1-x}Al_xO_y$, $Si_{1-x}Ti_xO_y$, as acidic catalysts. Mesoporous WO_3 can be used as the support for ruthenium, which currently holds the world record for photocatalytic conversion of CH_4 to CH_3OH and H_2. Mesoporous materials with semiconducting frameworks, such as SnO_2 and WO_3, can be also used in the construction of fuel cells.

Many applications of mesoporous metal oxides require both mesoscopic ordering and framework crystallinity. The mesoporous metal oxides of this invention are thermally stable and retain their mesoscopic ordering and structural integrity even after the nucleation of the high density of nanocrystallites within thick, robust channel walls. Development of such thermally stable, large-pore mesoporous metal oxide materials with nanocrystalline frameworks using lowcost, non-toxic,

and biodegradable polyalkylene oxide block copolymers has enormous potential for a variety of immediate and future industrial applications.

In practicing this invention, one can use any amphiphilic block polymer having substantial hydrophilic and hydrophobic components and can use any inorganic material that can form crown-ether-type complexes with alkylene oxide segments through weak coordination bonds. The inorganic material can be any inorganic compound of a multivalent metal species, such as metal oxides and sulphides, preferably the oxides. The metal species preferentially associates with the hydrophilic poly(ethylene oxide) (PEO) moieties. The resulting complexes then self-assemble according to the mesoscopic ordering directed principally by microphase separation of the block copolymer species. Subsequent crosslinking and polymerization of the inorganic species occurs to form the mesoscopically ordered inorganic/block-copolymer composites. The proposed assembly mechanism for these diverse mesoporous metal oxides uses PEO-metal complexation interactions, in conjunction with (for example) electrostatic, hydrogen bonding, and van der Waals forces to direct mesostructure formation.

As Indicated above, one can carry out the assembly process in non-aqueous media using metal halides as the inorganic precursors, which effectively slows the hydrolysis/condensation rates of the metal species and hinders subsequent crystallization. Restrained hydrolysis and condensation of the inorganic species appears to be important for forming mesophases of most of the non-silica oxides, because of their strong tendency to precipitate and crystallize into bulk oxide phases directly in aqueous media.

The procedures of the present invention enable close control of the porosity of the final structure by varying the proportions of PEO and PPO or PBO

and by adding an organic solvent to swell the PPO or PBO.

Because of their low cost, widespread use, and ease of preparation, we will first describe and exemplify the preparation of mesoporous silica, followed by the preparation of other metal oxides. We will then describe the multiphase assembly of meso-macro membranes, which we will exemplify with silica membranes.

Mesoporous silicas

In accordance with this invention, we have synthesized a family of high quality, hydrothermally stable and ultra large pore size mesoporous silicas by using amphiphilic block copolymers in acidic media. One member of the family, to which we have assigned the designation SBA-15, has a highly ordered, two-dimensional hexagonal (*p6mm*) honeycomb, hexagonal cage or cubic cage mesostructures. Calcination at 500°C yields porous structures with high BET surface areas of 690 - 1040 m^2/g, and pore volumes up to 2.5 cm^3/g, ultra large *d*(100) spacings of 74.5 - 450 Å, pore sizes from 46 - 500 Å and silica wall thicknesses of 31 - 64 Å. SBA-15 can be readily prepared over a wide range of specific pore sizes and pore wall thicknesses at low temperature (35 - 80°C) using a variety of commercially available, low-cost, non-toxic, and biodegradable amphiphilic block copolymers, including triblock polyoxyalkylenes, as described below. In general, all microphase-separating, domain-partitioning copolymer systems can be considered as candidates for the synthesis of such mesostructured materials, depending on solution composition, temperature, processing conditions, etc. The pore size and thickness of the silica wall is selectively controlled by varying the thermal treatment of SBA-15 in the reaction solution and by the addition of cosolvent organic molecules, such as 1,3,5-trimethylbenzene (TMB). The organic template can be easily removed by heating at 140°C for 3 h, yielding the mesoporous SBA-15 product, which is thermally stable in boiling water.

Transparent films, fibers, and monolithic materials with mesoscopic order can also be prepared by a similar process utilizing the same family of triblock polyoxyalkylene copolymers, yielding mesoporous structure in bulk. These materials are similarly synthesized in acidic media at low temperatures (20-80°C), and display a variety of well-ordered copolymer phases with mesostructures of about 100-500 Å. They can be processed (e.g., molded) into a variety of bulk shapes, which are also transparent. In addition, it is possible to use polymer processing strategies, such as shear alignment, spin casting, and fiber drawing to induce orientational order in these materials. After calcination at 350°C these monoliths and films retain their macroscopic shape and mesoscopic morphology. To our knowledge, these are the first reported thermally stable, transparent, monolithic, large pore-size materials with well-ordered mesostructure. Their dielectric constants can be varied to low values via the Lorentz-Lorenz relationship by tuning the pore volume fraction from 0.6 to as much as 0.86. The fluid sol processability, extraordinary periodic pore and cage structures, high pore volume fraction and inexpensive synthesis make them excellent low dielectric materials for inter-level dielectrics (LID) for on-chip interconnects to provide high speed, low dynamic power dissipation and low cross-talk noise.

To produce the highly ordered, ultra large pore silica mesostructures we adopted an $S^+I^-X^-I^+$ synthesis processing strategy. This synthesis methodology is distinctly different from the S^+I^- route (pH > 3) used to make the M41S family of mesoporous materials: the two methods employ conditions that are on opposite sides of the isoelectric point of aqueous silica (pH = 2). For example, mesoporous silica SBA-15 can be synthesized using block copolymers, which that have a polyoxyethylene-polyoxypropylene-polyoxyethylene (PEO-PPO-PEO) sequence centered on a (hydrophobic) polypropylene glycol nucleus terminated by two primary hydroxyl groups; see Table 1 The synthesis is

carried out in acidic (e.g., HCl, HBr, H_2SO_4, HNO_3, H_3PO_4) media at 35 - 80°C using either tetraethylortho-silicate (TEOS), tetramethylorthosilicate (TMOS), or tetrapropoxysilane (TPOS) as the silica source.

Hexagonal SBA-15 has a wheat-like macroscopic morphology, a highly ordered (four to seven peaks in the X-ray diffraction pattern), two-dimensional hexagonal (*p6mm*) mesostructure, BET surface areas up to 1040 m^2/g, pore volumes to 2.5 cm^3/g, and thick silica walls (31 - 64 Å). The thick silica walls in particular are different from the thinner-walled MCM-41 mesostructures made with conventional low molecular weight cationic surfactants. The pore size and the thickness of the silica wall can be adjusted by varying the heating temperature (35 - 140°C) or heating time (11 - 72 h) of the SBA-15 in the reaction solution and by adding organic swelling agents such as 1,3,5-trimethylbenzene. The thick walls of the hexagonally ordered pores of these materials produce a novel combination of a high degree of both mesoscopic organization and hydrothermal stability. Based on the above properties, SBA-15 materials have potential applications in catalysis, separations, chemical sensors, and adsorbents.

Transparent films and monoliths have been synthesized with similar PEO-PPO-PEO copolymers as structure-directing agents in an acidic sol-gel reaction. These materials can be synthesized with various amounts of water, acid, silicate source, and polymer to yield different mesophase structures depending upon the polymer and processing conditions used. The materials consist of a collection of aggregates of an organic polymer component, such as the amphiphilic copolymer Pluronic F127, which for a hexagonal array that organizes a polymerized silica matrix in the interstices between the polymer aggregates. Such morphologies are formed by interactions among the block copolymer and the oligomeric silicate species, and solidified as the silica polymerizes to form a monolithic structure. The polymer is not strongly incorporated into

the silica walls, as inferred from the remarkably low temperature (150°C) needed to remove the polymer, and supporting ^1H nuclear magnetic resonance (NMR) relaxation measurements. These structures possess characteristic length scales of 100-200 Å and have very large domain sizes (>1 μm), yet retain good transparency. Upon calcination the monoliths become opaque, though retain their bulk shape and possess mesoscopically ordered, hexagonally arranged pores (100-200 Å diameter), which impart high internal surface areas to the materials (ca. 1000 M^2/g).

Synthesis of highly mesoscopically ordered ultra-large-pore, and hydrothermally stable mesoporous silica.

Referring to Figures 1a,b,c and d, there is shown, approximately to scale, two prior art inorganic oxide porous structures and the SBA-15 produced in accordance with this invention. As shown in Figures 1a and 1b Faujasite, a sub-nanoporous zeolite has a pore size of less than 1 nm. MCM-41, a mesoporous molecular sieve material, shown at Figure 1c, has a pore size of about 8nm. In contrast, as shown in Figure 1d, SBA-15, the ultra large pore mesoporous silica material produced by this invention, has a pore size of about 20nm, in this particular example.

Mesoporous silica SBA-15 was synthesized at 35 - 80°C using a hydrophilic-hydrophobic-hydrophilic PEO-PPO-PEO triblock copolymer as the structure-directing-agent. 4.0 g of Pluronic P123 ($PE0_{20}PP0_{70}PE0_{20}$) was dissolved in 30 g water and 120 g (2 M) HCl solution while stirring at 35°C. To the resulting homogeneous solution 8.50 g TEOS was added while stirring at 35°C for 22 h. The mixture was then aged at 100°C without stirring for 24 h. The solid product was filtered, washed, and air-dried at room temperature. Calcination was carried out in air by slowly increasing the temperature (from room temperature to 500°C over 8 h) and heating at 500°C for 6 h.

X-ray diffraction is an important means for characterizing the SBA-15 family of materials. Figures 2a and 2b show small-angel XRD patterns for as-synthesized and calcined hexagonal mesoporous silica SBA-15 prepared by using the polyoxyalkylene triblock copolymer $PE0_{20}PP0_{70}PE0_{20}$ (Pluronic P123). The chemical composition of the reaction mixture was 4 g of the copolymer : 0.041 M TEOS : 0.24 M HCl : 6.67 M H_2O. The XRD patterns were acquired on a Scintag PADX diffractometer equipped with a liquid nitrogen cooled germanium solid-state detector using Cu Kα radiation. The X-ray pattern of as-synthesized hexagonal SBA-15 (Figure 2a) shows four well-resolved peaks that are indexable as (100), (110), (200), and (210) reflections associated with *p6mm* hexagonal symmetry. The as-synthesized SBA-15 possesses a high degree of hexagonal mesoscopic organization indicated by three additional weak peaks that are present in the 2Θ range of 1 - 3.5°, corresponding to the (300), (220), and (310) scattering reflections, respectively. The intense (100) peak reflects a d-spacing of 104 Å, corresponding to a large unit cell parameter (a = 120 Å). After calcination in air at 500°C for 6 h, the XRD pattern (Figure 2b) shows that the p6mm morphology has been preserved, although the peaks appear at slightly higher 2Θ values with $d(100)$ = 95.7 Å and a cell parameter (a_0) of 110 Å. Six XRD peaks are still observed, confirming that hexagonal SBA-15 is thermally stable. A similarly high degree of mesoscopic order is observed for hexagonal SBA-15 even after calcination to 850°C.

SEM images (Figures 3a, 3b) reveal that as-synthesized hexagonal SBA-15 has a wheat-like morphology with uniform particle sizes of about ~80 μm, and that these consist of many rope-like macrostructures. The SEM's were obtained on a JEOL 6300-F microscope. Calcined hexagonal SBA-15 at 500°C in air shows a similar particle morphology, reflecting the thermal stability of the macroscopic shape and structure. TEM images (Figure 3c, 3d) of calcined SBA-15 with different sample orientations

show well ordered hexagonal arrays of mesopores (one-dimensional channels) and further confirm that SBA-15 has a two-dimensional p6mm hexagonal structure. The TEM's were acquired using a 2000 JEOL electron microscope operating at 200 kV. For the TEM measurements, samples were prepared by dispersing the powder products as a slurry in acetone and subsequently deposited and dried on a holey carbon film on a Ni grid. From high-dark contrast in the TEM images, the distance between mesopores is estimated to be about 110 Å, in agreement with that determined from XRD data.

Nitrogen adsorption-desorption isotherm plots and the corresponding pore-size distribution curves are shown in Figure 4 for calcined hexagonal SBA-15 samples that were prepared using the copolymer $PEO_{20}PPO_{70}PEO_{20}$. The sample corresponding to the measurements shown in Figures 4a and 4b was prepared by reaction at 35°C for 20 h, heating at 100°C for 48 h, and subsequent calcination in air at 500°C, yielding a hexagonal SBA-15 product material with a mean pore size of 89 Å, a pore volume of 1.17 cm^3/g, and a BET surface area of 850 m^2/g. The sample corresponding to the measurements shown in Figures 4c and 4d was prepared under identical conditions but additionally used TMB as an organic swelling agent to increase the pore size of the subsequent product material. Using TMB yields hexagonal mesoporous SBA-15 silica with a mean pore size of 260 Å, a pore volume of 2.2 cm^3/g, and a BET surface area of 910 m^2/g. The isotherms were measured using a Micromeritics ASAP 2000 system. Data were analyzed by the BJH (Barrett-Joyner-Halenda) method using the Halsey equation for multilayer thickness. The pore size distribution curve was obtained from an analysis of the adsorption branch of the isotherm. The pore volumes were taken at $P/P_0 = 0.983$ signal point. Prior to the BET measurements, the samples were pretreated at 200°C overnight on a vacuum line. In both Figures 4a and 4c, three well-distinguished regions

of the adsorption isotherm are evident: (1) monolayer-multilayer adsorption, (2) capillary condensation, and (3) multilayer adsorption on the outer particle surfaces. In contrast to N2 adsorption results for MCM-41 mesoporous silica with pore sizes less than 40 Å, a clear type H_1 hysteresis loop in the adsorption-desorption isotherm is observed for hexagonal SBA-15 and the capillary condensation occurs at a higher relative pressure (P/P_0 ~ 0.75). The approximate pore size calculated using the BJH analysis is significantly smaller than the repeat distance determined by XRD, because the latter includes the thickness of the pore wall. Based on these results, the thickness of the pore wall is estimated to be ca. 31 Å (Table 1) for hexagonal SBA-15 prepared using the $PEO_{20}PPO_{70}PEO_{20}$ copolymer.

Heating as-synthesized SBA-15 in the reaction solution at different temperatures (80 - 140°C) and for different lengths of time (11 72 h) resulted in a series of structures with different pore sizes (47 - 89 Å) and different silica wall thicknesses (31 - 64 Å) (as presented in Table 1). The pore sizes and the wall thicknesses determined for hexagonal SBA-15 from TEM images (such as shown in Figures 5a, 5b) are in agreement with those estimated from X-ray and N_2 adsorption measurements. The walls are substantially thicker than those typical for MCM-41 (commonly 10-15 Å) prepared using alkylammonium ion surfactant species as the structure directing-agents. Higher temperatures or longer reaction times result in larger pore sizes and thinner silica walls, which may be caused by the high degree of protonation of the long hydrophilic PEO blocks of the copolymer under the acidic $S^+X^-I^+$ synthesis conditions. EOH moieties are expected to interact strongly with the silica species and to be closely associated with the inorganic wall. Increasing the reaction temperature results in increased hydrophobicity of the PEO block group, and therefore on average smaller numbers of the EOH groups that are associated with the silica wall (see below) and thus increased pore sizes.

The pore size of hexagonal mesoporous SBA-15 can be increased to ~300 Å by the addition of cosolvent organic molecules such as 1,3,5-trimethylbenzene (TMB). In a typical preparation, 4.0 g of Pluronic P123 was dissolved in 30 g water and 120 g (2 M) HCl solution with stirring at room temperature. After stirring to dissolve completely the polymer, 3.0 g TMB was added with stirring for 2 h at 35°C. 8.50 g TEOS was then added to the above homogeneous solution with stirring at 35°C for 22 h. The mixture was then transferred to a Teflon autoclave and heated at 100 -140°C without stirring for 24 h. The solid product was subsequently filtered, washed, and air-dried at room temperature.

Figure 6 shows the typical XRD patterns of hexagonal SBA-15 prepared by adding an organic swelling agent. The chemical composition of the reaction mixture was 4 g of the copolymer : 3 g TMB : 0.041 M TEOS : 0.24 M HCl : 6.67 M H_2O. The X-ray pattern of as-synthesized product (Figure 6a) shows three well-resolved peaks with *d* spacings of 270, 154, and 133 Å at very low angle (2Θ range of 0.2 - 1°), which are indexable as (100), (110), and (200) reflections associated with p6mm hexagonal symmetry. The (210) reflection is too broad to be observed. The intense (100) peak reflects a d-spacing of 270 Å, corresponding to an unusually large unit cell parameter (a = 310 Å). After calcination in air at 500°C for 6 h, the XRD pattern (Figure 6b) shows improved resolution and an additional broad (210) reflection with d spacing of 100 Å. These results indicate that hexagonal SBA-15 is thermally stable, despite its unusually large lattice parameter. The N_2 adsorption -desorption results show that the calcined product has a BET surface area of 910 m^2/g, a pore size of 260 Å, and a pore volume of 2.2 cm^3/g. TEM images confirm that the calcined products have highly ordered, hexagonal symmetry with unusually large pore sizes (Figures 5c, 5d).

Figure 7 shows the change of the pore size and the *d*-spacing of the XRD *d*(100) peak as a function of the TMB/copolymer mass ratio for

calcined hexagonal SBA-15. The pore sizes of calcined SBA-15 were measured from the adsorption branch of the N_2 adsorption-desorption isotherm curve by the BJH (Barrette-Joyner-Halenda) method using the Halsey equation for multilayer thickness. The pore size data for the MCM-41 sample were taken from ref. 4. The chemical compositions of the reaction mixture were 4 g of the copolymer : x g TMB : 0.041 M TEOS : 0.24 M HCl : 6.67 M H_2O for SBA-15 and $NaAlO_2$: 5.3 C_{16}TMACl : 2.27 TMAOH : 15.9 SiO_2 :x g TMB : 1450 H_2O for the MCM-41 (C_{16}TMACl = cetyltrimethylammonium chloride, TMAOH = tetramethyl- ammonium hydroxide). The ratios used in this study ranged from 0 to 3, with the *d*(100) spacing and pore size increasing significantly, up to 320 Å and 300 Å, respectively, with increasing TMB/copolymer ratio. The increased pore size is accompanied by retention of the hexagonal mesostructure, with the X-ray diffraction patterns of each of these materials exhibiting 3 - 4 peaks.

To the best of our knowledge, hexagonal SBA-15 has the largest pore dimensions thus far demonstrated for mesoscopically ordered porous solids. As shown in Figure 7, the *d*(100) spacing and pore size of calcined MCM-41 prepared by using cationic surfactant species can also be increased, but compared to SBA-15, the change is much less. In addition, although MCM-41 pore sizes of ca. 100 Å can be achieved by adding auxiliary organic species (e.g., TMB), the resulting materials have significantly reduced mesostructural order. The XRD diffraction patterns for such materials are substantially less resolved, and TEM micrographs reveal less ordering, indicating that the materials possess lower degrees of mesoscopic order. This is particularly the case near the high-end of this size range (~100 Å) for which a broad single peak is often observed. These materials also tend to suffer from poor thermal stability as well, unless additional treatment with wellTEOS (which reduces the pore size) is carried out. From our results, a family of highly ordered mesoporous

SBA-15 silica can be synthesized with large uniform and controllable pore sizes (from 89 - 500 Å) by using PEO-PPO-PEO copolymer species as amphiphilic structure-directing agents, augmented by the use of organic swelling agents in the reaction mixture. The pore size for hexagonal SBA-15 determined by TEM images (Figures 5c, 5d) is in agreement with that established from separate N_2 adsorption measurements.

Magic-Angle Spinning ^{29}Si NMR spectra (Figure 8) of as-synthesized hexagonal SBA-15 show three broad peaks at 92, 99, and 109 ppm, corresponding to Q^2, Q^3, and Q^4 silica species, respectively. From the relative peak areas, the ratios of these species are established to be $Q^2 : Q^3 : Q^4 = 0.07 : 0.78 : 1$. These results indicate that hexagonal SBA-15 possesses a somewhat less condensed, but similarly locally disordered, silica framework compared to MCM-41.

TGA and DTA analyses (Figure 9) of hexagonal SBA-15 prepared using $PEO_{20}PPO_{70}PEO_{20}$ show total weight losses of 58 wt% apparently consisting of two apparent processes: one at 80 OC (measured using TGA) yields a 12 wt% loss, accompanied by an endothermic DTA peak due to desorption of water, followed by a second 46 wt% weight loss at 145°C with an exothermic DTA peak due to desorption of the organic copolymer. A Netzsch Thermoanalyzer STA 409 was used for thermal analysis of the solid products, simultaneously performing TGA and DTA with heating rates of 5 $Kmin^{-1}$ in air.

The desorption temperature of the large block copolymer (~150°C) is much lower than that of cationic surfactants (~360°C), so that the organic copolymer species can be completely removed and collected without decomposition by heating SBA-15 in an oven (air) at 140°C for 3 h. (The possibility to recover and reuse the relatively expensive triblock copolymer structure-directing species is an important economic consideration and benefit to these materials.) It should be noted that the pure block copolymer $PEO_{20}PPO_{70}PEO_{20}$ decomposes at 270 OC, which

is substantially lower than that of cationic surfactants (~360°C) during calcination. For comparison, the TGA of the copolymer $PEO_{20}PPO_{70}PEO_{20}$ impregnated in SiO_2 gel shows that the copolymer can be desorbed at 190°C, which is ~50°C higher than required for hexagonal SBA-15. Removal of the organic species from as-synthesized SBA-15 at these relatively low temperatures (e.g., 140°C) suggests the absence of strong electrostatic or covalent interactions between the copolymer species and the polymerized silica wall, together with facile mass transport through the pores. The possibility to recover and reuse the relatively expensive triblock copolymer structure-directing species is an important economic consideration and advantage of these materials.

Hexagonal SBA-15 can be synthesized over a range of copolymer concentrations from 2 - 6 wt% and temperatures from 35 - 80° C. Concentrations of the block copolymer higher than 6 wt% yielded only silica gel or no precipitation of silica, while lower copolymer concentrations produced only dense amorphous silica. At room temperature, only amorphous silica powder or products with poor mesoscopic order can be obtained, and higher temperatures (> 80°C) yield silica gel. Like TEOS, tetramethylorthosilicate (TMOS) and tetrapropoxysilane (TPOS) can also be used as the silica sources for the preparation of hexagonal SBA-15.

SBA-15 can be formed in acid media (pH<1) using HCl, HBr, HI, HNO_3, H_2SO_4, or H_3PO_4. Concentrations of HCl (pH 2 - 6) above the isoelectric point of silica (pH 2) produce no precipitation or yield unordered silica gel. In neutral solution (pH 7), only disordered or amorphous silica is obtained. We also measured the precipitation time (t) of the silica as a function of the concentration of HCl and Cl^-. The [Cl^-] concentration was varied by adding extra NaCl, while keeping the H^+ concentration constant. From these measurements, log (t) is observed to increase linearly with log C (where C is the concentration of HCl or Cl^-).

Slopes of 0.31 for [Cl^-] and 0.62 for HCl indicate that Cl^- influences the synthesis of SBA-15 to a lesser extent than does H^+. Based on these results, we propose that the structure-directed assembly of SBA-15 by the polyoxyalkylene block copolymer in acid media occurs by a $S^+X^-I^+$ pathway. While both the EO and PO groups of the copolymer are positively charged in acidic media, the PO groups are expected to display more hydrophobicity upon heating to 35 - 80°C, thereby increasing the tendency for mesoscopic ordering to occur. The protonated polyoxyalkylene (S^+), the anionic inorganic (X^-) bonding, S^+X^-, and the positive silica species (I^+) are cooperatively assembled by hydrogen bonding interaction forces. Assembly of the surfactant and inorganic species, followed by condensation of silica species, results in the formation of hexagonal SBA-15 mesophase silica. At high pH values (2 - 7), the absence of sufficiently strong electrostatic or hydrogen bonding interactions leads to the formation of amorphous or disordered silica.

One of the limitations of calcined MCM-41 materials prepared without additional treatment with TEOS is their poor hydrothermal stability. As shown in Figure 10, both as-synthesized and calcined (500°C for 6 h) MCM-41, prepared with $C_{16}H_{33}N(CH_3)_3Br$ as previously described, show well resolved hexagonal XRD patterns (Figures 10a, 10b). However, after heating in boiling water for 6 h, the structure of calcined MCM-41 is destroyed and the material becomes amorphous, as evidenced by the absence of XRD scattering reflections in Figure 10c. By contrast, all of the calcined hexagonal SBA-15 samples prepared using the PEO-PPO-PEO block copolymers are stable after heating in boiling water for 24 h under otherwise identical conditions. For calcined hexagonal SBA-15 prepared by using the $PEO_{20}PPO_{70}PEO_{20}$ copolymer and after calcination in air at 500°C and subsequent heating in boiling water for 6 h, the (210) reflection becomes broader, the (300), (220), and (310) peaks become weaker, while the (100) peak is still observed with

similar intensity (Figure 10d). After heating in boiling water for 24 h, the intensity of the (100) Bragg peak (Figure 10e) is still unchanged. Nitrogen BET adsorption isotherm measurements carried out after such hydrothermal treatment shows that the monodispersity of the pore size, surface area, and pore volume are retained. The results confirm that calcined hexagonal SBA-15 silica is significantly more hydrothermally stable than calcined hexagonal MCM-41 silica, most likely because SBA-15 has a thicker silica wall. This is an improved one-step alternative to two-step post-synthesis treatments that use tetraethylorthosilicate (TEOS) to stabilize mesoporous MCM-41 by reforming and structuring the inorganic wall with additional silica.

Preparation of mesoscopically ordered silica-copolymer monoliths and films.

A typical preparation of monolithic silica-copolymer mesostructures is outlined below. A series of samples was made with varying amounts of Pluronic F127 $PEO_{100}PPO_{65}PEO_{100}$ triblock copolymer, while holding other processing conditions constant. A calculated amount of a 20 wt% EtOH/ Pluronic F127 solution (between 0.7 and 3.5 ml) is transferred into a 30 ml vial. 0.72 ml of an acidic solution of HCl (pH 1.5) is added to the polymer solution while stirring, followed by addition of 1.0 ml of tetraethylorthosilicate (TEOS). The solution is stirred until homogeneous, and allowed to gel uncovered under ambient conditions. After gelation (~ 2 days) the samples are covered for 2 weeks at room temperature. At the end of this period the gels have shrunk, yet done so uniformly to retain the shape of the container. Further research has shown that addition of a small amount of 3-glycidoxypropyltrimethoxysilane can prevent shrinkage. The cover is removed and the materials are dried at room temperature to eliminate excess solvent. The F127 series materials produced are transparent up to 38 wt% polymer, after which the polymer macro-phase

separates creating a white opaque material. Figures 11a and 11b show optical photographs of two of the monoliths produced. These monoliths were produced using a 2:1 ratio of water to TEOS at pH 1.4 and room temperature, with aging for approximately 1 month. Note the high degree of transparency and only one crack in the 34 wt% sample. Subsequent research has allowed us to produce crack-free monoliths by varying the aging time and temperature. The monoliths pictured are approximately 3-mm thick; although thicker monoliths can be produced, the aging time for these samples increases significantly to eliminate cracking.

These monoliths were analyzed using XRD, TEM, and NIVIR to determine mesostructural morphology, as well as the mechanism of the structure formation. The F127 polymer series above showed an aggregation point of roughly 25 wt% F127, below which the polymer was disordered and homogeneously dispersed within the matrix and above which aggregation of the polymers led to silica-copolymer mesophases. The copolymer weight percents required to produce specific phases vary depending upon the exact conditions and copolymer used, however this example may be considered representative, though by no means all inclusive, of the results observed.

XRD patterns of powdered samples obtained from the monoliths show a single diffraction peak with increasing intensity for increasing polymer concentration with a maximum at 38 wt%. Below 27 wt% F127, no XRD intensity is observed. The *d*(100) peak is centered at 112 Å for 27-34 wt% and increases to 120 Å for the 38 wt% sample. The change in the location of the peak is due to phase changes in the material, as observed by TEM and NMR. TEM reveals well ordered silica-copolymer mesophases in the samples with higher copolymer concentration, such as the lamellar phase in the 38 wt% sample shown in Figure 12. The image shows that the material has an extremely well ordered lamellar mesoscopic structure with a repeat distance of ~105 nm. The image

region is 990 x 1200 nm. The large background stripes are artifacts produced by the microtome cutting process and are otherwise unrelated to the morphology of the material. Lower concentrations of copolymer produced hexagonal, gyroid, or micellar phases with spacings of about 110 Å. The domain sizes for these structures is quite large, well over 1 μm^2 for the lamellar phase, which makes it surprising that only one XRD peak is observed, although others have shown that single XRD patterns do not always imply poorly ordered materials (F. Schüth). Below 27 wt% no mesostructural ordering is observed.

NMR spectroscopy was utilized to provide information about copolymer-silicate interactions on the molecular level. ^1H $T_{1\rho}$ relaxation and two-dimensional ^{29}Si-^1H and ^{13}C-^1H heteronuclear correlation NMR experiments reveal that the polymer is rigidly incorporated in the silicate at 11 wt% and begins to microphase separate at 20 wt%. At 27 wt% the PEO and PPO are 80% separated from the silicate, and at 38 wt% the PPO is fully separated (>10Å) from the matrix. This indicates that a phase change has occurred in progressing from copolymer concentrations of 27 to 34 wt% in the samples, where some PPO-^{29}Si correlation intensity is still observed. Some PEO was observed to be associated with the matrix at all concentrations, implying that the polymerizing silica and PEO blocks are compatible. This suggests that the material is produced by polymerization of silicate oligomers that selectively swell the PEO block of the composite mesostructure.

It is possible to use this chemistry and processing to produce thin SBA-15 silica-copolymer films by either spin-, drop-, or dip-casting. Such films can serve as robust permeable coatings for use in separation or chemical sensing applications or as host matrices for optically or electrically active guest molecules for use in optoelectronic devices. Figure 13 shows a photograph and X-ray diffraction pattern of an optically transparent hexagonal SBA-15-copolymer film formed by drop-casting the

reaction solution (2 ml TEOS, 0.6 ml H_2O, 0.80 g Pluronic P104, 1 ml dimethylformamide) onto a glass slide and drying at room temperature. The film is 50-μm thick, crack-free and transparent. The X-ray diffraction pattern of this film shows well resolved peaks that are indexable as (100), (110), (200), and (210) reflections associated with *p6mm* hexagonal symmetry in which the one-dimensional axes of the ca. 200 Å aggregates are highly ordered horizontally in the plane of the film.

High quality films can be produced generally as follows. A mixture of 5 ml tetraethylorthosilicate and 0.75-3.0 ml H20 (pH=1.4) is stirred for approximately 30 min or until the silicate has hydrolyzed sufficiently to become miscible with water and thereby form a homogeneous solution. An appropriate amount (generally between 10-40 wt%) of block copolymer, such as Pluronic P104 polyethyleneoxide-polypropyleneoxide-polyethyleneoxide copolymer, is dissolved in the solution. An additive such as ethanol, dimethy1formamide, or tetrahydrofuran can be added to vary the viscosity and coating properties. The mixture is allowed to age, then is dip-, drop-, or spin-coated onto a glass or Si wafer substrate. Thin films with variable thicknesses can also be produced using spin coating.

The XRD patterns confirm that these thin films have highly ordered hexagonal (*p6mm*), cubic (1m3m), or 3-d hexagonal ($p6_3/mmc$) mesostructures. They are highly ordered and can easily be shear aligned. BET measurements show that the thin films have narrow pore size distributions, pore sizes of 20-120 Å, pore volumes up to 1.7 cm^3/g and BET surface areas up to ~1500 m^2/g. SEM images of these thin films show a uniformly flat surface. The thickness of the films can be adjusted from 100 nm - 1 mm by varying the concentration of the solution, aging time and coating time.

The examples shown above use $PEO_{20}PPO_{70}PEO_{20}$ copolymer species as the structure-directing agents. Highly ordered, ultra large pore size SBA-15 materials can also be synthesized by using PEO-PPO-PEO

block copolymers with different ratios of EO to PO and without adding supplemental organic swelling agents, such as TMB. Table 1 summarizes the physicochemical properties of mesoporous silica prepared by using triblock and reverse triblock copolymers. The *d*(100)-spacings from X-ray diffraction measurements can be in the range of 74.5 - 118 Å, with pore sizes of 46 - 100 Å established by N_2 adsorption measurements. The EO/PO ratio and intramolecular distribution and sizes of the corresponding blocks affects the formation of SBA-15. A lower EO/PO ratio with a symmetric triblock PEO-PPO-PEO copolymer architecture favors the formation of *p6mm* hexagonal SBA-15. For example, Pluronic L121, $PEO_5PPO_{70}PEO_5$, at low concentrations (0.5 - 1 wt %) forms hexagonal SBA-15, while use of higher concentrations of this copolymer (2 - 5 wt%) leads to an unstable lamellar mesostructured silica phase. Higher EO/PO ratios of the block copolymer, e.g. $PEO_{100}PPO_{39}PEO_{100}$ or $PEO_{80}PPO_{30}PEO_{80}$, yield cubic SBA-15 silica, including an *Im3m* morphology. These cubic mesophase materials yield large 54 - 80 Å mesoscopically ordered pores and high BET surface areas (up to 1000 m^2/g). Hexagonal mesoporous silica SBA-15 can also be synthesized by using reverse PPO-PEO-PPO triblock copolymer configuration, for example, $PPO_{19}PEO_{33}PPO_{19}$.

In general, any microphase-separating, domain-partitioning copolymer architecture can be considered promising for the synthesis of such mesostructured materials, according to the specifications imposed by processing conditions and ultimately the product properties desired. Additionally, cubic (*Pm3m*) and hexagonal (*p6mm*) mesostructures can be formed by using Brij 56, $C_{16}H_{33}(OCH_2CH_2)_{10}OH$ ($C_{16}EO_{10}$) surfactant species, with the pore sizes controllable from 25 - 40 Å and BET surface areas up to 1070 m^2/g. Brij 76 ($C_{18}EO_{10}$) yields the three-dimensional hexagonal (*P6$_3$/mmc*) and two-dimensional hexagonal (*p6mm*) mesostructures with similar pore sizes and surface areas; see Table 2.

Films and monoliths can be produced with several variations of the solution conditions and/or sol-gel parameters, such as the ratio of water to TEOS, aging time, acidity, additives, temperature, and choices of copolymer or nonionic surfactants. Materials for specific applications can be formulated by appropriate modification of these parameters. Heat treatment after gelation can also produce harder materials that are less likely to crack.

We have found that silica-surfactant mesophases and MCM-41-type mesoporous materials can be aligned using liquid crystal processing strategies, including imposition of magnetic, shear, or electric fields. Similarly, polymer processing of the silica-copolymer composites is expected to be equally advantageous for producing aligned ultra large mesopore hydrothermally spH materials. For example, it should be possible to induce orientational ordering of the silica-copolymer composites and resultant mesoporous materials by applying shear to the sol-gel/copolymer system as it dries. Concerning variations on processing SBA-15-copolymer thin films (0.1-100 μm), use of shear alignment strategies, including spin-casting and dip-casting (i.e., drawing a vertical coverslip from a reservoir of the reaction solution), have been shown to induce larger degrees of orientational order than provided by drop-cast preparations. Moreover, guest molecules such as conducting or optically active organic species can be introduced to the reaction solution(s) and incorporated into the silica-copolymer monoliths, films or powders prior to or during processing. We have demonstrated the efficacy of this for the inclusion of conducting polymer moieties, such as poly(3,4-ethylenedioxythiophene) in SBA-15 silica-copolymer monoliths and spin-, drop-, and dip-cast films.

Methods currently available for the preparation of inorganic-organic mesophases or mesoscopically ordered porous materials typically involve one of five pathways that rely on Coulombic or hydrogen-bonding

interactions, represented by the shorthand notations S^+I^-, $S^+X^-I^+$, S^-I^+, $S^-X^+I^-$, or S^0I^0. The most popular route used in syntheses of mesoporous materials has been the S^+I^- approach in basic media, but the S^-I^+ and $S^-X^+I^-$ syntheses generally yield unstable non-silica based mesoporous materials. Furthermore, the surfactants used as the structure-directing agents in these cases (e.g., alkylammonium, alkylamine) are expensive and/or environmentally noxious. The S^0I^0 synthesis route generally yields disordered or worm-like mesoporous solids due to the absence of strong electrostatic or hydrogen bonding interactions. The materials and synthesis method described here are less expensive, non-toxic, and considerably more versatile than the cases described above. They can be used to tune material properties, such as mesoscopic ordering, pore size, hydrothermal stability, monolith shape, orientational alignment, and compatibility with a wide range of guest molecules to a significantly greater extent than possible with the current state-of-the-art.

The ultra large mesopores in calcined SBA-15 materials provide new opportunities in chromatographic separations of large molecules, such as proteins, enzymes, or polymers. In addition, these materials have promise for new applications in environmental remediation, such as the clean up of polycyclic aromatics, porphyrins, other large organics, and heavy metals from process streams or soils. These properties can be enhanced and tailored by functionalizing molecular moieties along the inorganic walls to provide chemical as well as size selective specificity of adsorption interactions.

To the best of our knowledge there have been no reports of mesoscopically ordered silica monoliths or films with large characteristic structural length scales (>50 Å). The large dimensions of the inorganic-copolymer aggregates and large pore sizes of the composite or mesoporous materials detailed herein are superior to conventional mesoporous solids due to their thermal stability, transparency, monolithic

form, and ability to incorporate large guest molecules. SBA-15 mesoporous silica also has distinct advantages over dense silica, particularly for applications requiring a lower dielectric constant material. SBA-15 has much lower density, long range mesoscopic order and possibilities for obtaining materials with high degrees of structural anisotropy, compared to dense silica. The improvements substantially exceed those provided by MCM-type materials, as discussed earlier. This has attractive implications for the development of low dielectric constant materials, particularly for reducing the capacitance of interconnects, which are among the most severely limiting factors in improving integrated and optical circuit performance. As shown in Figure 14, the quest for materials with dielectric constants significantly below 2 appears to be well within reach; calcined SBA-15 materials have been prepared with porosities of 0.6-0.86, which lead to calculated optical dielectric constants of 1.1-1.4. One can produce aligned morphologies or structures with unconnected spherical cavities to eliminate transverse channel connectivities, which are undesirable for dielectric materials applications.

Use of block copolymers with a hydrophobic core also produces the unique ability to stabilize hydrophobic guest molecules that would not otherwise be compatible with the hydrophilic sol-gel reaction, such as some optically active dyes and polymers. Before now all optical moieties incorporated into sol-gel materials were either water soluble or had to be chemically grafted onto a compatible polymer. The inclusion of a hydrophobic region within our silicates, yet still smaller then optical wavelengths, allows an entirely new area of monoliths and coatings to be developed using hydrophobic dyes and optically active organics while retaining optical transparency. Furthermore, inclusion of guest conducting or optically active species, such as polymers and/or metal nanoparticles, in the pores can create quantum-effect materials. The controllability of the SBA-15 pore sizes, inorganic wall composition, organic composition, and

guest species composition permit the properties (e.g., optoelectronic, mechanical, thermal, etc.) to be tuned over an enormous range. Indeed, sequential introduction of guest species, for example a conducting polymer coating on the interior of the inorganic wall, followed by a second polymer or metal/semiconductor species in the pore center, could lead to the first mesoscopically ordered arrays of nanosized coaxial quantum wires.

Generalized block copolymer syntheses of mesoporous metal oxides

Mesoporous metal oxides were synthesized at 30 - 70 °C using poly(alkylene oxide) block copolymers $HO(CH_2CH_2O)_x(CH_2CH(CH_3)O)_y(CH_2CH_2O)_xH$ (EO_x-PO_y-EO_x) or $HO(CH_2CH_2O)_x(CH_2CH(CH_3CH_2)O)_yH$ (EO_x-BO_y) block copolymers as the structure-directing agents. In a typical synthesis, 1 g of poly(alkylene oxide) block copolymer was dissolved in 10 g of ethanol (EtOH). To this solution, 0.01 mole of the inorganic chloride precursor was added with vigorous stirring. The resulting sol solution was gelled in an open petri dish at 40 - 60 °C in air. The aging time differs for different inorganic systems. Alternatively, the sol solution can be used to prepare thin films by dip coating. The as-made bulk samples or thin films were then calcined at 400 °C for 5 hours to remove the block copolymer surfactants. For the Al and $Si_{1-x}Al_x$ systems, calcination was carried out at 600 °C for 4 hr. For WO_3, calcination at 300 °C is sufficient to yield ordered mesoporous oxides.

X-ray diffraction (XRD) is an important technique for characterizing these metal oxide mesostructures. Table 3 summarizes the synthetic conditions, including the inorganic precursors and aging temperatures and times for the mesostructured inorganic/copolymer composites (before calcination) using $EO_{20}PO_{70}EO_{20}$ as the structure-directing agent. A broad array of mesostructured composites have been successfully prepared,

covering the first-, second- and third-row transition metals and some main group elements as well. The ordering lengths shown in Table 3 correspond to the largest *d* value observed from the low-angle XRD patterns; it ranges from 70 to 160 Å for the different systems. High-order low-angle diffractions are also observed for most of these systems. Quantitative elemental chemical analysis suggests that the frameworks of these mesostructured composites are made up of metal-oxygen-chlorine networks.

Upon calcination, mesoporous TiO_2, ZrO_2, Nb_2O_5, Ta_2O_5, Al_2O_3, WO_3, SiO_2, SnO_2, HfO_2, and mixed oxides $Si_{1-x}Ti_xO_y$, $Zr_{1-x}Ti_xO_y$, $Al_{1-x}Ti_xO_y$, $Si_{1-x}Al_xO_y$ are obtained. X-ray diffraction, transmission and scanning electron microscopy imaging (TEM & SEM), and nitrogen adsorption/desorption are three crucial techniques for characterization of these materials. Table 4 summaries the analysis results, including the ordering length, pore size, wall thickness, wall structure, porosity and Brunauer-Emmet-Teller (BET) surface area.

Figure 15 shows typical XRD patterns for mesostructured zirconium oxides prepared using $EO_{20}PO_{70}EO_{20}$ as the structure-directing agent before and after calcination. The as-made zirconium inorganic/polymer mesostructure (Figure 15a) shows three diffraction peaks with *d* = 115, 65, and 59 Å. After calcination, the diffraction peaks appear at higher 2θ angles with *d* = 106, 60, and 53 Å (Figure 15b). Both sets of diffraction peaks can be indexed as the (100), (110), and (200) reflections from 2-dimensional hexagonal mesostructures with lattice constants a_0 = 132 and 122 Å, respectively. Similar XRD results are obtained in other mesoporous metal oxides. The ordering lengths of these mesoporous metal oxides (Table 4) are substantially larger than those of materials previously reported.

Thermogravimetric experiments indicate that the block copolymer is completely removed upon calcination at 400 °C. The appearance of

low-angle diffraction peaks indicates that mesoscopic order is preserved in the calcined metal oxide materials. This is confirmed by TEM images obtained from mesoporous samples. As examples, Figures 16 - 26 show TEM images of mesoporous ZrO_2, TiO_2, SnO_2, WO_3, Nb_2O_5, Ta_2O_5, Al_2O_3, HfO_2, $SiTiO_4$, $SiAlO_{3.5}$, and $ZrTiO_4$ recorded along the [110] and [001] zone axes of the 2-dimensional hexagonal mesostructures. In each case, ordered large channels are clearly observed to be arranged in hexagonal arrays. The pore/channel walls are continuous and have thicknesses of ~ 3.5 - 9 nm. They are substantially thicker than those typical of metal oxides prepared using alkyammonium ion surfactant species as the structure-directing agents. In addition, energy dispersive X-ray spectroscopy (EDX) measurements made on the calcined samples show the expected primary metal element signals with trace of Cl signal, which confirms that the inorganic walls consist predominantly of metal-oxygen networks.

Furthermore, selected area electron diffraction patterns (ED) recorded on mesoporous ZrO_2, TiO_2, SnO_2, andWO_3 show that the walls of these materials are made up of nanocrystalline oxides that show characteristic diffuse electron diffraction rings (Figures 16 - 18 and 20 insets). Wide-angle X-ray diffraction studies of calcined samples also clearly show broad peaks that can be indexed according to the corresponding oxide crystalline phase. Figure 15d shows a wide-angle diffraction pattern for the calcined ZrO_2 sample. The sizes of the nanocrystals in the calcined materials are estimated to be ~ 2 nm using the Scherrer formula. In addition, bright-field and dark-field (BF/DF) TEM imaging were employed to study the distribution of these nanocrystals. Figures 27 and 28 show such images recorded on same area of one thin mesoporous TiO_2 and ZrO_2 sample. As can be seen in the dark field image (Figures 27b, 28b), the oxide nanocrystals (~ 2 nm) are uniformly embedded in a continuous amorphous inorganic matrix to form

semicrystalline wall structures. This is the first time that the combination of electron diffraction, X-ray diffraction, and bright field/dark field TEM imaging has been used to conclusively demonstrate that our mesoporous metal oxides have nanocrystalline framework.

Figures 29 - 36 show BET isotherms that are representative of mesoporous hexagonal ZrO_2, TiO_2, Nb_2O_5, Ta_2O_5, Al_2O_3, WO_3, $SiTiO_4$, and $ZrTiO_4$. Barrett-Joyner-Halenda (BJH) analyses show that the calcined hexagonal mesoporous metal oxides exhibit pore sizes of 35 - 140 Å, BET surface areas of 100 - 850 M^2/g, and porosities of 40 - 60%. The pore sizes are again substantially larger than the previous reported values. For most of the isotherms obtained on these metal oxides, three well-distinguished regions of the adsorption isotherm are evident: (1) monolayer-multi layer adsorption, (2) capillary condensation, and (3) multilayer adsorption on the outer particle surfaces. In contrast to N_2 adsorption results obtained for mesoporous metal oxides prepared using low-molecular-weight surfactants with pore sizes less than 4 nm, large hysteresis loops that resemble typical H_1- and H_2- type isotherms are observed for these mesoporous metal oxides.

The foregoing examples used $EO_{20}PO_{70}EO_{20}$ copolymer species as the structure-directing agent. Mesoporous metal oxides with other mesostructures can be synthesized by using EO_x-PO_y-EO_x or EO_x-BO_y block copolymers with different ratios of EO to PO or BO. For example, when $EO_{75}BO_{25}$ copolymer is used as the structure-directing agent, mesoporous TiO_2 with cubic mesostructure can be prepared. Figure 37 shows typical XRD patterns for mesostructured titanium oxides prepared using $EO_{75}BO_{70}$ as the structure-directing agent, before and after calcination. The as-made titanium inorganic/ polymer mesostructure (Figure 35a) shows six diffraction peaks with d = 100, 70, 58, 44, 41, 25 Å, which can be indexed as (110), (200), (211), (310), (222), (440) reflections of an Im3m mesophase. After calcination, the diffraction

peaks appear at higher 2θ angles with d = 76, 53, and 43 Å (Figure 35b). These diffraction peaks can be indexed as the (110), (200), and (211) reflections from Im3m mesostructures. The cubic mesostructure is confirmed by the TEM imaging (Figures 38 39).

Films and monoliths (Figure 40) can be produced by varying such synthetic conditions as the solvent, the ratio of inorganic/polymer, aging temperature, aging time, humidity, and choice of the block copolymer. Liquids that are common solvents for inorganic precursors and the block copolymers (e.g. methanol, ethanol, propanol , butanol) can be used during the synthesis. The temperature, the amount of water added, and the pH can adjusted to control formation of the mesostructures. Materials for specific applications can be formulated by appropriate modification of these parameters.

The advantages and improvements over existing practice can be summarized as follows:

(1) Robust, thick channel walls (35 - 90 Å) which give enhanced thermal and chemical stabilities.

(2) Very large pore sizes (3.5 - 14 nm)

(3) Use of low-cost inorganic precursors

(4) Versatile synthetic methodology using non-aqueous media that can be generally applied to vastly different compositions, among which mesoporous SnO_2, WO_3, and mixed oxides $SiTiO_4$, $ZrTiO_4$, Al_2TiO_5 are synthesized for the first time.

(5) For the first time, conclusive demonstration of the nanocrystallinity of the framework in mesoporous ZrO_2, TiO_2, SnO_2, WO_3 using XRD, ED and BF/DF TEM imaging

(6) Mesoporous metal oxides with various physical properties including semiconducting, low dielectric-constant, high dielectric-constant, and negative thermal expansion.

Crystallization of inorganic species during cooperative inorganic/organic self-assembly can lead to macroscopic phase separation of the inorganic and organic components. This is because crystallization energies often dominate the interaction energies that stabilize the inorganic-organic interface, thereby disrupting the establishment of mesostructural order. This is particular the case for non-lamellar phases. In the present invention, this situation is successfully circumvented by using conditions that initially produce a mesoscopically ordered material with an amorphous inorganic wall structure (Figures 15c and 35c) within which a high density of nanocrystals can subsequently be nucleated upon calcination. The thick wall and the noncrystallized inorganic matrix prevent this partially crystalline structure from collapsing by effectively sustaining the local strain caused by the nucleation of the nanocrystals. The coexistence of mesoscopic ordering and framework nanocrystallinity is extremely important for catalysis, sensor, and optoelectronic applications.

To the best of our knowledge, there has been no previous report of mesoporous metal oxide synthesis with such simplicity and versatility. The formation, with such unprecedented simplicity and generality, of large-pore mesoscopically ordered metal oxides suggests that the same general inorganic/ block polymer assembly mechanisms may be operating. In fact, it is well documented that alkylene oxide segments can form crown-ether type complexes with many inorganic ions, through weak coordination bonds. The multivalent metal species (M) can associate preferentially with the hydrophilic PEO moieties, as indicated in Scheme 1, because of their different binding capabilities with poly(ethylene oxide) (PEO) and poly(propylene oxide) (PPO). The resulting complexes then self-assemble according to the mesoscopic ordering directed principally by the microphase separation of the block copolymer species, and

subsequently cross-link and polymerize (Scheme 1) to form the mesoscopically ordered inorganic/polymer composites.

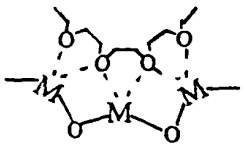

Scheme 1

The proposed assembly mechanism for these diverse mesoporous metal oxides uses PEO-metal chelating interactions in conjunction with electrostatics, van der Waals forces, etc., to direct mesostructure formation.

A unique feature of the current synthetic methodology is use of inorganic precursors in non-aqueous media. Because of the lower electronegativies of the transition metals compared to silicon, their alkoxides are much more reactive towards nucleophilic reactions such as hydrolysis and condensation. There has been some work on the nonhydrolytic sol-gel chemistry of inorganic oxides, a non-hydrolytic route involving carbon-oxygen bond cleavage instead of the metal- oxygen bond which has a general tendency to delay crystallization of the metal oxides, a very important for the first step of our inorganic-copolymer cooperative self-assembly process. In addition, the hydrolytic route to metal oxides often leads to difficulties in controlling stoichiometry and homogeneity. Homogeneity depends on the rate of homocondensation (i.e. formation of M-O-M and M'-O-M') versus the rate of heterocondensation, which can be hardly controlled in the hydrolytic process because of the different reactivities of the various precursors towards hydrolysis and condensation. However, in principle, the non-hydrolytic process should favor the formation of homogeneous binary oxides from different metal precursors because of the decreased

difference in hydrolysis and condensation rates for different inorganic sources in non-aqueous media. This has been successfully demonstrated in the mesoporous mixed oxides syntheses using the methods of this invention.

This utilization of block copolymer self-assembly in conjunction with chelating complexation for inorganic/organic cooperative assembly in the non-aqueous media make it possible to synthesize mesoporous materials with vastly different compositions exemplified in Table 4.

Cooperative Multiphase Assembly of meso-macro silica membranes

Here we describe a novel procedure for the synthesis of artificial coral silica membranes with 3-d meso-macro structures. This process utilizes multiphase media while including microphase separation block copolymer/silica composite and macrophase separation between strong electrolytes and the composite in a single step. We find that strong electrolytes such as NaCl, LiCl, KCl, NH_4Cl, KNO_3, or even transition metal cationic salts such as $NiSO_4$, can be used to prepare meso-macro silica membranes that are formed at the interface of droplets of these inorganic salt solution. It is well known that in nature, macroscopic ordered silica structure such as diatom and coral are grown through a protein modified process in the ocean environments that are rich in inorganic salts such as NaCl. The process used in this study may be significant in understanding the formation of diatom and coral in nature which also can be considered as a 3-phase media process: the environment of the cell, the cell membrane and the aqueous media within the cell.

The silica membranes (size ~ 4 cm x 4 cm, thickness ~ 5 mm) with 3-d meso-macro silica network structures that we have prepared show oriented continuous rope, tyroid, and grape vine or dish pinwheel, and gyroid, morphologies depended on the electrolyte strength of the

inorganic salts or amphiphilic block copolymer templates. The macropore size (0.5 ~ 100 μm) can be controlled by inorganic salts and evaporation rate of the solvent. The mesoscopic structures can be highly ordered 2-d honeycomb (pore size 40 ~ 90 Å) or 3-d cubic packing, and controlled by the amphiphilic block copolymer templates. These artificial coral meso-macro silica membranes are thermally stable and exhibit a large surface areas up to 1000 cm^2/g and pore volumes up to 1.5 cm^3/g.

The silica membranes were prepared by the use of two-step sol-gel chemistry. First oligomeric silica sol-gel was obtained by pre-hydrolysizing of tetraethoxysiliane (TEOS) in ethanol solution by an acid-catalyzed process . Second, the oligomeric silica sol-gel was added into a mixture solution of poly(ethylene oxide)-*block*-ploy(propylene oxide)-*block*-poly(ethylene oxide) (PEO-PPO-PEO) triblock copolymer and inorganic salts in water and ethanol. The final composition of this mixture was range of 1 TEOS: (6.8 ~ 34) x 10^{-3} copolymer: 0.51 ~ 3.0 inorganic salt: 18 ~ 65 H_2O: 0.002 ~ 0.04 HCl: 11 ~ 50 EtOH. The silica membranes with 3-d meso-macro structures were obtained after drying at room temperature, washing with water to remove the inorganic salts, and calcination to completely remove the organic block copolymer,.

In a typical synthesis, 2.08 g TEOS (Aldrich) were added to 5 g ethanol, 0.4 g water and 0.4 g (0.1 M) of HCl solution with stirring at room temperature for 0.5 h, then heated at 70°C without stirring for 1 h. After cooling to room temperature, 1 g $EO_{20}PO_{70}EO_{20}$ (Pluronic P123, Aldrich/ BASF, average molecular weight 5800), 1 g NaCl, 10 g ethanol and 10 g water were added to this solution with stirring at room temperature for 1 h. The resultant solution was transferred into an open petri dish, allowed to evaporate at room temperature. After complete drying, the solid membrane was removed from the dish, 20 g water added and then heated in a sealed container at 100°C for 3 days to dissolved the inorganic salts. After cooling to room temperature, the solid silica

membranes were washed with de-ionic water and dried at room temperature. The as-synthesized silica membranes were calcined at 500°C for 6 h in air to completely remove all organic block copolymers.

Figure 41 shows several representative scanning electron microscope (SEM) images, obtained on a JEOL 6300-F microscope, of the silica membranes and inorganic salt (NaCl) crystal co-grown with the membranes by sol-gel chemistry. The silica membranes prepared from NaCl solution show 3-d macroscopic network structures and a coral-like morphology (Figure 4la). The reticular 3-d network (thickness of ~ 1 μm) of the silica membrane is made up of continuous rope-like silica which exhibits highly mesoscopic ordering (see below). The silica membranes can be as large as ~ 4 cm x 4 cm depended on the size of the container that is used. The thickness of the silica membranes can be varied from 10 μm to 5 mm.

As shown in Figure 4lb, the whole silica membrane shows similar local macroscopic structure that is not long-range ordering. The average macropore size of the silica membranes is about ~2 μm (±0.4) (Figure 4la) and can be varied from ~0.5 μm to ~100 μm by changing the evaporation rate or the electrolyte strength of the inorganic salts. For example, when a small amount of ethylene glycol is added into the sol-gel solution to slow the evaporation rate, a small macropore size (~0.5 μm) is obtained as shown in Figure 4lc. Of interest is finding that when the evaporation rate is low, the thickness of the silica network is decreased several hundreds nanometer as shown in Figure 41c. When the evaporation rate is high, the macropore size of the silica membranes can be as large as ~10 μm, the framework thickness is increased (as shown in Figure 41d) and the macroscopic structure of the silica membranes is changed to a 2-d honey comb channel structure.

The electrolyte strength of the inorganic salts also can be used to control the macropore size. By using stronger electrolytes, for example,

$MgS0_4$, the macropore size can be as much as ~20 μm. In addition, the morphology of the silica membrane can be modified through changing the concentration of inorganic salts. Low concentrations of the inorganic salts result in an inhomogeneous silica membrane. While high concentrations, result in the grape vine morphology that makes up the silica membrane as shown in Figure 41e.

The morphologies of the inorganic salt crystals are also affected by the organic block copolymer. For example, without the amphiphilic block copolymer, cubic crystals of NaCl as large as ~100 μm can be grown in the solution of water and ethanol, however, in the presence of the surfactant under our synthesis conditions, most NaCl crystals show an acicular (~1 μm in diameter) morphology (Figure 4If), with a length of as much as 1 cm. When $NiSO_4$ is used as the inorganic salts in our synthesis condition, a disk-like morphology of $NiSO_4$ crystal is observed at the bottom of the silica membranes. This suggests that the crystallization of the inorganic salts can also be directed by block copolymers.

Besides NaCl, other inorganic salts such as LiCl, KCl, NH_4Cl, Na_2SO_4, $MgSO_4$, $NiSO_4$, $MgCl_2$, chiral $NaClO_3$, and organic acids such as, malic acid, can be used to form the silica membranes. Figure 42 shows several representative scanning electron microscope (SEM) images of the meso-macroporous silica membranes prepared by using block copolymer P123 (a-c), or P65 (d) in different inorganic salt solutions. The morphology of the silica membranes is dependent on the electrolyte strength of the inorganic salts. For example, when LiCl, KCl, and NH_4Cl are used, with electrolyte strengths comparable to that for NaCl, a similar coral-like morphologies (Figures 42a, b, c) are observed, although the network morphology of the silica membranes is somewhat different. However, when the inorganic salts with stronger electrolyte strengths such as Na_2SO_4, $MgSO_4$, are used in the synthesis, the macroscopic

structures consist silica networks made up of toroid, pinwheel, dish, and gyroid morphologies (Figure 43).

The macroscopic structure is also affected by the block copolymer. When higher aver-age molecular weight block copolymers such as Pluronic F127 ($EO_{106}PO_{70}EO_{106}$) is used, cubic morphology is observed by SEM (Figure 43a). This morphology results from silica grown around cubic NaCl crystals, suggesting a macroscopic inorganic crystal templating process for the mesoporous silica growth. When block copolymers such as Pluronic P65 ($E0_{26}PO_{39}EO_{26}$) is used, the silica membrane with large macropore size is obtained (Figure 42d).

The mesoscopic ordering in these silica membranes formed by the cooperative self-assembly of inorganic silica species/amphiphilic block copolymer is mainly controlled by the block copolymer while can be characterized by the low-angle X-ray diffraction patterns (Figure 44) and transmission electron microscope (TEM) (Figure 45). The XRD patterns of Figure 44 were acquired on a Scintag PADX diffractometer using Cu Ka radiation. For the TEM of Figure 45 measurements, the sample was prepared by dispersing the powder products as a slurry in acetone and subsequently deposited and dried on a hole carbon film on a Cu grid. As shown in Figure 44a, the coral-like silica membranes synthesized by using P123 triblock copolymer after removal of NaCl by washing, shows a typical hexagonal (*p6mm)* XRD pattern for mesoporous materials with four diffraction peaks (a = 118 Å), which is similar to that of SBA-15 described above. After calcination at 500°C in air for 6 h, the four-peak XRD pattern is also observed and the intensity of the diffraction peaks is increased, suggesting that the *p6mm* mesoscopic ordering is preserved and thermally stable, although the peaks appear at slightly larger 20 values, with a = 111 Å. The cell parameters of mesoscopic ordering on the silica membranes can be varied by using different triblock copolymers. For example, a = 10 1 Å for Plunroin P103 ($EO_{17}PO_{85}EO_{17}$) (Figure 44b)

and a = 73.5 Å for Plunronic P65 ($E0_{26}PO_{39}EO_{26}$) (Figure 44c), these materials have 2-d hexagonal (*p6mm*) mesoscopic highly ordered structures.

These results suggest that the presence of the inorganic salts such as NaCl does not greatly effect the cooperative self-assembly of block copolymer/silica to form highly ordered mesostructure. Figures 45a,b show TEM images of calcined silica membranes prepared by using P123 block copolymer in NaCl solution at different orientations, confirming that silica network of the membranes is made up of a 2-d *p6mm* hexagonal mesostructure, with a well-ordered hexagonal array and one-dimensional channel structure. TEM images (Figure 45 c, d) of the silica membranes with small macropore size (~0.5 μm from SEM) prepared by adding a small amount of ethylene glycol show that the rope-like networks of the silica membranes is made up of loop-like mesoscopic silica with oriented 1-d channel arrays parallel to the long axis. These rope-like silicas form a 3-d network macroporous structure. It should be noted that when higher molecular weight block copolymer F127 is used as the mesoscopic structure-directing agents, a silica membrane with cubic mesostructure (a = 217 Å) can be obtained, based on XRD and TEM results.

SEM images of the silica membranes after calcination at 500 °C in air show that the coral-like macrostructure is retained, demonstrating that the coral-like meso-macro silica membranes prepared with inorganic salts are thermally stable. Thermal gravimetric and differential thermal analyses (TGA and DTA) (Figure 46) in air of the silica membranes prepared by using P123 block coploymer in NaCl solution after removal of the inorganic salts, show total weight losses of only 24 weight % (Figure 46 top). A Netzsch Thermoanalyzer STA 409 was used for thermal analysis of the solid products, simultaneously performing TGA and DTA with heating rates of 5 $Kmin^{-1}$ in air. At 100°C TGA registers a 18 weight % loss accompanied by an endothermic DTA peak caused from

desorption of water, this is followed by a 6 weight % TGA loss at 190°C which coincides with an exothermic DTA peak associated with decomposition of the organic block coploymer. By comparison, the silica membranes obtained without removed the inorganic salts show total weight losses of 50 weight % (Figure 46 bottom). At 100°C TGA registers a 4 weight % loss from physical adsorption of water, followed by a 46 weight % TGA loss at 200°C from decomposition of the organic block copolymer.

The above observations confirm that the interaction between silica species and block copolymer species is weak, and after washing with water 84 weight % of the block copolymer in the silica membranes is removed. After washing by water and without calcination, these silica membranes already show similar nitrogen sorption behavior to that for calcined silica membranes, (Figure 47a, b) so that after washing, both macroporous (~ 2 μm) and mesoporous (60 Å) channels are already accessible. The isotherms of Figure 47 were measured using a Micromeritics ASAP 2000 system. Data were calculated by using the BdB (Broekhoff and de Boer) model. The pore size distribution curve was obtained from an analysis of the adsorption branch of the isotherm. The pore volume was taken at $P/P_0 = 0.985$ signal point. The BET sample was pre-treated at 200°C overnight on the vacuum line.

The representative nitrogen adsorption/desorption isotherms and the corresponding pore size distribution calculated by using Broekhoff and de Boer's model are shown in Figure 48. The isotherms of Figure 48. The isotherms were measured using a Micromeritics ASAP 2000 system. Data were calculated by using the BdB (Broekhoff and de Boer) model. The pore size distribution curve was obtained from an analysis of the adsorption branch of the isotherm. The pore volume was taken at $P/P_0 = 0.985$ signal point. The BET sample was pre-treated at 200°C overnight on the vacuum line. The coral-like silica membranes prepared using P123

block copolymers in a NaCl solution show a typical isotherm (type IV) of cylindrical channel mesoporous materials with H_1-type hysteresis, and exhibit a narrow pore size distribution at the mean value of 84 Å. This material has a Brunauer-Emmett-Teller (BET) surface area of 660 m^2/ 9, and a pore volume of 1.1 cm^3/g. The mesoscopic pore size of the silica membranes prepared in NaCl solution depended on the amphiphilic block copolymer, for example, the materials prepared by using P103 and P65 show similar isotherms and exhibit pore sizes of 77 and 48 Å, BET surface areas of 720 and 930 m^2/g, and pore volumes of 1.12 and 0.99 cm^3/g respectively (Figure 48). When large molecular weight F127 block copolymer is used as the templates, the silica membrane with cubic mesoscopic structure shows the isotherms with a large H_2-type hysteresis (Figure 49a) much different with that for hexagonal mesoscopic array silica membranes and does not fits to cylinders model by using BdB model to calculate the pore size distribution. (Figure 49b) However, using spheres model, it shows quite narrow pore size distribution at a mean of 10.5 nm, and exhibit a BET surface area of 1003 m^2/g, pore volume of 0.8 cm^3/g (Figure 49b). The silica membranes prepared by using nonionic oligomeric surfactant $C_{16}H_{33}EO_{10}$ also high BET surface area of 710 m^2/g and pore volume of 0.64 cm^3/g, but slight smaller a mean pore size of 3.6 nm (Figures 50a,b).

In order to understand the formation of the coral-like meso-macro silica membranes, we have carefully investigated the macroscopic structures in different areas (Figure 51) of the as-made silica membranes prior to washing. As shown in Figures 51a-d, without washing out the inorganic salt (LiCl) the macroscopic coral-like structures of the membrane have been already formed in the middle region of the silica membrane. On the other hand, the image recorded in the top region of the silica membrane is quite different than that from the middle region and show disordered pillow windows that have similar average macro-window

size compared that in the middle region. These results suggest that the silica membrane grown at the air interface is different than that water interface. Figure 51d shows the SEM image of the silica membrane prepared by LiCl recorded at the bottom region, suggesting that the mosaic-like inorganic salt LiCl crystals, which are confined by XRD and chemical analysis, are formed in the bottom of the silica membranes. The shape of the pillow-like LiCl crystals is somewhat similar to the fenestrated morphology observed at the top region of the silica membrane. SEM images of the silica membrane prepared by using NiS04 as the inorganic salt recorded on the top, middle, bottom regions of the membrane are shown in Figures 51e-h. Without washing out the inorganic salt ($NiSO_4$) (Figures 51e,f) SEM images reveal a disk-like window morphology at the top of the membrane, while inside this window, a coral-like morphology can be seen (Figure 46f). However, at the bottom of the membrane, grape vine-like silica macrostructures with disk-like inorganic salt $NiSO_4$ crystals are observed (Figure 51g, h). The size of disk-like $NiSO_4$ crystals is the same as the window size of the silica membrane at the top. These results are consist with initial phase separation between the coral-like silica macrostructure and inorganic salts, followed by formation of the silica macrostructure above the inorganic salts.

In order to further confirm the formation of the materials, we investigate the change of composition as a function of the evaporation time (Figure 52). The chemical composition of the starting reaction mixture was I g P123 block coploymer: 0.0 1 mol TEOS: I g LiCl : 4 x 10^{-5} mol HCl: 0.55 mol H_20: 0.33 mol EtOH. As shown in Figure 52, in the beginning, the concentration (weight %) of ethanol is decreased rapidly, and the concentration of water and SiO_2 and inorganic salt LiCl are increased since a large amount of ethanol is evaporated. After about 3 h, silica-block copolymer gel starts to form, in liquid phase, the concentration

of silica is rapidly decreased and the concentration of LiCl is rapidly increased. When the silica mesostructure is formed as determined by XRD, almost all the ethanol has evaporated (in liquid phase, a concentration lower than 1%) and only a trace amount of silica is found in the liquid phase, suggesting that the silica/organic block copolymer composition has been already solidified at this time at the interface with salt water. When the concentration of salt LiCl is near saturation concentration (45%), the crystallization of the inorganic salt LiCl occurs. At this time, the formation of mesostructured silica has been almost completed. These results further indicate that the macroscopic silica structure is formed first at the interface of inorganic salt water, and sequentially, when the solution of the inorganic salt reaches saturation concentrations, crystal of inorganic salts are formed in the bottom of the membrane.

Based on above results, we postulate that macroscopic silica structure is formed around a droplet of inorganic salt solution as illustrated in Scheme A (Figure 53). Ethanol is first evaporated, then, water. As the inorganic salt solution becomes more concentrated, two domains are formed, one a water-rich domain, where most inorganic salt is located, another a water-poor domain, where silica and block copolymer compositions are located. The formation of two domains results in tri- phase separation, a droplet of inorganic salt solution phase separated by silica-block copolymer gel. The droplet of the solution serves as a template for the growth of silica-block copolymer composites. Once the macrostructure is rigidified, the inorganic salt solution approaches to the bottom of the container progressively. The cooperative self-assembly of silica/block copolymer occurs at the interface of the droplet, and results in coral-like mesomacroscopic silica structure. On the other hand, when the silica is formed at the interface of air and salt water,

the droplet of the salt solution becomes flatters, resulting in the fenestrated membrane at the top.

Referring to Figure 54, progressively higher magnifications are shown of a section of a meso-macro silica membrane made in accordance with this invention. The membrane is shown in Figure 54a which has a macropore structure, as shown in Figure 54b. However the walls defining the macropores have a mesoporous structure.

In summary, artificial coral silica membranes with 3-d meso-macro structures have been synthesized by a novel process of an acidic catalyzed silica sol-gel chemistry in the present of inorganic salts. Inorganic salts play an important role on the formation of meso-macro silica membranes that are grown at the interface of a droplet of inorganic salt solution. The results are of general important for understanding multiphase processes such as the formation of diatoms coral silica structures in nature. The silica membranes (size ~ 4 cm x 4 cm, thickness ~ 5 mm) with 3-d meso-macro silica network structures show oriented continuous rope, toroid, and grape vine, or dish, pinwheel, gyroid, and cubic cage morphologies depending on the electrolyte strength of the inorganic salts or amphiphilic block copolymer templates. The macropore size (0.5 ~ 100 μm) can be controlled by inorganic salts and the evaporation rate of the solvent. The mesoscopic structures can be highly ordered 2-d honeycomb (pore size 40 ~ 90 Å) or 3-d cubic packing and are controlled by the amphiphilic block copolymer templates. The coral-like mesomacro silica membranes are thermally stable and exhibit large surface areas (to 1000 cm^2 /g) and pore volume (to 1.1 cm^3/g). We anticipate that these new process ceramics material with structure and design on multiple length scales will have many applications in the areas, including separation, sorption, medical implant, catalysis, and sensor array applications.

The example shown above in forming meso-macro silica membranes used Pluronic P123 block copolymer, $EO_{20}PO_{70}EO_{20}$ as the template to control mesoscopic ordering of the silica membranes. Besides P123, other surfactants can also be used in the synthesis. For example, one could use:

(1) a diblock copolymer, poly(ethylene oxide)-*block*-poly(propylene oxide); poly(ethylene oxide)-*block*-poly(butylene oxide) (Dow Company); B50-6600, BL50-1500;

(2), a triblock copolymer, poly(ethylene oxide)-*block*-poly(propylene oxide)-*block* poly(ethylene oxide); (BASF) poly(ethylene oxide)-*block*-poly(butylene oxide)-*block* poly(ethylene oxide) (Dow Company); such as Pluronic L64, L121, L122, P65, P85, P103, P104, P123, PF20, PF40, PF80, F68, F88, F98, F 108, F 127;

(3) a reversed triblock copolymer Pluronic 25R8, 25R4, 25R2

(4) a star di-block copolymer (BASF), Tetronic 901, 904, 908; and

(5) a reversed star di-block copolymer Tetronic 90R1, 90R4, 90R8.

The inorganic salts can be electrolyte, such as KCl, NaCl, LiCl, NH_4Cl, MgCl, $MgSO_4$, KNO_3, $NaClO_3$, Na_2SO_4, $NiSO_4$, $CoCl_2$, water organic acid, such as DL tartaric acid, citric acid, malic acid. We claim that dissolvable alkali salts, alkaline earth salts, transition metal, sulfate, nitrate, halide, chlorate, per chlorate.

The preparation of meso-macro silica membrane are emulsion chemistry latex sphere template; phase separation and solvent exchanged; inorganic salts templating which was developed by ourselves here. This discovery should have great signification for understanding the formation of the diatom and coral in nature, The macromesoporous materials would have many applications in the areas of sorption, catalysis, separation, sensor arrays, optoelectionic devices. The materials and synthesis method described here are very versatile in that

they can be used for many fields of application and for synthesis of any inorganic-surfactant composites, for example, aluminophosphate-based, TiO_2, ZrO_2, Al_2O_3, Nb_2O_5, Ta_2O_5, Cr_2O_3, Fe_2O_3, $ZrTiO_4$, Al_2SiO_5, HfO_2, meso-macroporous silica membranes. These materials would have many applications on sorption, catalysis, separation, sensor arrays, optoelectionic devices.

Table 1. Physicochemical Properties of Mesoporous Silica (SBA) prepared using Polyoxyalkylene Block Copolymers.

Block Copolymer	Formal	Mesophase	d(Å)[a]	BET surface area (m^2/g	pore size[b] (Å)	pore volume(m^3/g)	Wall[c] thickness (Å)
Pluronic L121	$PEO_5PPO_{70}PEO_5$	lamellar	116				
Pluronic L121	$PEO_5PPO_{70}PEO_5$	hexagonal	118(117)	633	100	1.04	35
Pluronic F127	$PEO_{106}PPO_{70}PEO_{106}$	cubic	124(118	742	54	0.454	
Pluronic F88	$PEO_{100}PPO_{39}PEO_{100}$	cubic	118(101)	696	35	0.363	
Pluronic F68	$PEO_{80}PPO_{30}PEO_{80}$	cubic	91.6(88.9)				
Pluronic P123	$PEO_{20}PPO_{70}PEO_{20}$	hexagonal	104(95.7)	692	47	0.557	64
Pluronic P123	$PEO_{20}PPO_{70}PEO_{20}$	hexagonal	105(97.5)*[d]	780	60	0.795	53
Pluronic P123	$PEO_{20}PPO_{70}PEO_{20}$	hexagonal	103(99.5)*[e]	820	77	1.03	38
Pluronic P123	$PEO_{20}PPO_{70}PEO_{20}$	hexagonal	108(105)*[f]	920	85	1.23	36
Pluronic P123	$PEO_{20}PPO_{70}PEO_{20}$	hexagonal	105(104)*[g]	850	89	1.17	31
Pluronic P103	$PEO_{17}PPO_{85}PEO_{17}$	hexagonal	97.5(80.6)	768	46	0.698	47
Pluronic P65	$PEO_{20}PPO_{30}PEO_{20}$	hexagonal	77.6(77.6)	1003	51	1.26	39
Pluronic P85	$PEO_{26}PPO_{39}PEO_{26}$	hexagonal	92.6(88.2)	962	60	1.08	42
Pluronic L64	$PEO_{13}PPO_{70}PEO_{13}$	hexagonal	80.6(80.5)	950	59	1.19	34
Pluronic 25R4	$PEO_{19}PPO_{33}PEO_{19}$	hexagonal	74.5(71.1)	1040	48	1.15	34
Tetronic 908		cubic	101(93.6)	1054	30	0.692	
Tetronic 901		cubic	73.9(70.1)				
Tetronic 90R4		cubic	7.39(68.5)	1020	45	0.910	- -

a, d(100) spacing or d value of characteristic reflection of the as-synthesized products and the value inside brackets is the d value after calcination at 500°C for 6 h; b, calculated from adsorption branch; c, calculated by a_o - pore size (a_o = 2x d(100)/√3).

* reaction at 35°C for 20 h, then heating: (d) at 80°C for 24 h; (e) at 80°C for 48 h; (f) at 90°C for 24 h; (g) at 100°C for 24 h.

Table 2. Physicochemical Properties of Mesoporous Silica (SBA) Prepared Using Nonionic Alkyl Polyethylene Oxide Surfactants.

Surfactant	Reaction Temperature	Mesophase	d(Å)[a]	BET surface area (m^2/g)	pore size[b] (Å)	pore volume (m^3/g)
$C_{16}EO_2$	RT	lamellar	64.3			
$C_{12}EO_4$	RT	cubic	45.3(44.7)	665	22	0.375
$C_{12}EO_4$	RT	lamellar (Lα)	45.7	570		
$C_{12}EO_4$	60°C	lamellar	42.4	606	24	0.392
$C_{16}EO_{10}$	RT	cubic	56.6(47.6)	1070	25	0.678
$C_{16}EO_{10}$	100°C	hexagonal	64.1(62.8)	910	35	1.02
$C_{16}EO_{20}$	RT	cubic	73.7(49.6)	602	22	0.291
$C_{18}EO_{10}$	RT	$P6_3/mmc$	63.5(51.0)	1150	31	0.826
$C_{18}EO_{10}$	100°C	hexagonal	77.4(77.0)	912	40	0.923
$C_{18}H_{35}EO_{10}$	RT	$P6_3/mmc$	49.1(47.7)	1004	27	0.587
$C_{12}EO_{23}$	RT	cubic	64.8(43.3)	503	16	0.241

Table 2 (continued)

Surfactant	Reaction Temperature	Mesophase	d(Å)[a]	BET surface area (m^2/g)	pore size[b] (Å)	pore volume (m^3/g)
Tween 20	RT	cubic	55.1(46.8)	795	19	0.370
Tween 40	RT	cubic	52.4(49.6)	704	20	0.363
Tween 60	RT	cubic	62.4(54.4)	720	24	0.516
Tween 60	RT	lamellar	28.7			
Tween 80	RT	cubic	62.2(53.9)	712	25	0.431
Span 40	RT	lamellar	55.5			
Triton X100	RT	cubic	41.8(35.5)	776	17	0.353
Triton X114	RT	cubic	42.2(36.7)	989	16	0.453
Teritor TMN 6	RT	cubic	44.3(39.9)	1160	23	0.568
Teritor TMN 10	RT	cubic	42.3(36.5)	804	20	0.379

a, *d*(100) spacing or d value of characteristic reflection of the as-synthesized products and the number inside brackets is the d value after calcination at 500°C for 6 h.

b, calculated from adsorption branch.

Table 3

System	Inorganic Precursor	Aging Temperature, °C	Aging time (day)	*d* (Å)
Zr	$ZrC1_4$	40	1	125
Ti	$TiC1_4$	40	7	123
Al	$AlC1_3$	40	2	130
Si	$SiC1_4$	40	2	171
Sn	$SnC1_4$	40	2	124
Nb	$NbC1_5$	40	2	106
Ta	$TaC1_5$	40	2	110
W	$WC1_6$	60	15	126
Hf	$HfC1_4$	40	1	124
Ge	$GeC1_4$	40	15	146
V	$VC1_4$	60	7	111
Zn	$ZnC1_2$	60	30	120
Cd	$CdC1_2$	40	7	111
In	$InC1_3$	60	30	124
Sb	$SbC1_5$	60	30	93
Mo	$MoC1_5$	60	7	100
Re	$ReC1_5$	60	7	121
Ru	$RuC1_3$	40	3	95
Ni	$NiC1_2$	40	2	100
Fe	$FeC1_3$	40	7	116
Cr	$CrC1_3$	40	4	117
Mn	$MnC1_2$	40	7	124
Cu	$CuC1_2$	40	7	98
SiAl	$AlC1_3/SiC1_4$	40	2	120
Si_2Al	$AlC1_3/SiC1_4$	40	2	120
ZrTi	$ZrC1_4/TiC1_4$	40	2	110
Al_2Ti	$AlC1_3/TiC1_4$	40	7	112
SiTi	$SiC1_4/TiC1_4$	40	3	103
ZrW_2	$ZrC1_4/WC1_6$	40	3	140
SnIn	$SnC1_4/InC1_3$	40	30	83

Table 4

Oxide	d_{100} (Å)	Wall Structure	Wall Thickness (Å)	Nanocrystal Size (Å)	Pore Size (Å)	BET Surface Area (m^2/g)	Porosity	Physical Properties
ZrO_2	106	Tetra. ZrO_2	65	15	58	150	0.43	dielectric
TiO_2	101	Anatase	51	24	65	205	0.46	semicond.
Nb_2O_5	75	Nb_2O_5	40	<10	45	196	0.50	dielectric
Ta_2O_5	68	Ta_2O_5	40	<10	35	165	0.50	dielectric
WO_3	95	WO_3	50	30	50	125	0.48	semicond.
SnO_2	106	Cassiterite	50	30	68	180	0.52	semicond.
HfO_2	105	amorphous	50	--	70	105	0.52	dielectric
Al_2O_3	186	amorphous	35	--	140	300	0.61	dielectric
SiO_2	198	amorphous	86	--	120	810	0.63	dielectric
$SiAlO_{3.5}$	95	amorphous	38	--	60	310	0.59	dielectric
$Si_2AlO_{5.5}$	124	amorphous	40	--	100	330	0.55	dielectric
Al_2TiO_5	105	amorphous	40	--	80	270	0.59	dielectric
$ZrTiO_4$	103	amorphous	35	--	80	130	0.46	dielectric
$SiTiO_4$	95	amorphous	45	--	80	495	0.63	dielectric
ZrW_2O_8	100	amorphous	45	--	50	170	0.51	NTE

THE CLAIMS

1. A method of forming a mesoscopically structured inorganic material, comprising:

combining an amphiphilic block polymer with an inorganic compound of a multivalent metal species under conditions whereby the block copolymer and inorganic compounds are self-assembled and polymerized into a mesoscopically structured composite; and

polymerizing the mesoscopically structured composite to form said mesoscopically structured inorganic material.

2. The method of claim 1 in which said block copolymer and inorganic compounds are combined in an aqueous or polar solvent and including the step, after polymerizing the mesoscopically structured composite, of evaporating said solvent to form a transparent mesostructured material with a uniform characteristic ordering length scale..

3. The method of claim 2 in which said transparent material is crack-free.

4. The method of claim 2 in which said transparent material has a large *d* spacing and thick inorganic walls

5. The method of claim 2 in which said transparent material is in the form of fibers.

6. The method of claim 2 in which said transparent material has a two dimensional hexagonal mesostructure.

7. The method of claim 2 in which said transparent material has a cubic mesostructure.

8. The method of claim 2 in which said transparent material has a lamellar mesostructure.

9. The method of claim 2 in which said wall thickness is at least 30 Å.

10. The method of claim 2 in which said mesoporous structure has a structural ordering length scale of at least 50 Å.

11. The method of claim 2 including the step of adding an organic cosolvent to said amphiphilic block polymer to increase the pore size and wall thickness of said mesoscopically structured inorganic material.

12. The method of claim 2 including the step of thermally treating said combination of amphiphilic block polymer and inorganic compound to increase the pore size and wall thickness, and thermal stability.

13. The method of claim 1 including the step, after polymerizing the mesoscopically structured composite, of removing said polymer to form a thermally stable mesoporous material.

14. The method of claim 1 including the step, after polymerizing the mesoscopically structured composite, of calcining or solvent extracting said mesoscopically structured inorganic oxide-block copolymer composite material to remove the organic species and thereby form a mesoporous multivalent metal oxide material with a high surface area.

15. The method of claim 14 in which said mesoporous structure has a porosity of at least 40%.

16. The method of claim 14 in which said pore size is at least 30 Å.

17. The method of claim 14 in which said *d* spacing is at least 60 Å.

18. The method of claim 14 in which said wall thickness is at least 30 Å.

19. The method of claim 14 in which said surface area is at least $100m^2/g$..

20. The method of claim 14 in which said mesoporous material is in the form of fibers.

21. The method of claim 14 in which said mesoporous material has a two dimensional hexagonal mesostructure.

22. The method of claim 14 in which said mesoporous material has a cubic mesostructure.

23. The method of claim 14 in which said mesoporous metal oxide material has a dielectric constant of 2 - 2.5.

24. The method of claim 1 in which, prior to combination with said inorganic compound, said block polymer is placed in an aqueous solution of inorganic salt and said inorganic compound is added to said block polymer

solution in the form of a sol gel to form said inorganic material as a meso-macro structure.

25. The method of claim 24 including the steps of polymerizing the meso-macro structured composite and calcining the polymerized composite to form a multivalent metal oxide material with macroporosity and a mesoporous surface area.

26. The method of claim 1 in which said block copolymer is a triblock polymer.

27. The method of claim 26 in which said triblock copolymer is a poly(ethylene oxide)-poly(alkylene oxide)- poly(ethylene oxide) polymer where the alkylene oxide moiety has at least three carbon atoms.

28. The method of claim 26 in which said triblock copolymer is a poly(ethylene oxide)-poly(propylene oxide)- poly(ethylene oxide) polymer.

29. The method of claim 26 in which said triblock copolymer is a poly(ethylene oxide)-poly(butylene oxide)- poly(ethylene oxide) polymer.

30. The method of claim 1 in which said block copolymer is a diblock polymer.

31. The method of claim 1 in which said block copolymer is a reversed triblock polymer.

32. The method of claim 1 in which said block copolymer is a star di-block polymer.

33. The method of claim 1 in which said block polymer is a reversed star di-block polymer.

34. The method of claim 1 wherein said inorganic compound, upon calcination, forms an oxide selected from TiO_2, ZrO_2, Nb_2O_5, Ta_2O_5, Al_2O_3, SiO_2, WO_3, SnO_2, HfO_2, $SiAlO_{3.5}$, $SiAlO_{5.5}$, Al_2TiO_5, $ZrTiO_4$, and $SiTiO_4$.

35. The method of claim 1 wherein said inorganic compound, upon calcination, forms SiO_2.

36. A mesoscopically structured composite of an amphiphilic block copolymer and a compound of a multivalent metal species.

37. A thermally stable mesoscopically ordered porous material comprised of a multivalent metal compound and having a narrow distribution of pore sizes in the mesoscopic size regime.

38. The mesostructured material of claim 37 having a high surface area, large *d* spacings and thick walls.

39. The mesostructured material of claim 36 in which said material is transparent..

40. The mesostructured material of claim 39 in the form of fibers.

41. The mesostructured material of claim 39 in the form of thin films.

42. The mesostructured material of claim 39 in the form of monoliths.

43. The mesostructured material of claim 36 comprising a two dimensional hexagonal mesostructure.

44. The mesostructured material of claim 36 comprising a cubic mesostructure.

45. The mesostructured material of claim 36 comprising a lamellar mesostructure.

46. The mesostructured material of claim 37 comprising a two dimensional hexagonal mesostructure.

47. The mesostructured material of claim 37 comprising a cubic mesostructure.

48. The mesostructured material of claim 37 comprising a lamellar mesostructure.

49. The mesostructured material of claim 37 in the form of fibers.

50. The mesostructured material of claim 37 in the form of thin films.

51. The mesostructured material of claim 37 in the form of monoliths.

52. The method of claim 14 in which said transparent material is in the form of a mesoscopically ordered, mesoporous, crack-free thin film.

53. The mesostructured material of claim 37 having a porosity of at least 40%.

54. The mesostructured material of claim 37 in which said pore size is at least 30 Å.

55. The mesostructured material of claim 37 having *d* spacings of at least 60 Å.

56. The mesostructured material of claim 37 having wall thicknesses of at least 30 Å.

57. The mesostructured material of claim 37 having a structural ordering length scale of at least 50 Å.

58. A mesoporous multivalent metal oxide material having a meso range pore size and a surface area of at least $100 m^2/g$.

59. The mesoporous metal oxide material of claim 58 having a dielectric constant of 2 - 2.5.

60. A macroporous multivalent metal oxide material having an ordered mesoporous surface area.

61. The mesostructured material of claim 37 wherein said multivalent metal compound is an oxide selected f rom TiO_2, ZrO_2, Nb_2O_5, Ta_2O_5, Al_2O_3, SiO_2, WO_3, SnO_2, HfO_2, $SiAlO_{3.5}$, $SiAlO_{5.5}$, Al_2TiO_5, $ZrTiO_4$, and $SiTiO_4$.

62. The mesostructured material of claim 37 wherein said multivalent metal compound is SiO_2.

63. A method of separating biomolecules from a biological specimen or synthesis mixture, comprising passing said biological specimen or mixture through a mesoporous multivalent metal oxide material.

64. The method of claim 63 in which said biomolecules comprise enzymes and/or proteins.

65. A method of separating biomolecules from a biological specimen or synthesis mixture, comprising passing said biological specimen or mixture through a macroporous multivalent metal oxide material having a mesoporous surface.

66. The method of claim 65 in which said biomolecules comprise enzymes and/or proteins.

67. A method of separating organics from a solution, comprising passing said solution through a mesoporous multivalent metal oxide material.

68. A method of separating organics from a solution, comprising passing said solution through a macroporous multivalent metal oxide material having a mesoporous surface.

69. A method of separating inorganics from a solution, comprising passing said solution through a mesoporous multivalent metal oxide material.

70. A method of separating inorganics from a solution, comprising passing said solution through a macroporous multivalent metal oxide material having a mesoporous surface.

71. A method of imparting adsorption and catalytic reaction selectivities to a macroporous multivalent metal oxide material having an ordered mesoporous surface area, comprising functionalizing separately the different mesoscopic and macroscopic pore surfaces of said material of to provide said selectivities.

FIG. 1a

SUB-NANOPOROUS ZEOLITES : < 1nm

FAUJASITE

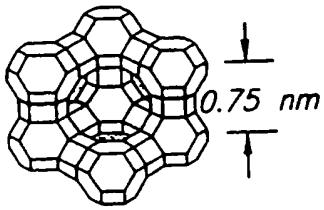

FIG. 1b

FIG. 1c

MESOPOROUS MOLECULAR SIEVES: 2- 10 nm

MCM-41

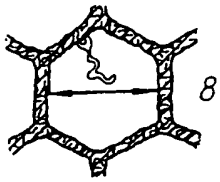

ULTRA LARGE PORE MATERIALS 5 - 50 nm

SBA-15

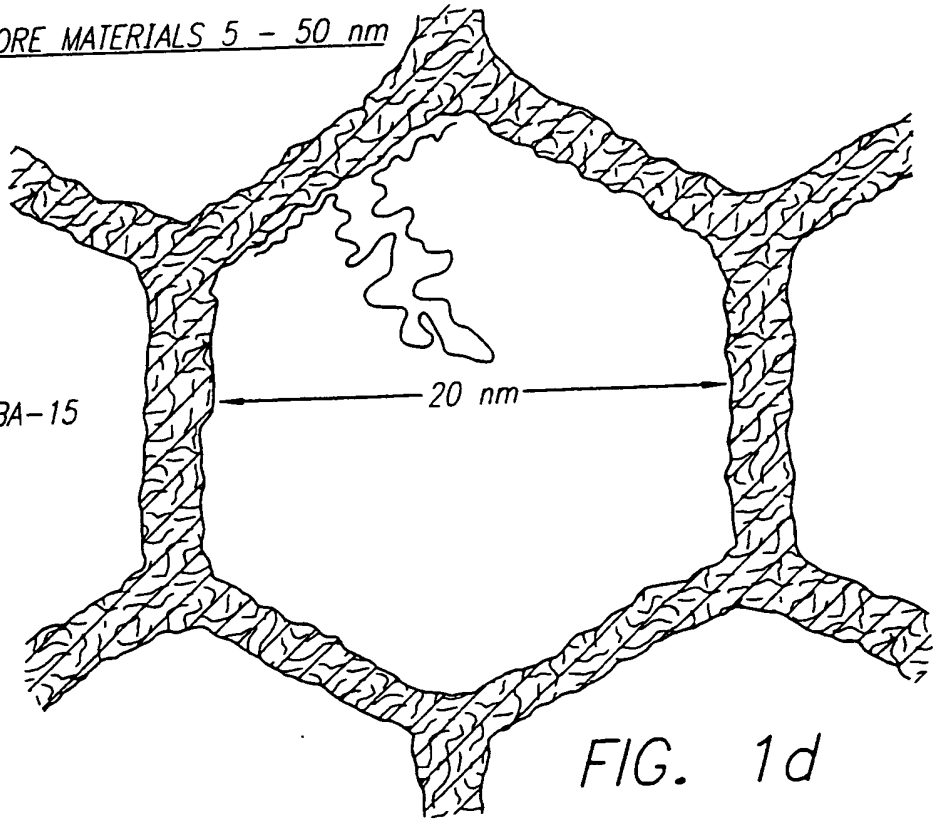

FIG. 1d

FIG. 2a

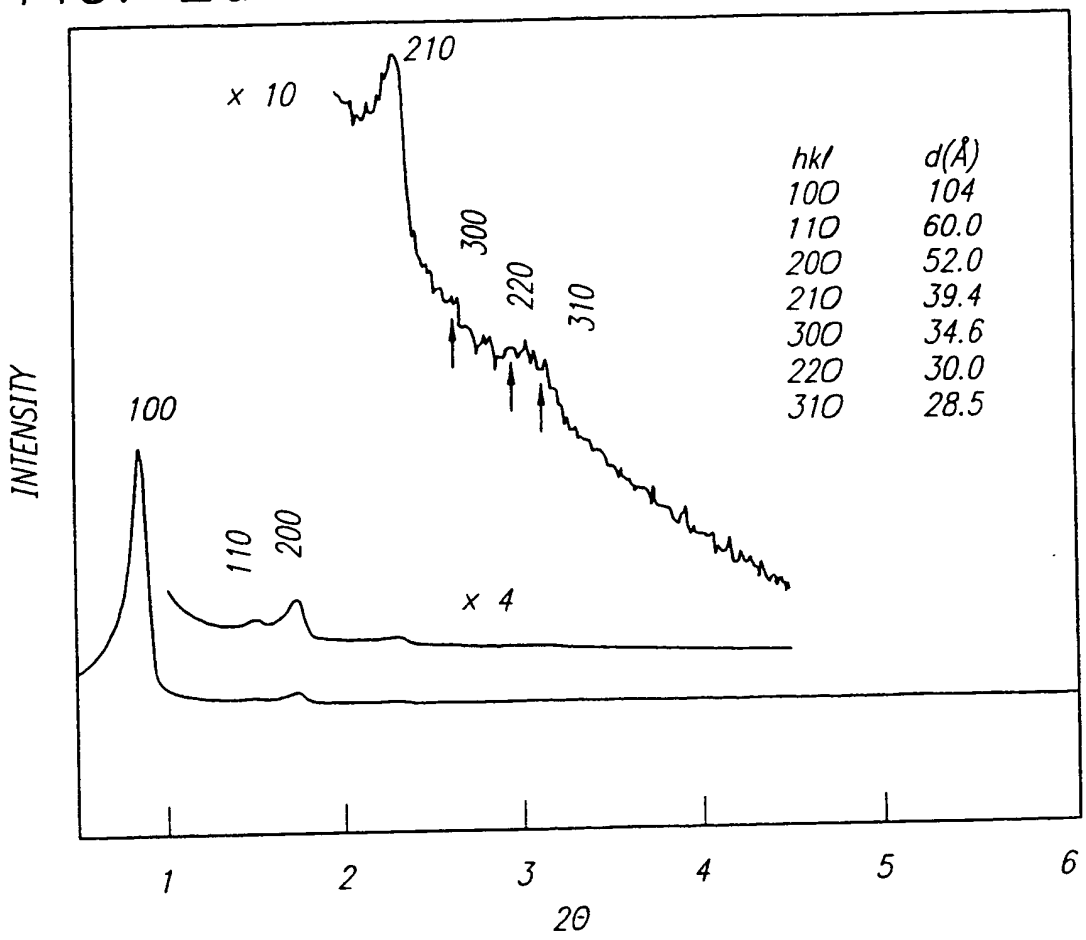
210
x 10
300
220
310
hkl d(Å)
100 104
110 60.0
200 52.0
210 39.4
300 34.6
220 30.0
310 28.5
100
110
200
x 4
INTENSITY
1
2
3
4
5
6
2θ

FIG. 2b

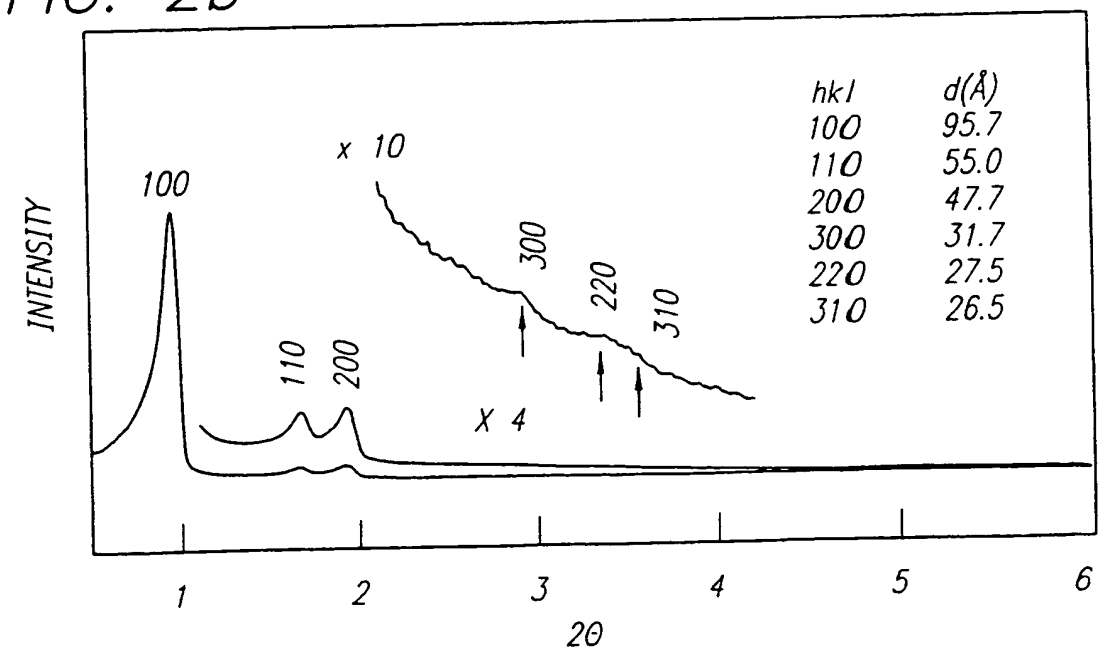
x 10
100
300
220
310
hkl d(Å)
100 95.7
110 55.0
200 47.7
300 31.7
220 27.5
310 26.5
110
200
X 4
INTENSITY
1
2
3
4
5
6
2θ

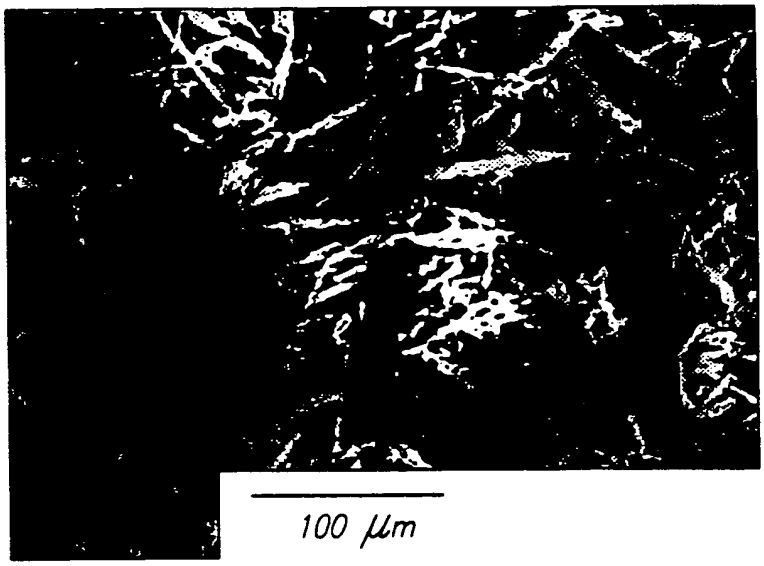

FIG. 3a

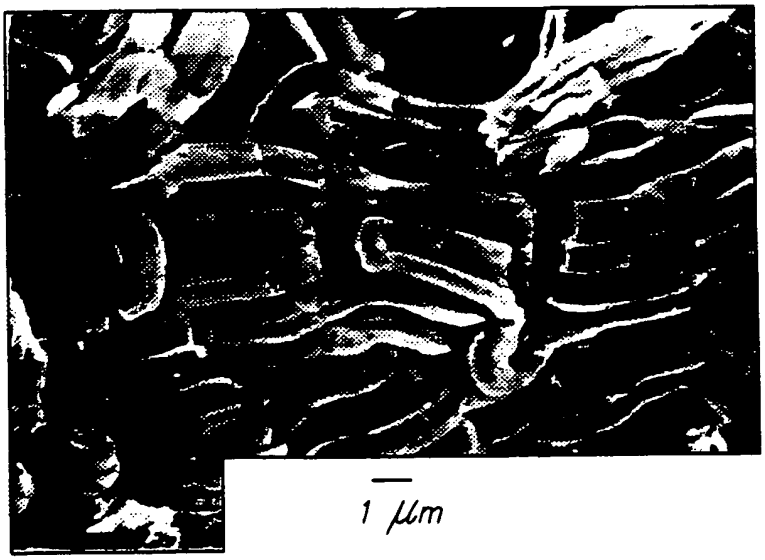

FIG. 3b

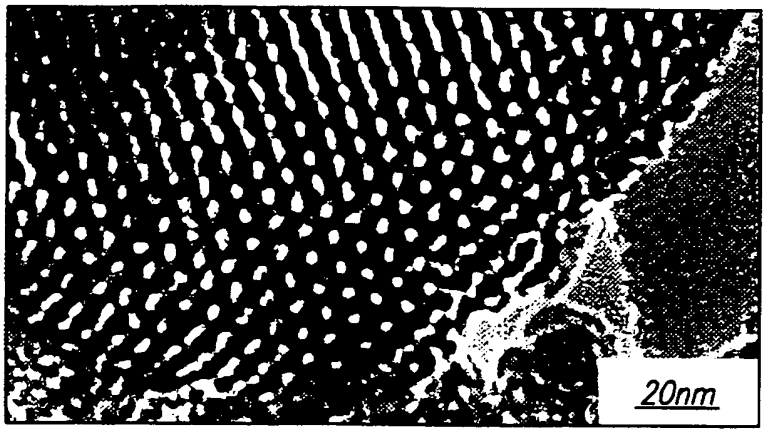

FIG. 3c

FIG. 3d

FIG. 4a

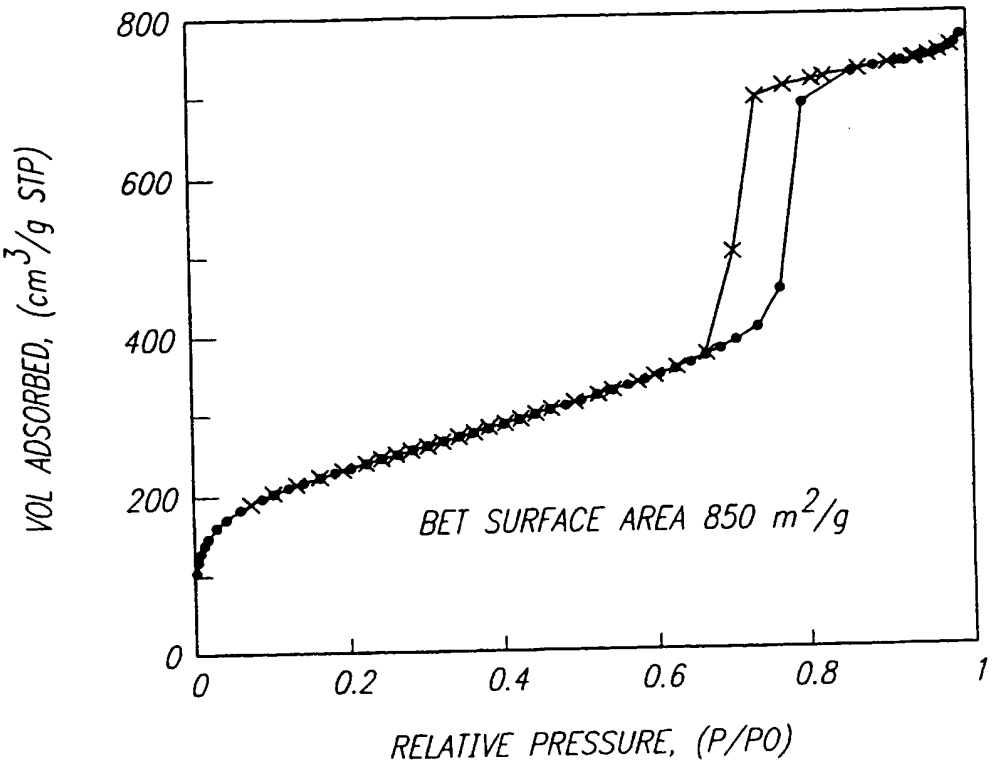
800
600
400
200
0
VOL ADSORBED, (cm3/g STP)
BET SURFACE AREA 850 m2/g
0
0.2
0.4
0.6
0.8
1
RELATIVE PRESSURE, (P/PO)

FIG. 4b

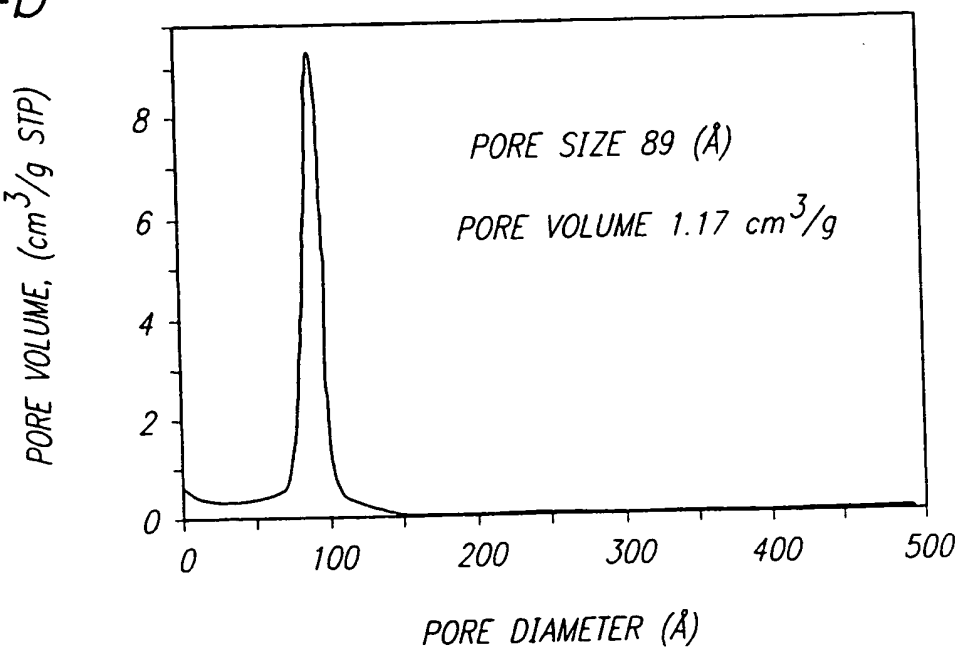
8
6
4
2
0
PORE VOLUME, (cm3/g STP)
PORE SIZE 89 (Å)
PORE VOLUME 1.17 cm3/g
0
100
200
300
400
500
PORE DIAMETER (Å)

FIG. 4c

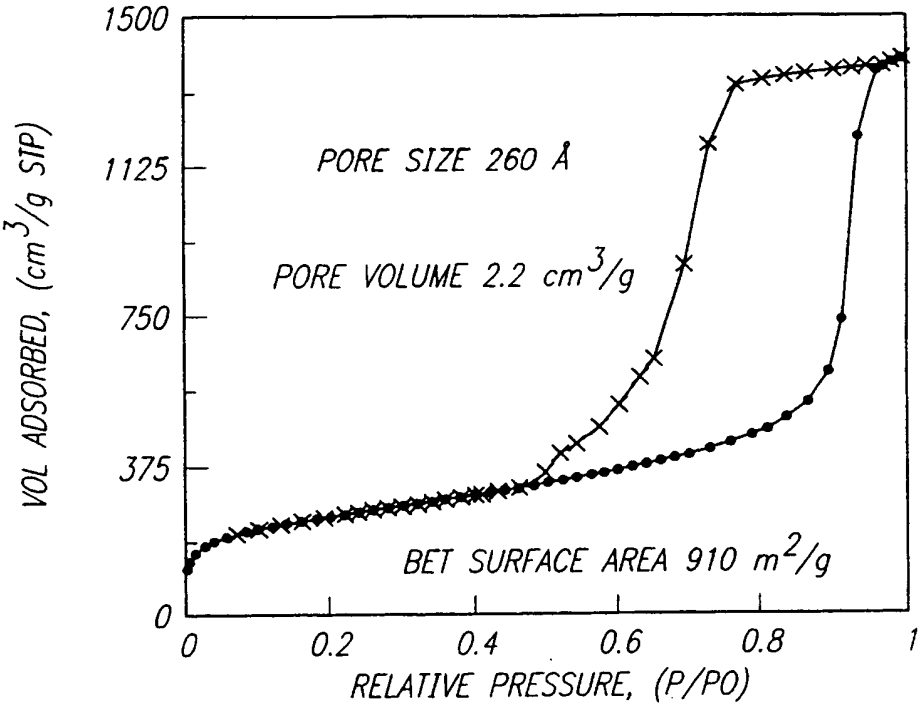

FIG. 4d

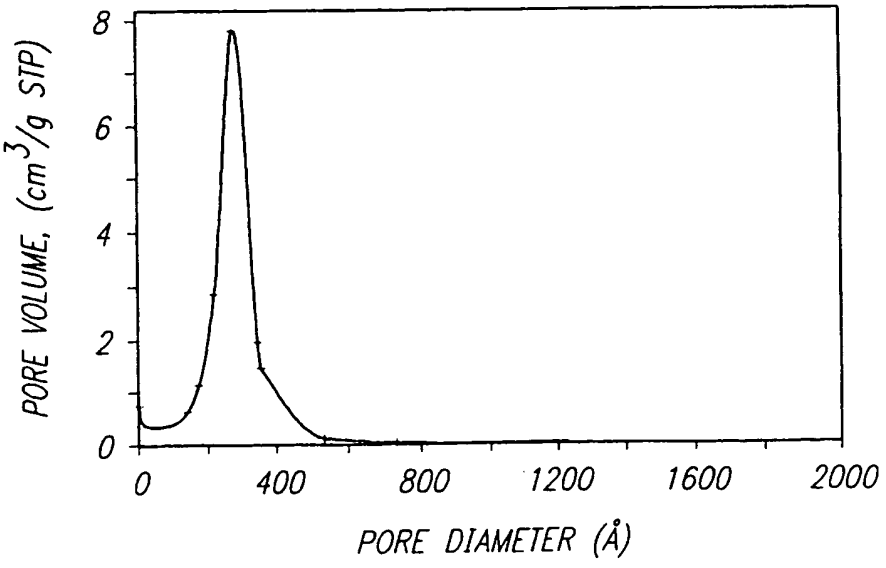

FIG. 5a

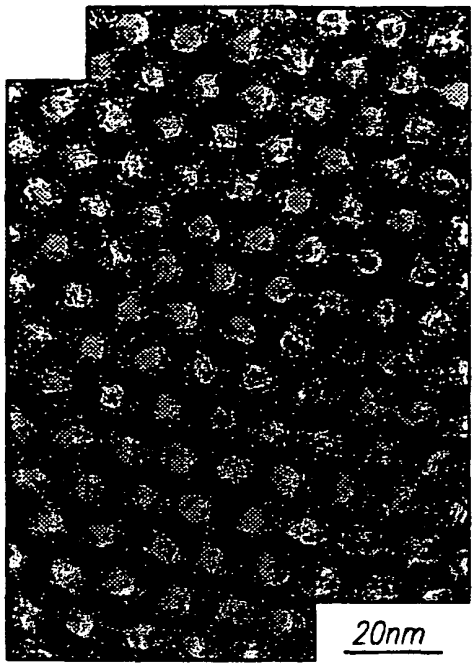

FIG. 5b

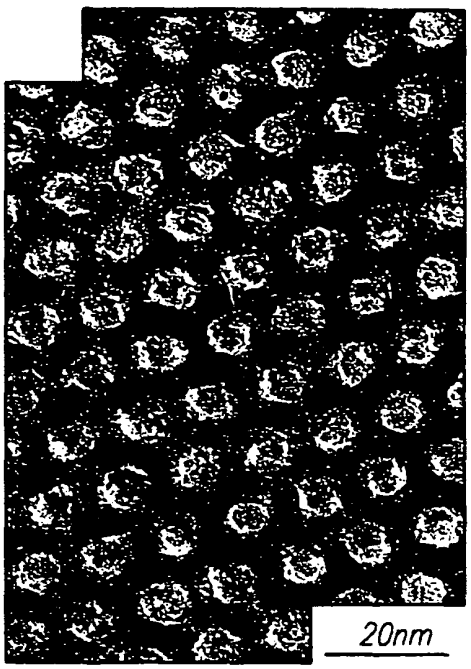

FIG. 5c

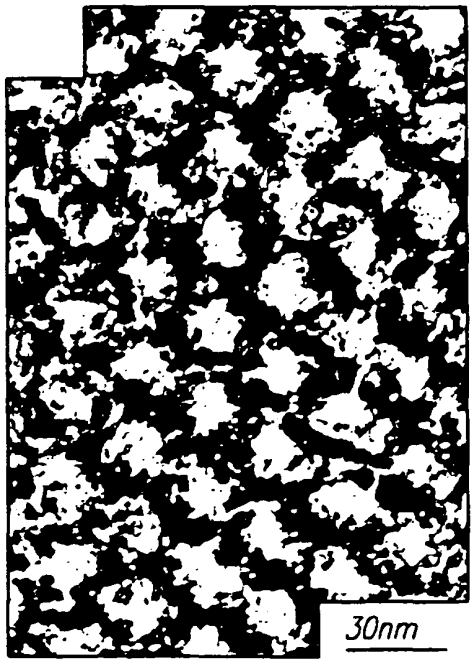

FIG. 5d

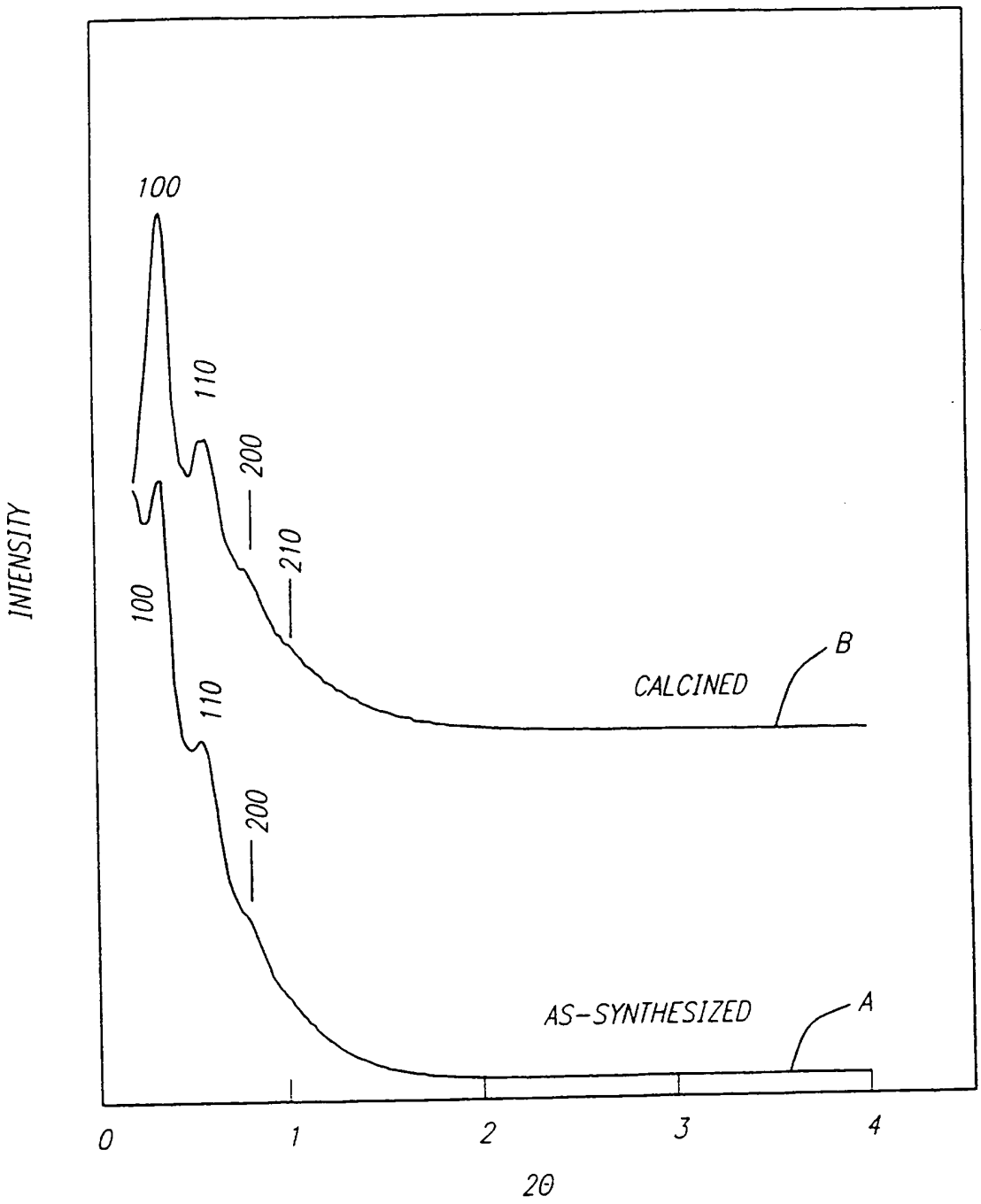

FIG. 6

FIG. 7

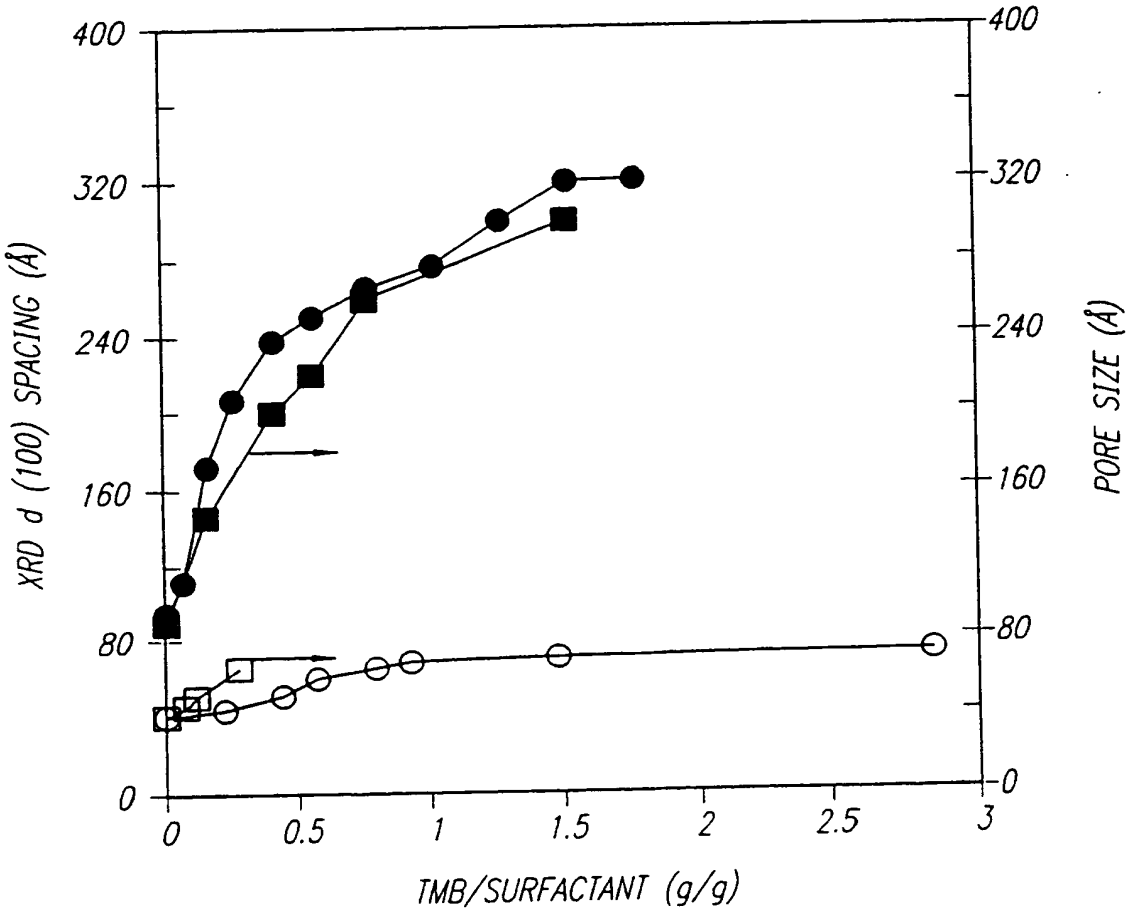

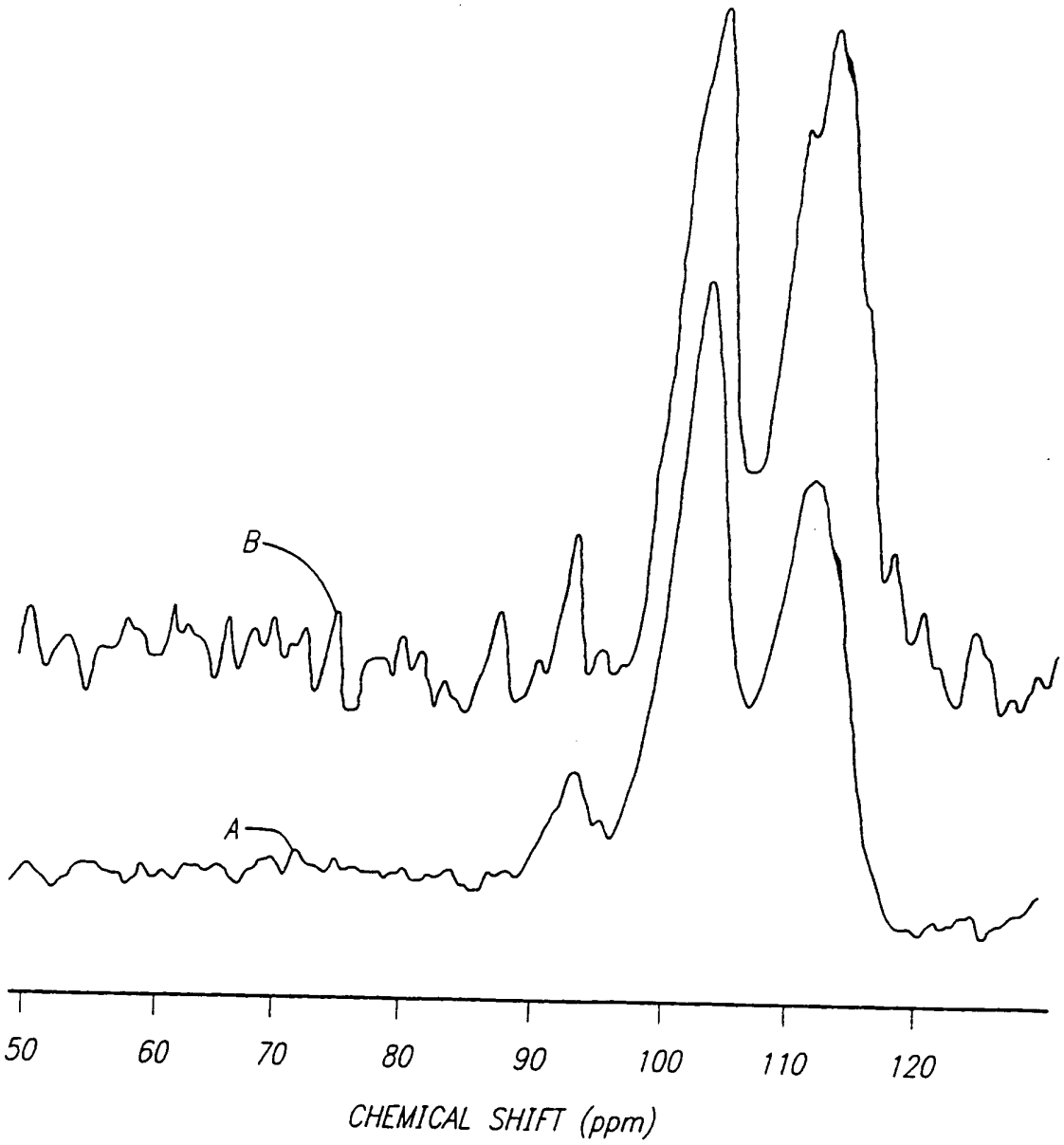

FIG. 8

FIG. 9

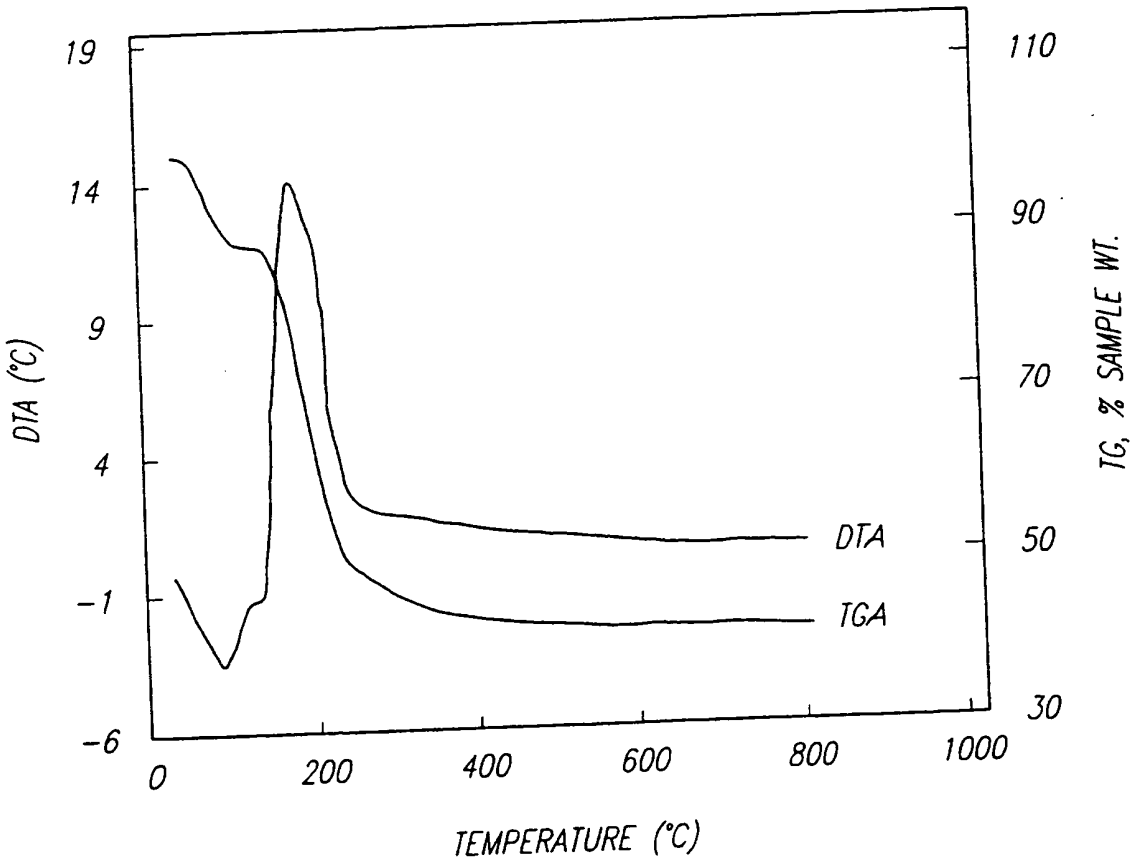

FIG. 10b

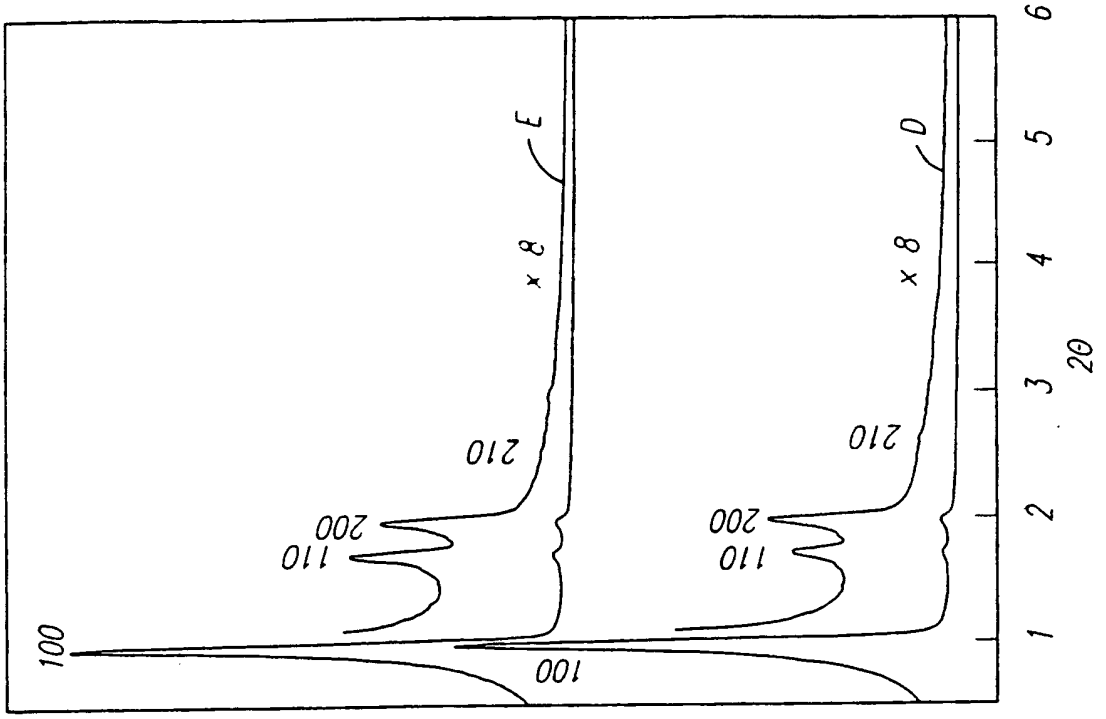

FIG. 10a

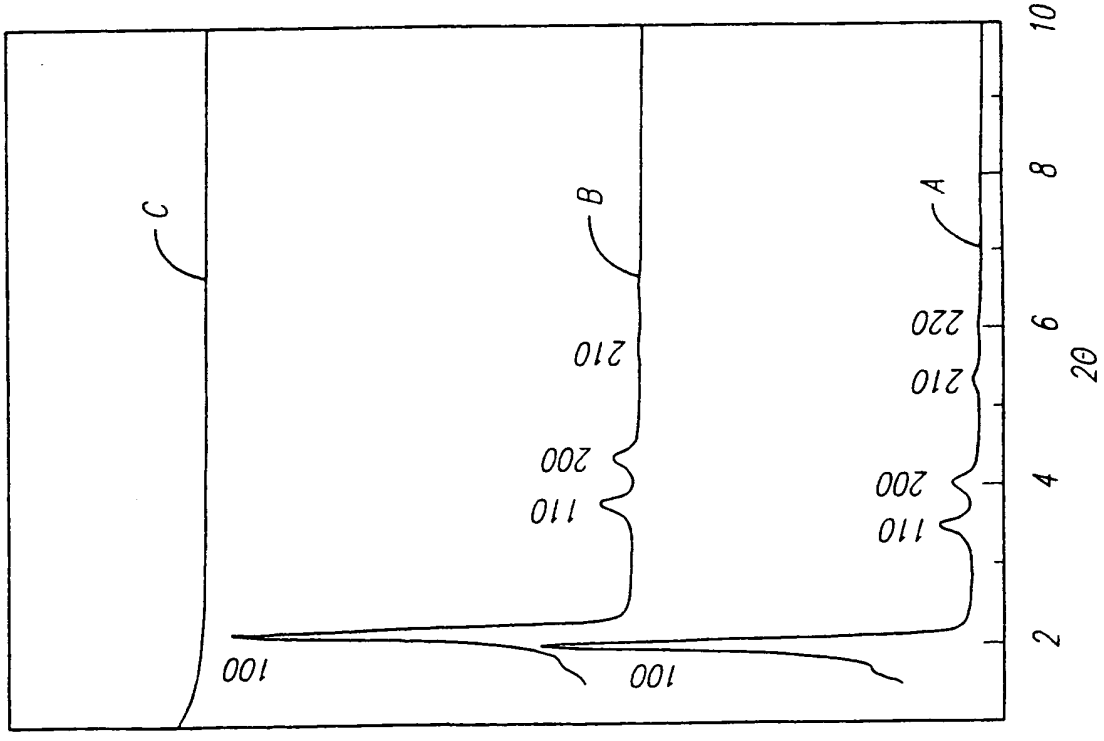

FIG. 11a

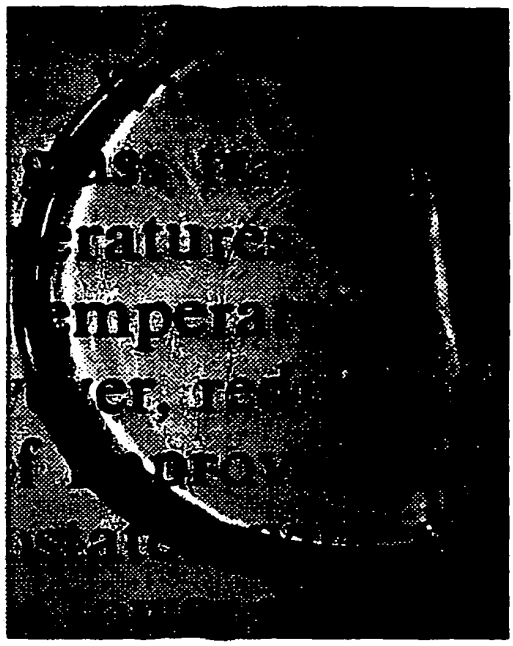

FIG. 11b

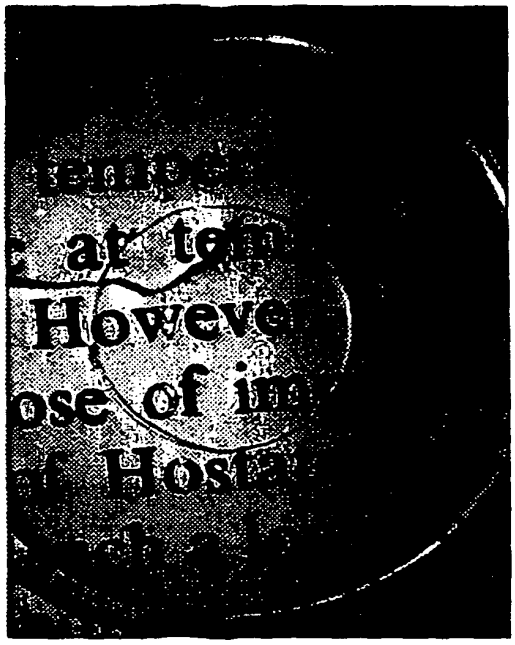

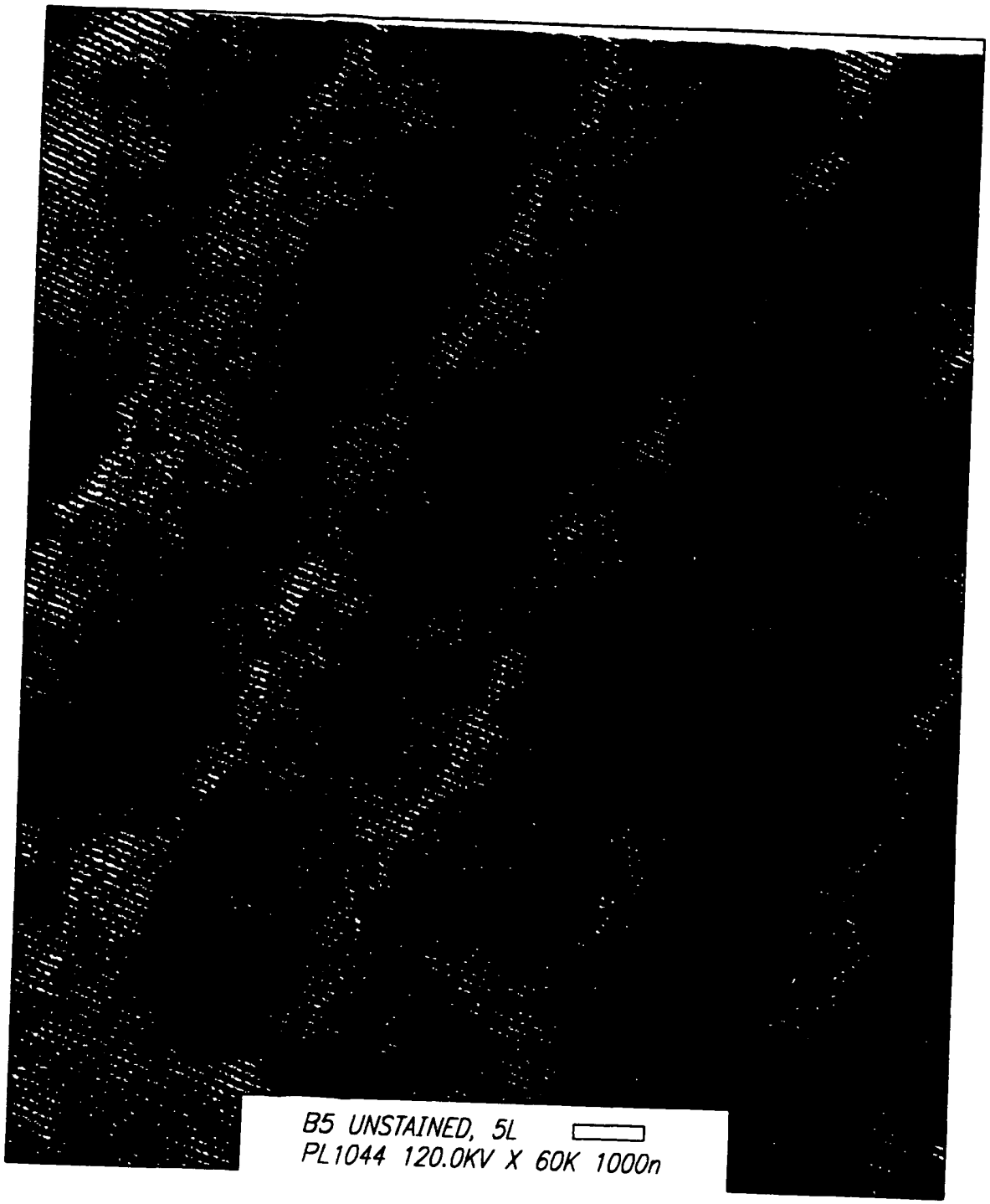

FIG. 12

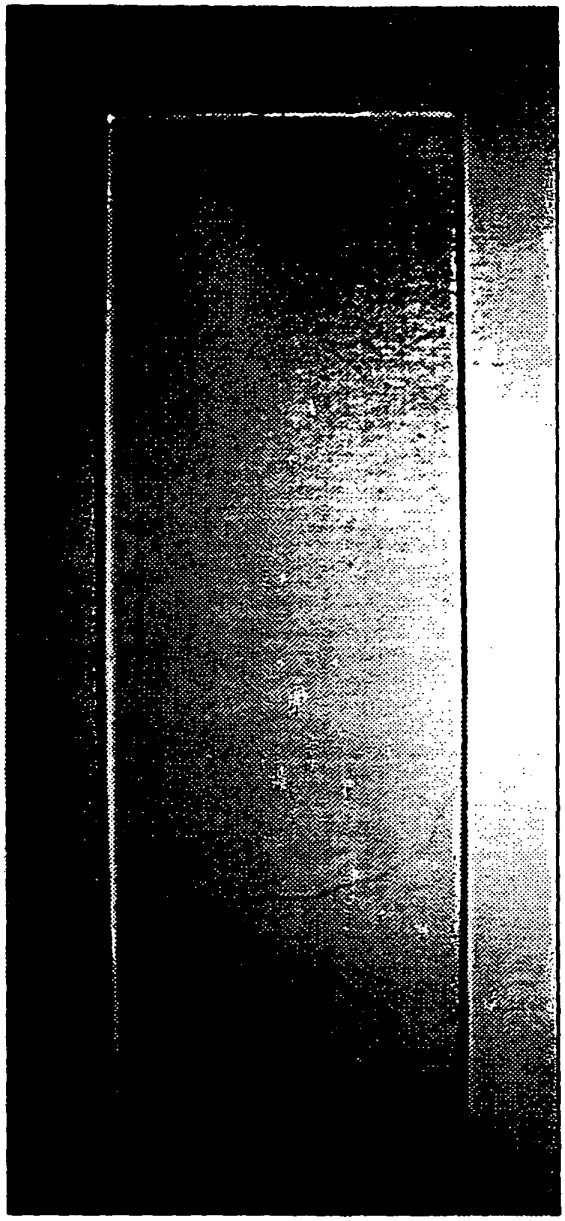

FIG. 13a

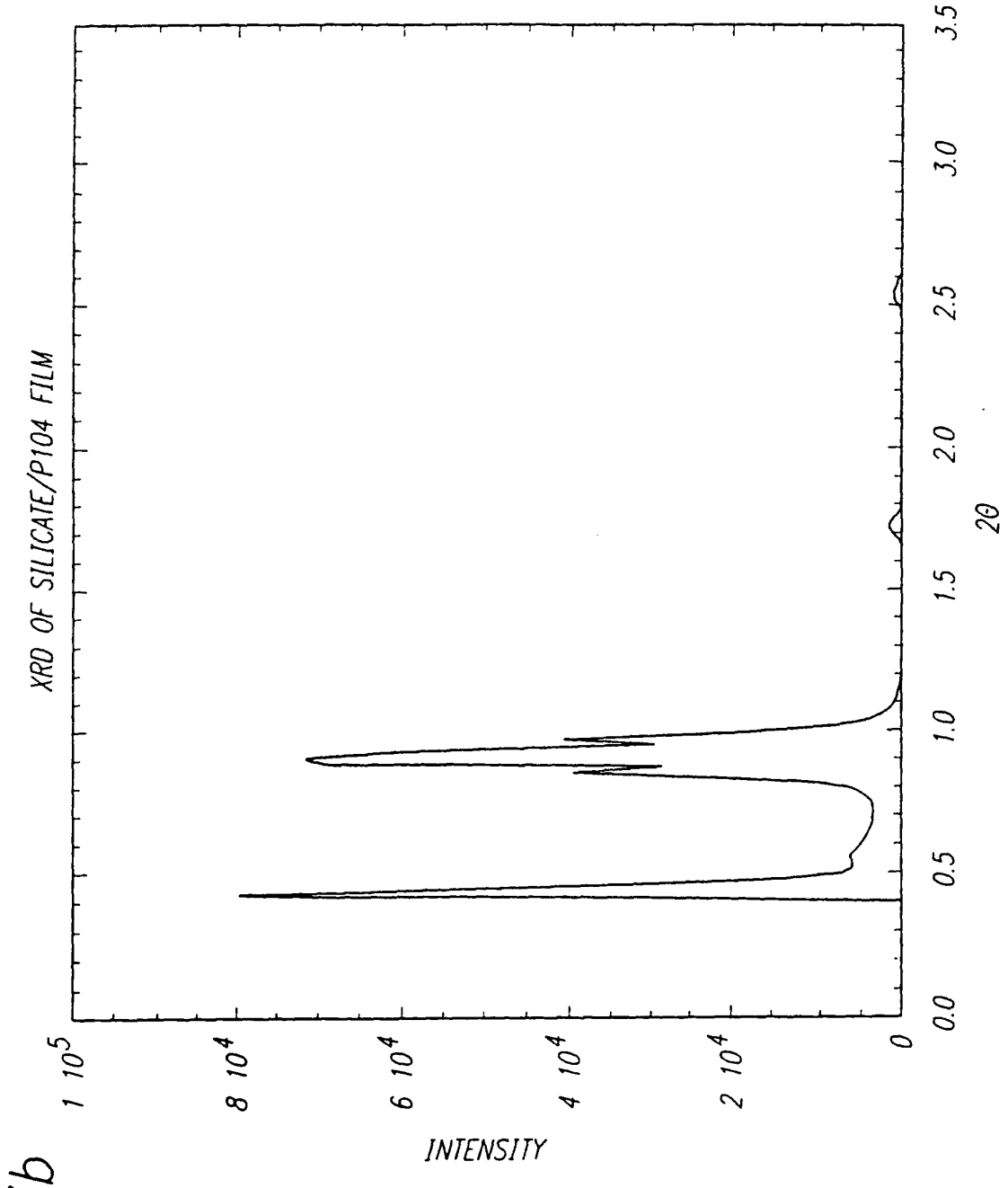

FIG. 13b

FIG. 14

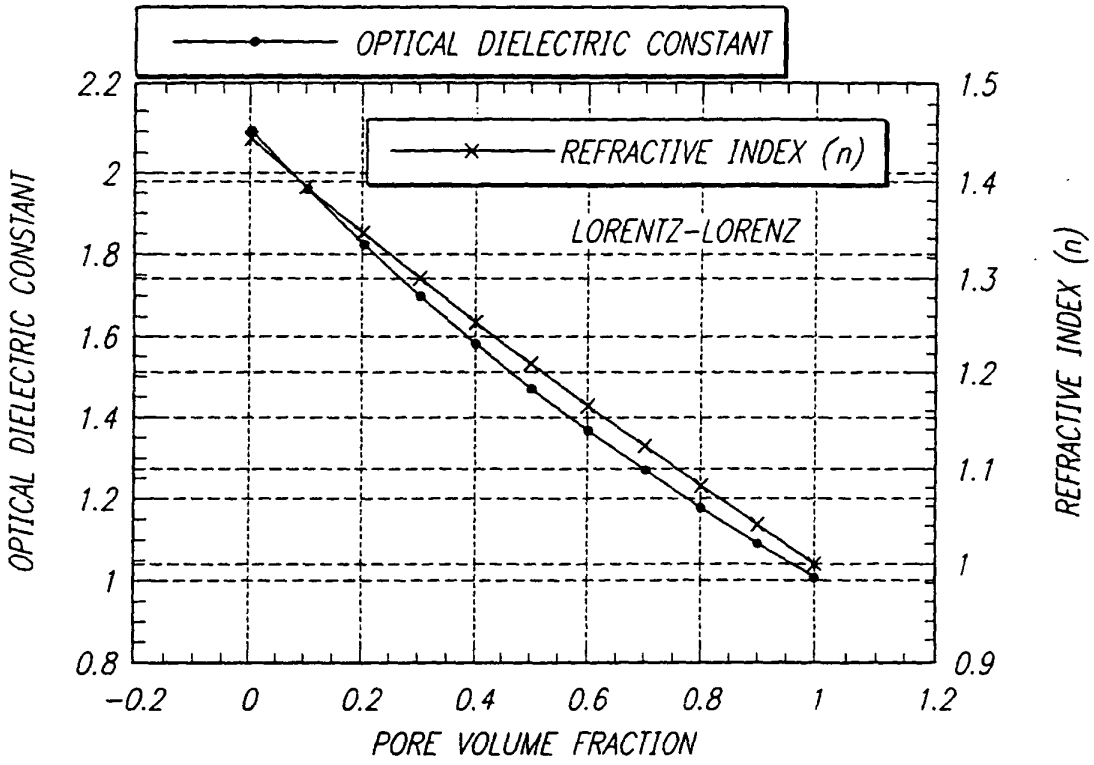

FIG. 15

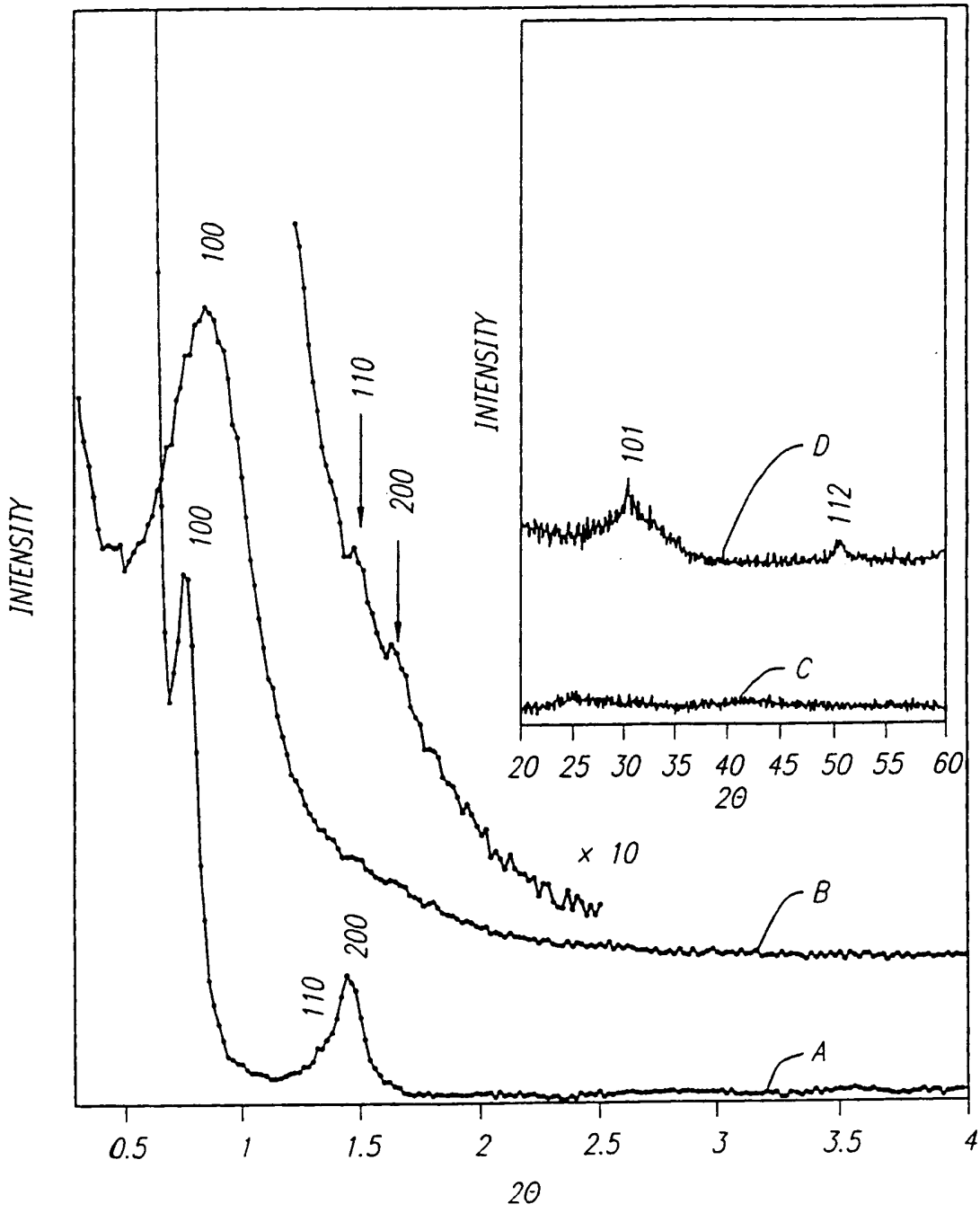

FIG. 16a

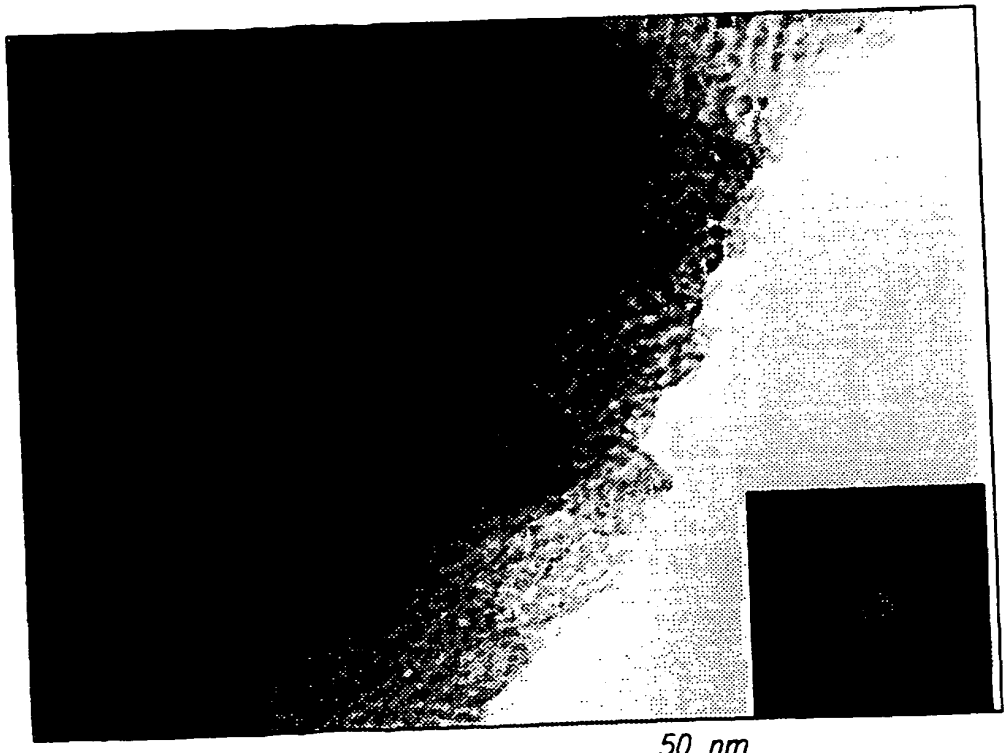

FIG. 16b

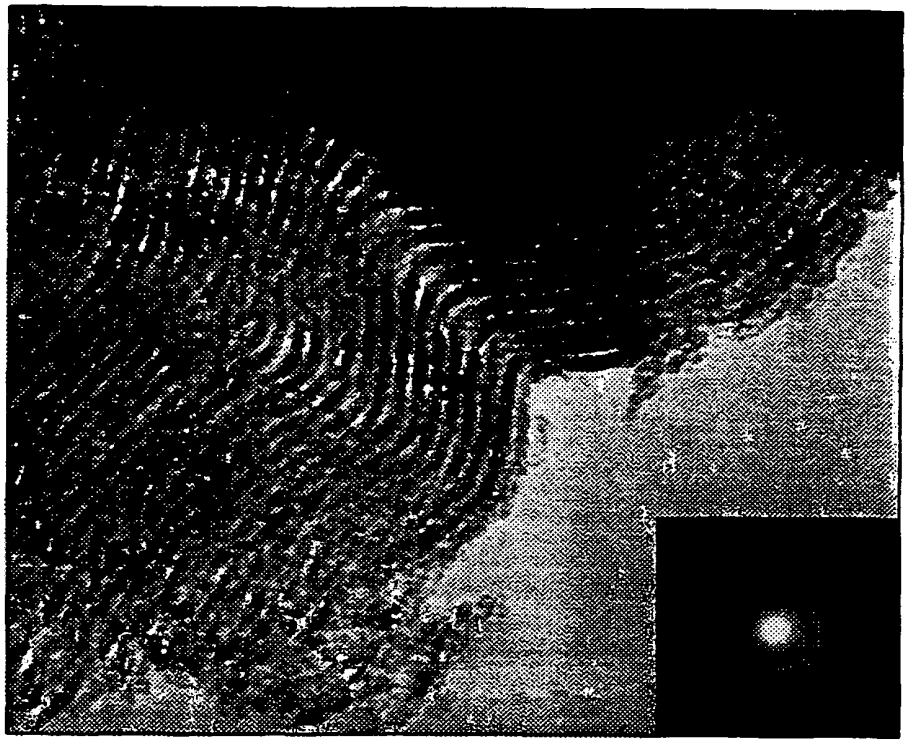

FIG. 17a

20 nm

FIG. 17b

20 nm

FIG. 18a

100 nm

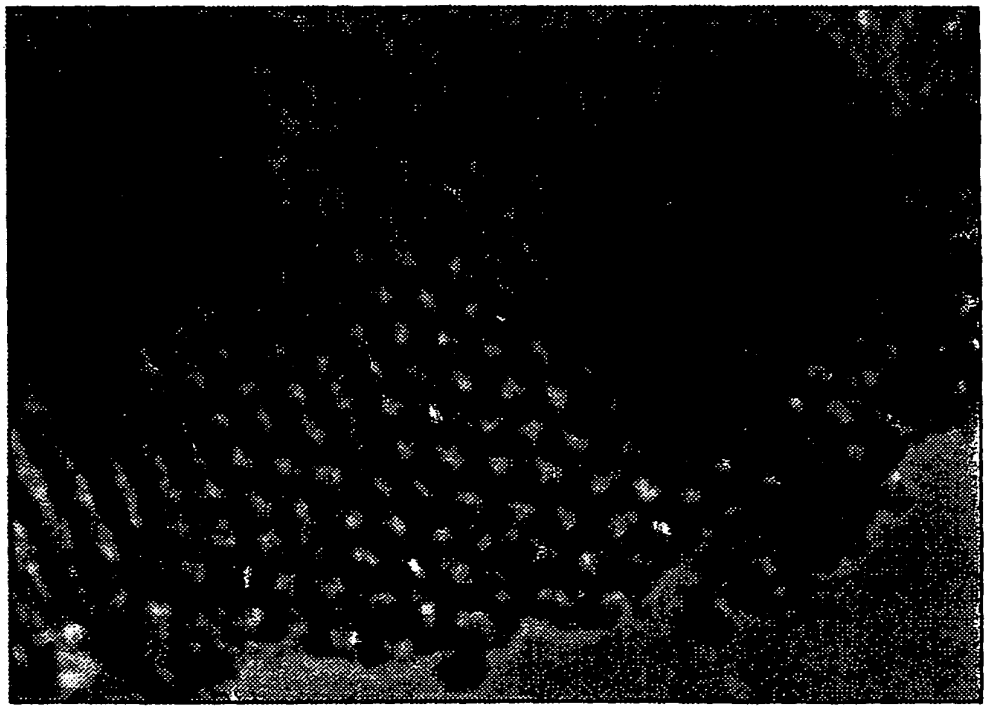

FIG. 18b

20 nm

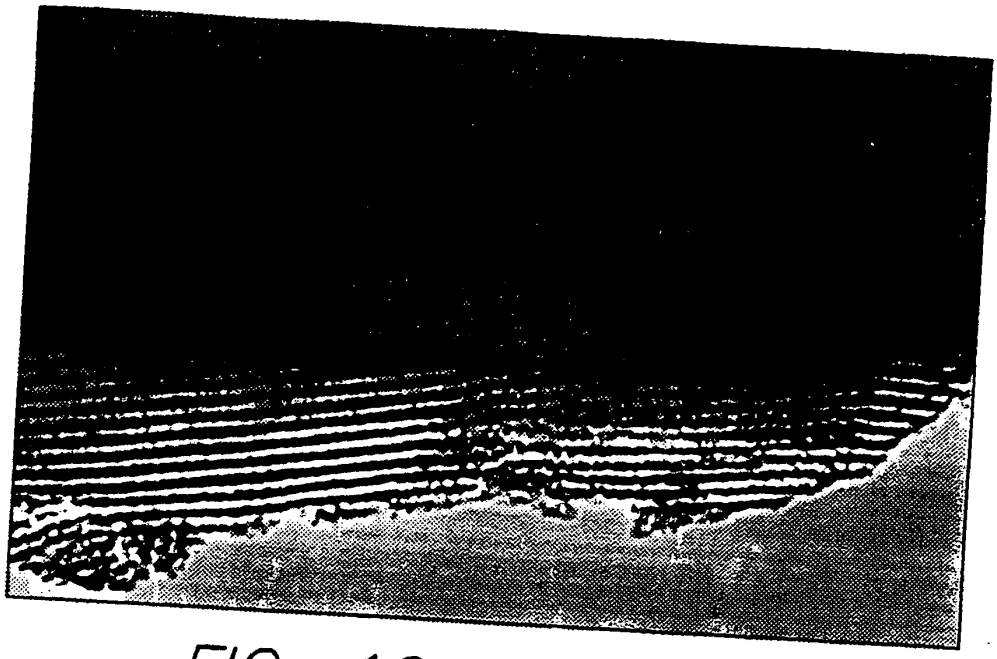

FIG. 19a

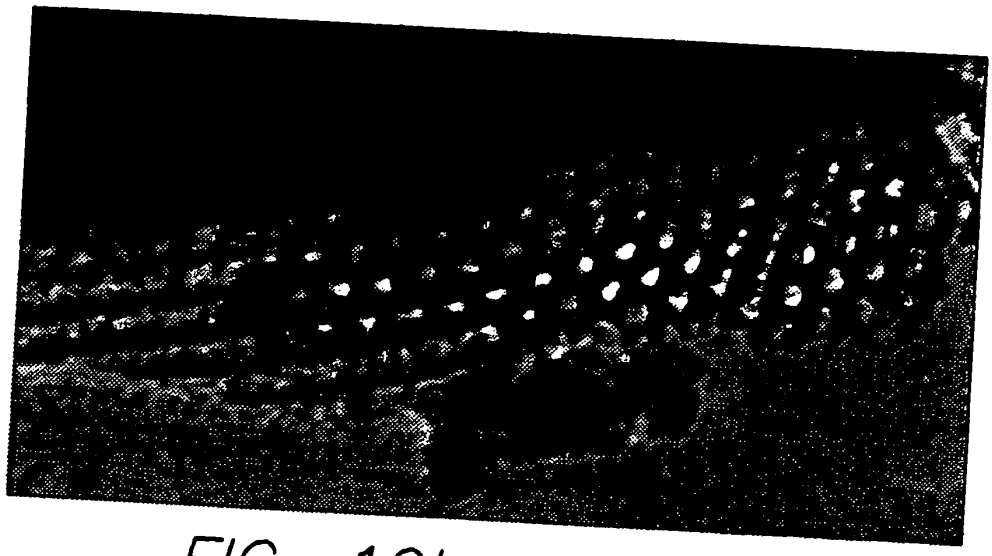

FIG. 19b

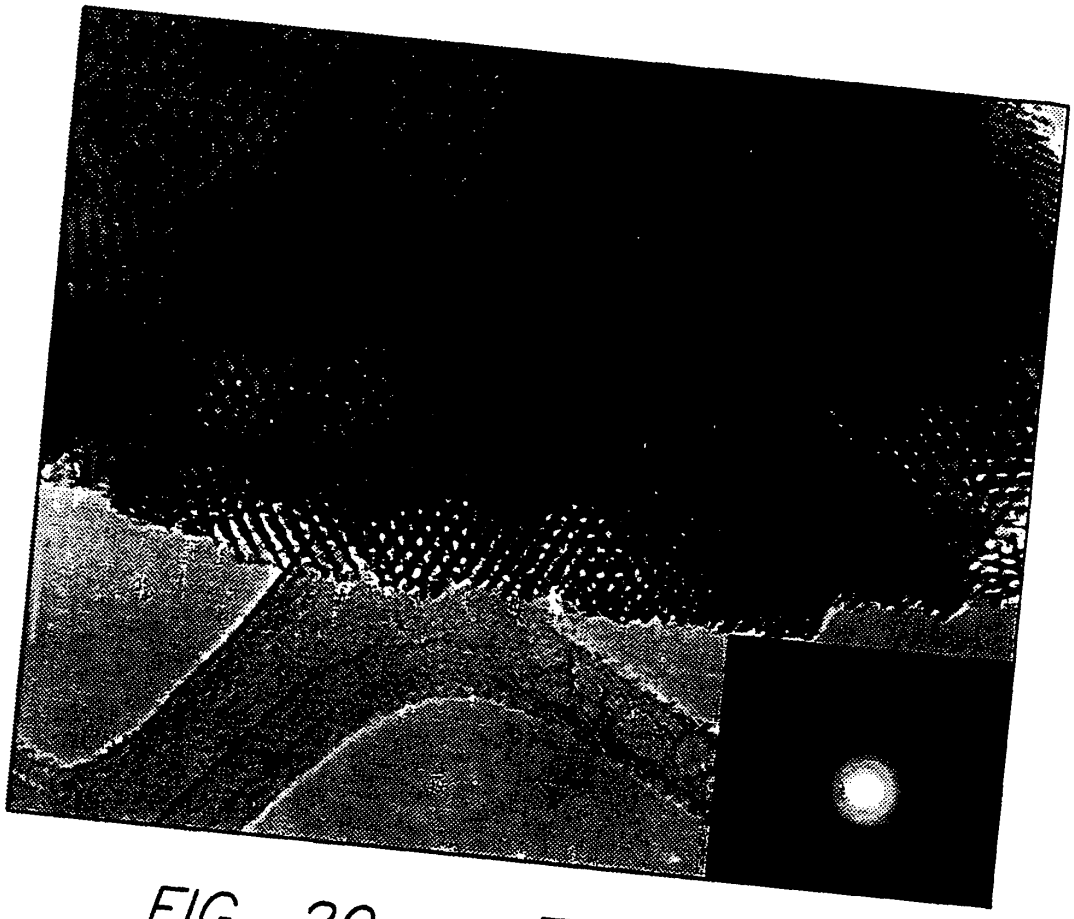

FIG. 20

20 nm

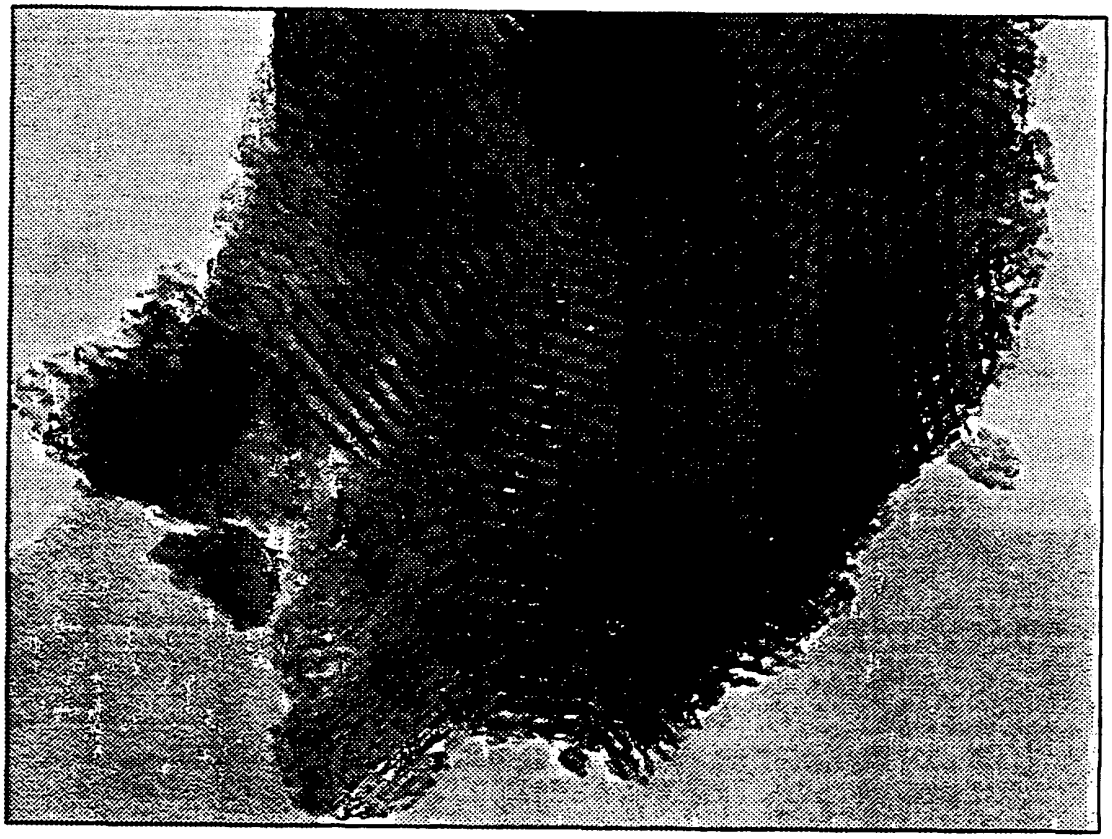

FIG. 21

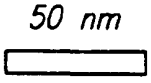

FIG. 22a

100 nm

FIG. 22b

50 nm

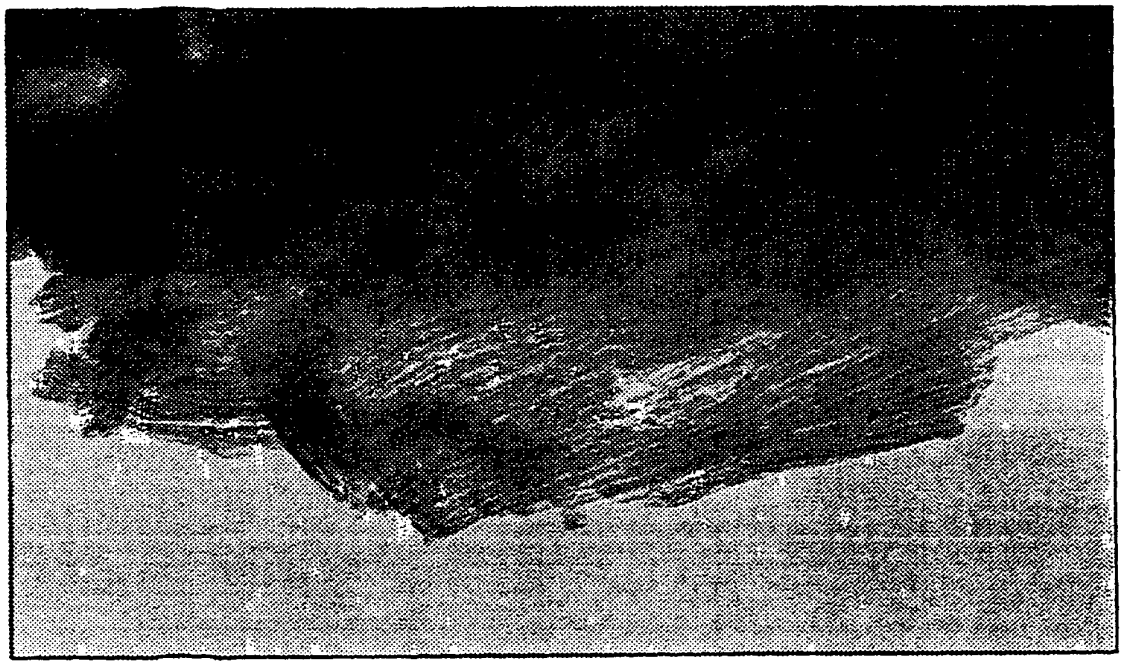

FIG. 23

50 nm

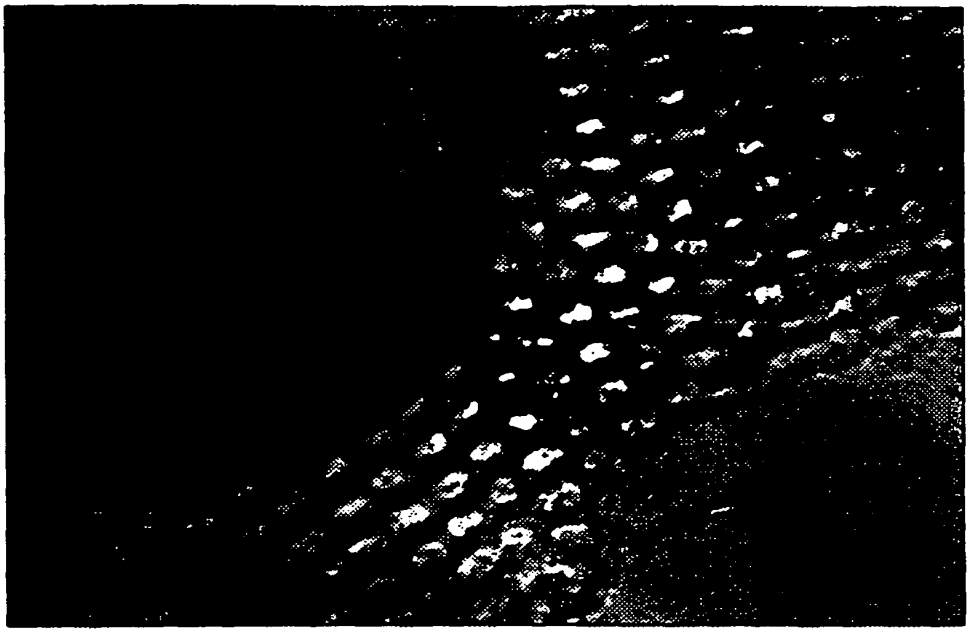

FIG. 24a

20 nm

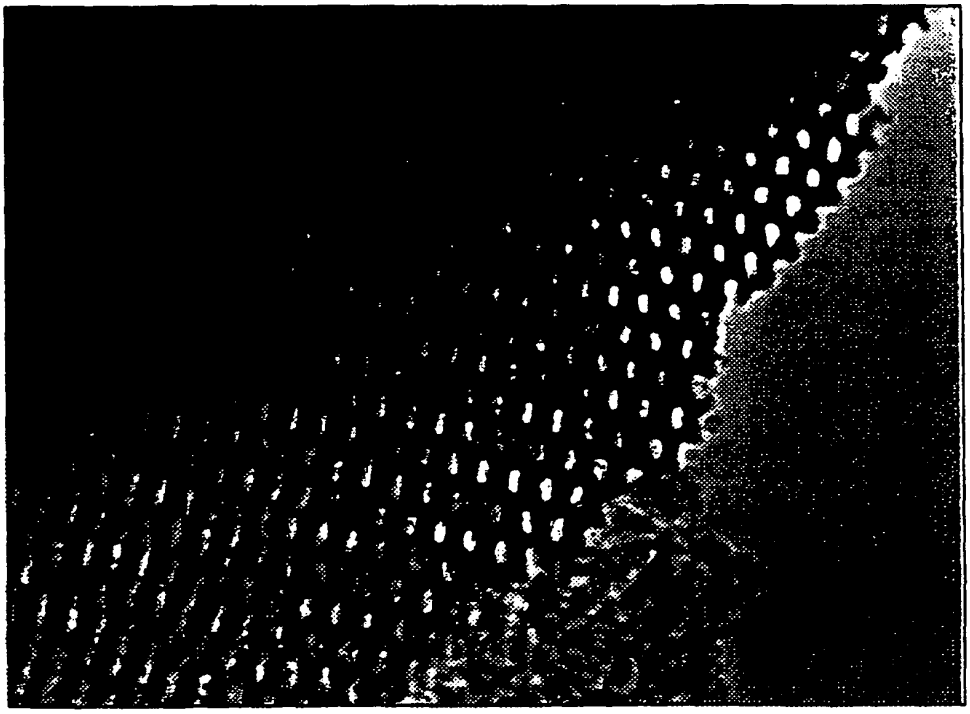

FIG. 24b

50 nm

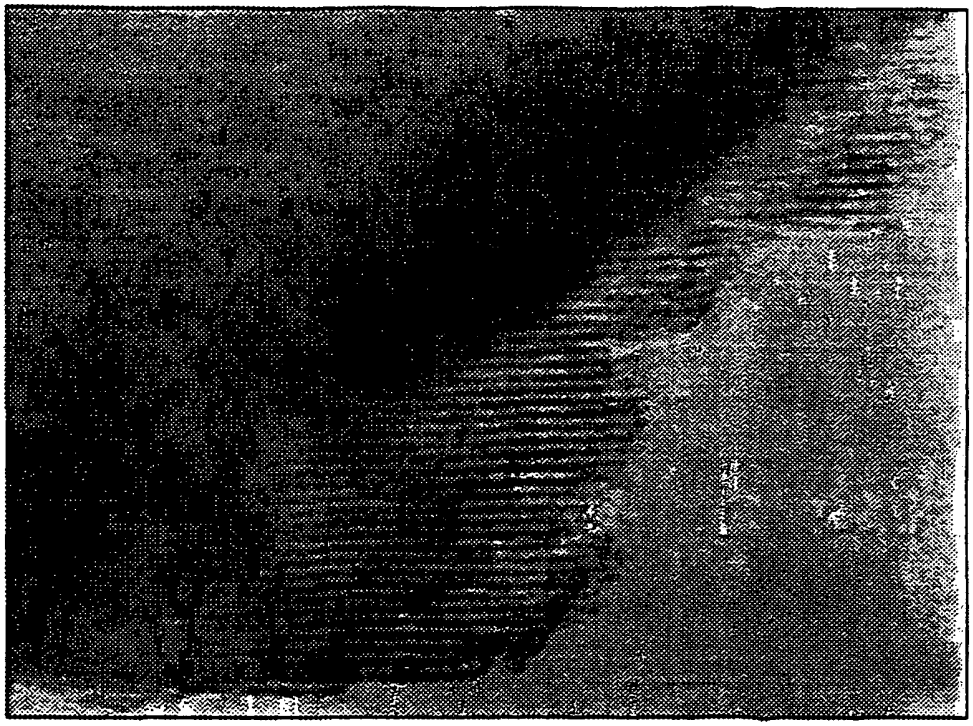

FIG. 25a

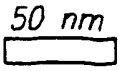

FIG. 25b

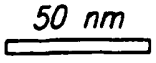

FIG. 26

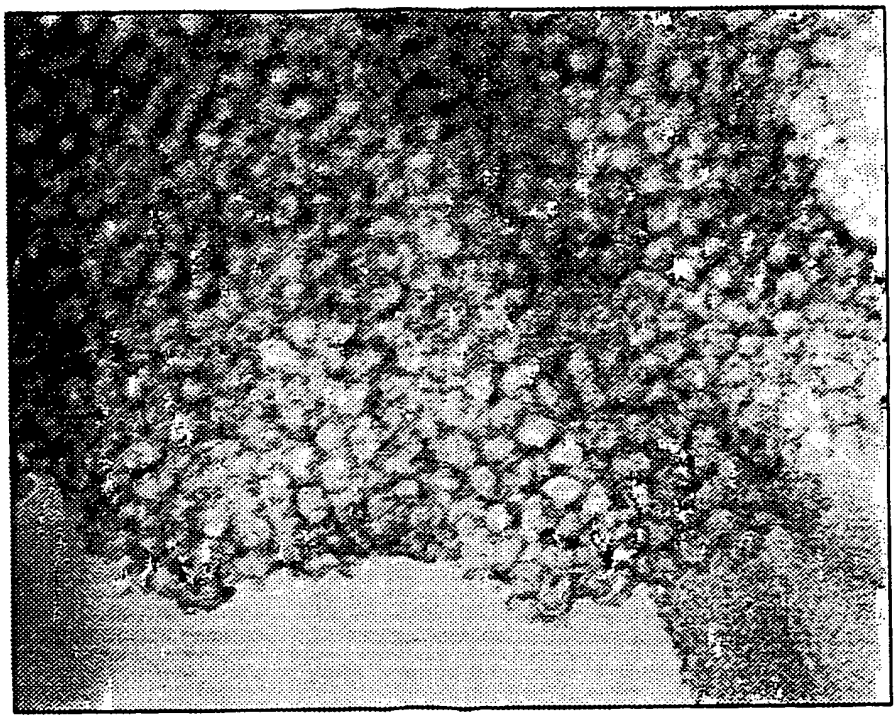

FIG. 27a 20 nm

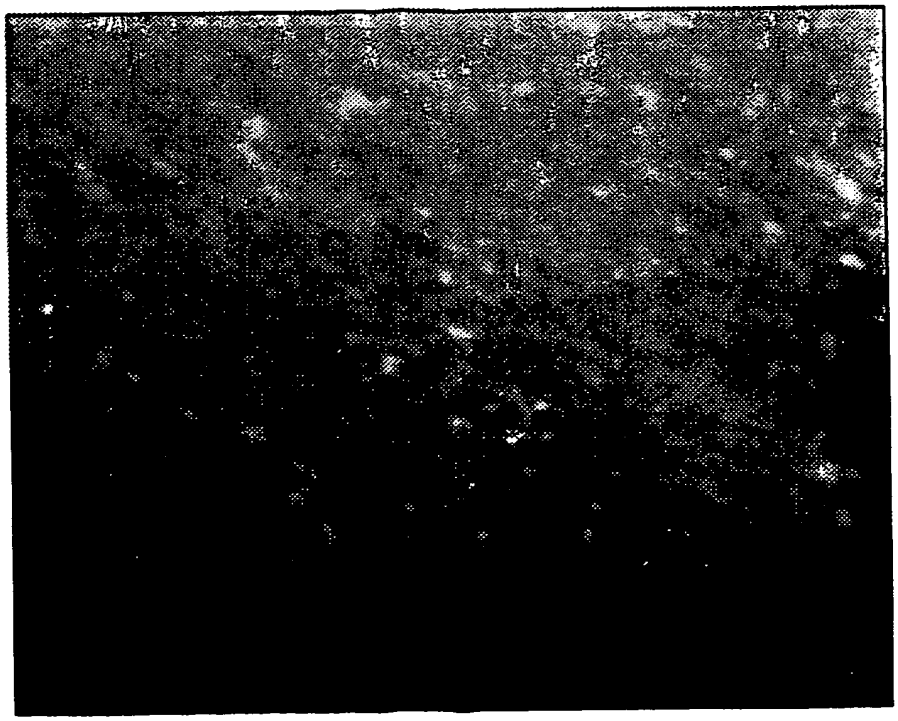

FIG. 27b 20 nm

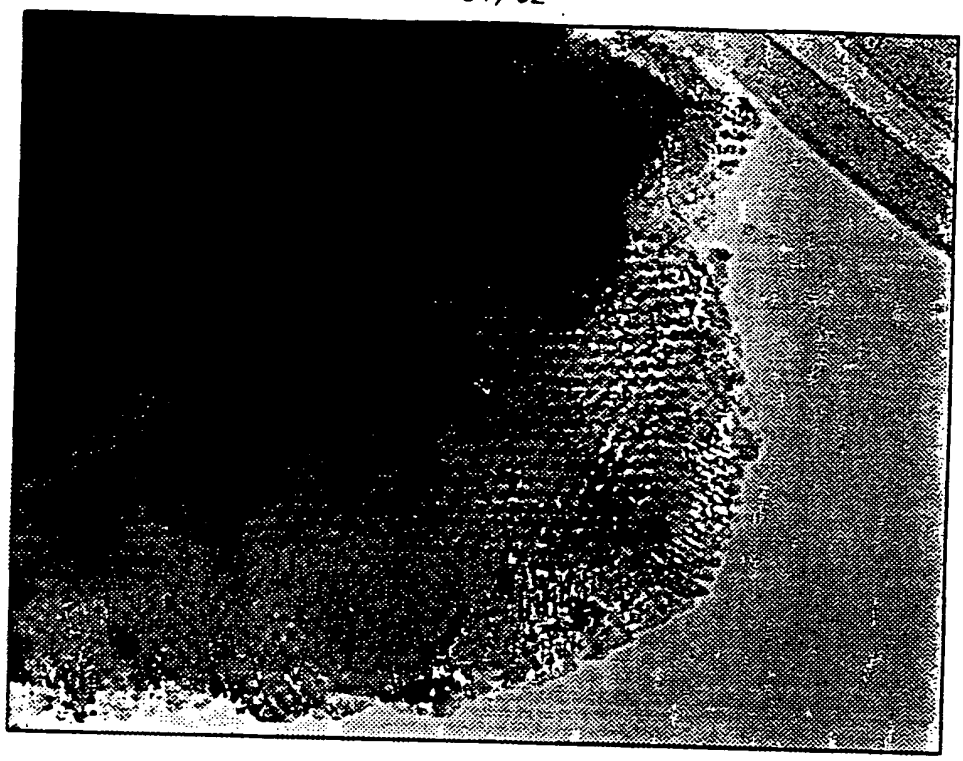

FIG. 28a

50 nm

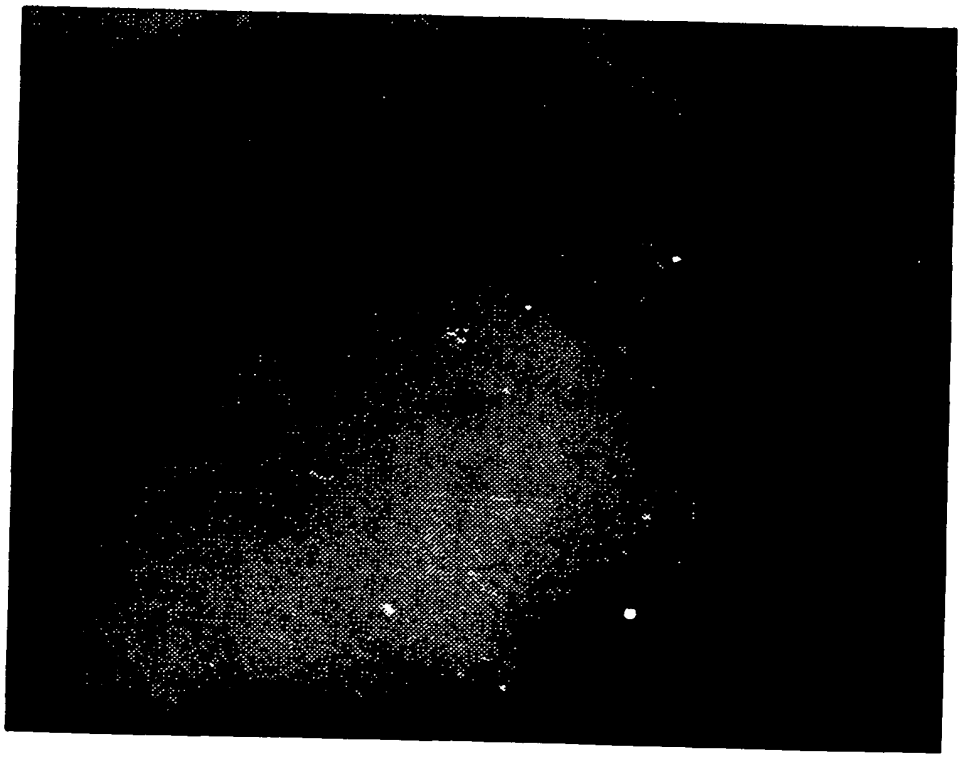

FIG. 28b

FIG. 29

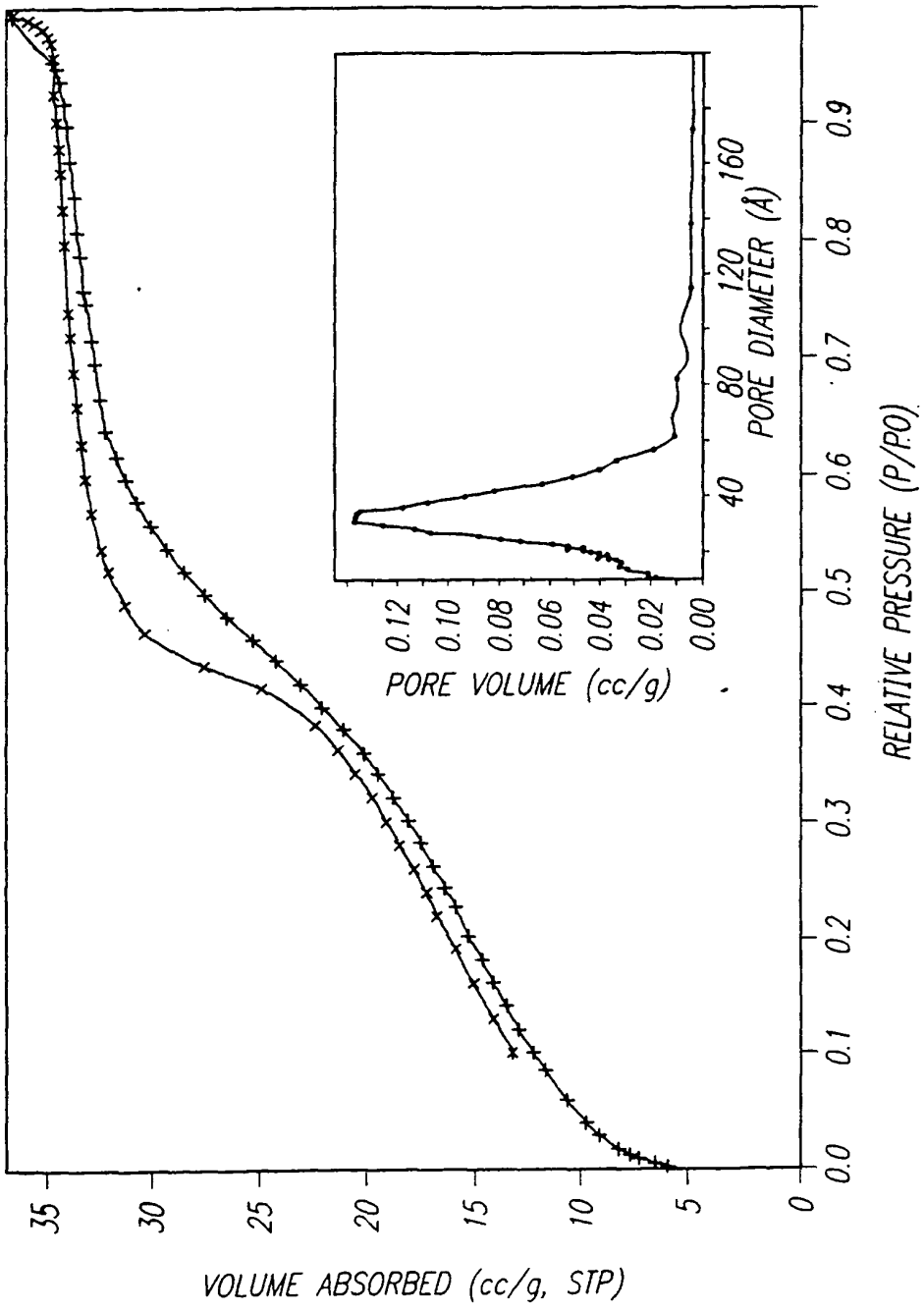

FIG. 30a

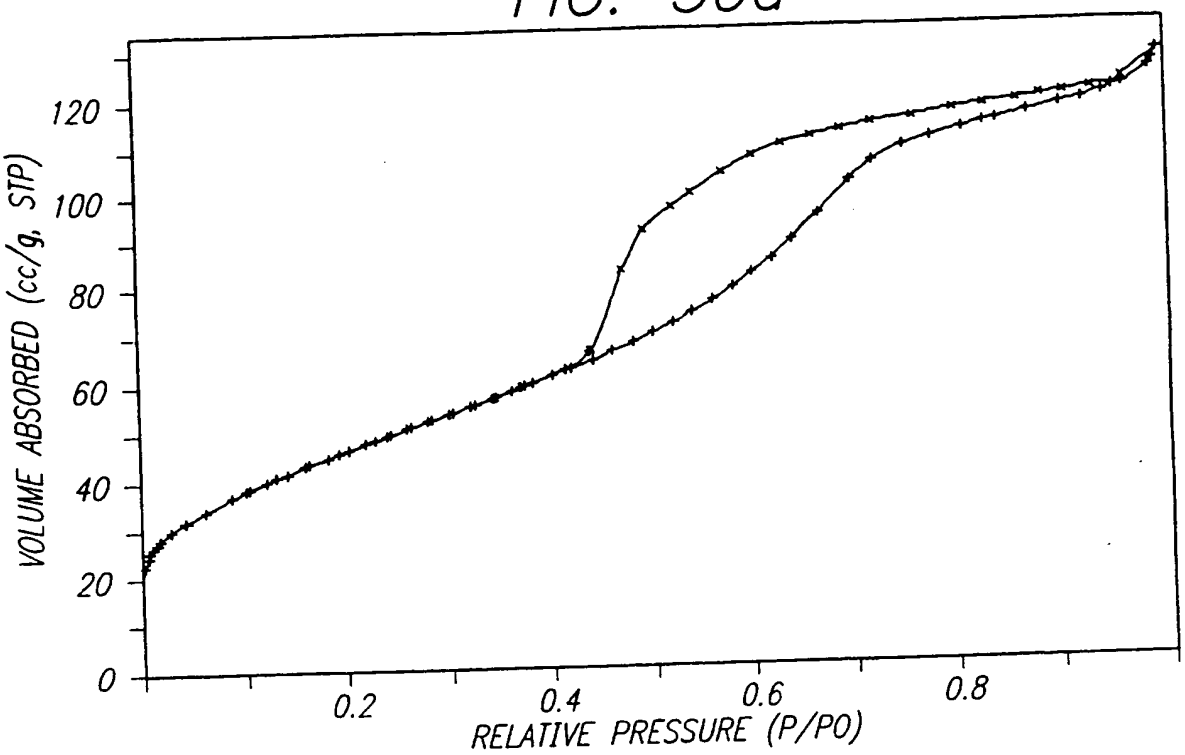

FIG. 30b

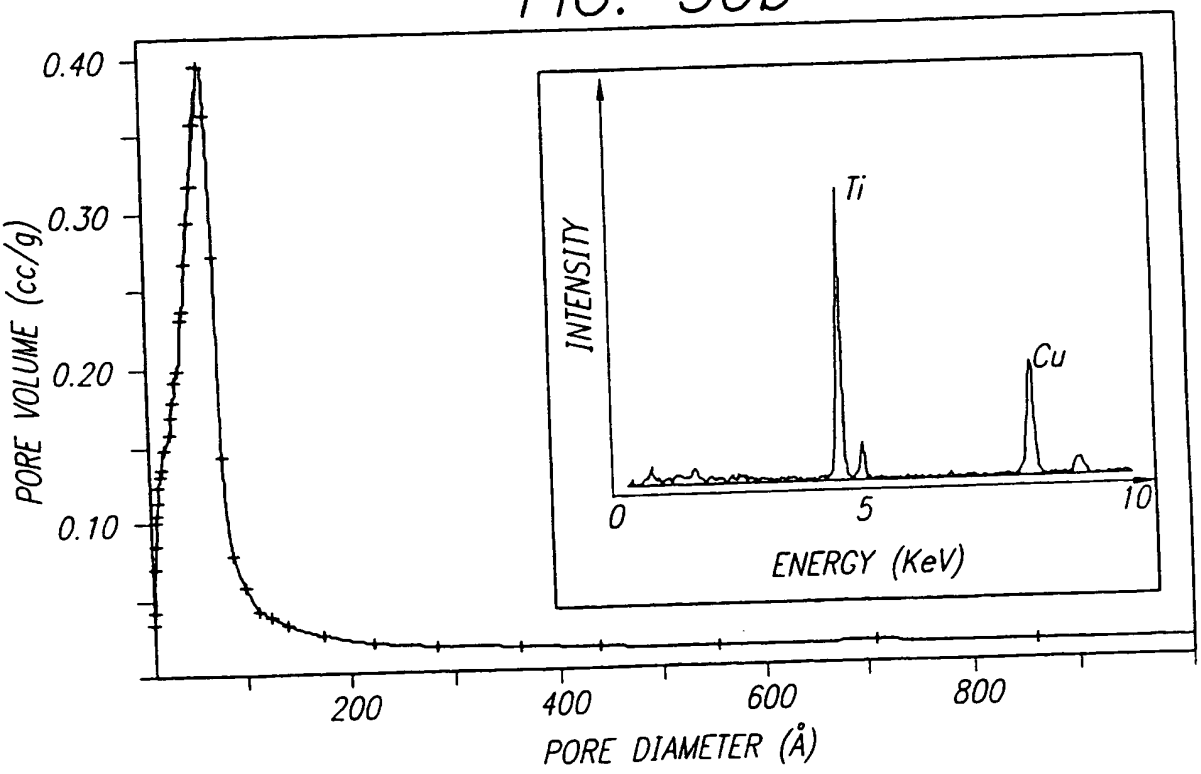

FIG. 31

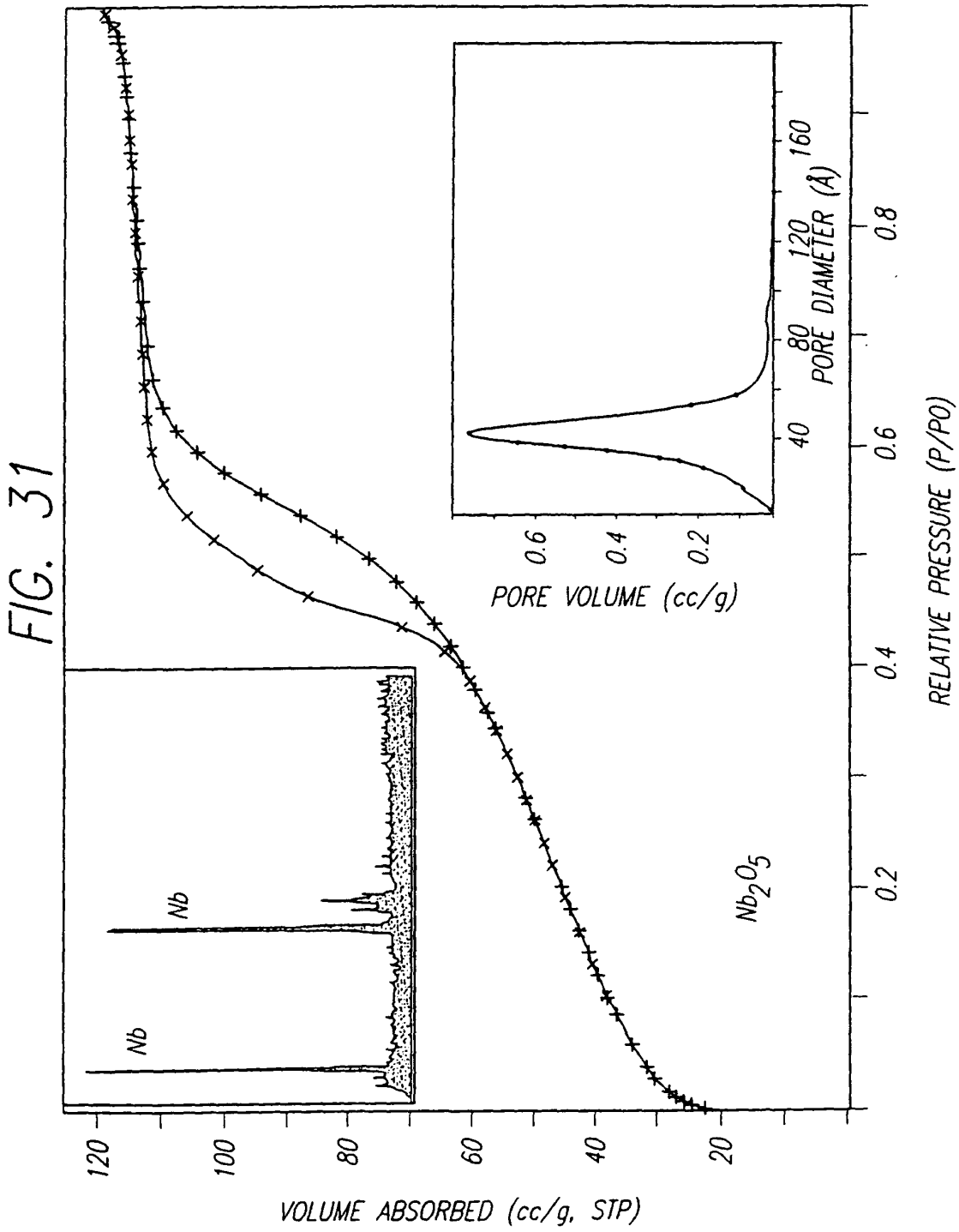
VOLUME ABSORBED (cc/g, STP)
120
100
80
60
40
20
RELATIVE PRESSURE (P/PO)
0.2
0.4
0.6
0.8
Nb_2O_5
Nb
Nb
PORE VOLUME (cc/g)
0.6
0.4
0.2
PORE DIAMETER (Å)
40
80
120
160

FIG. 32

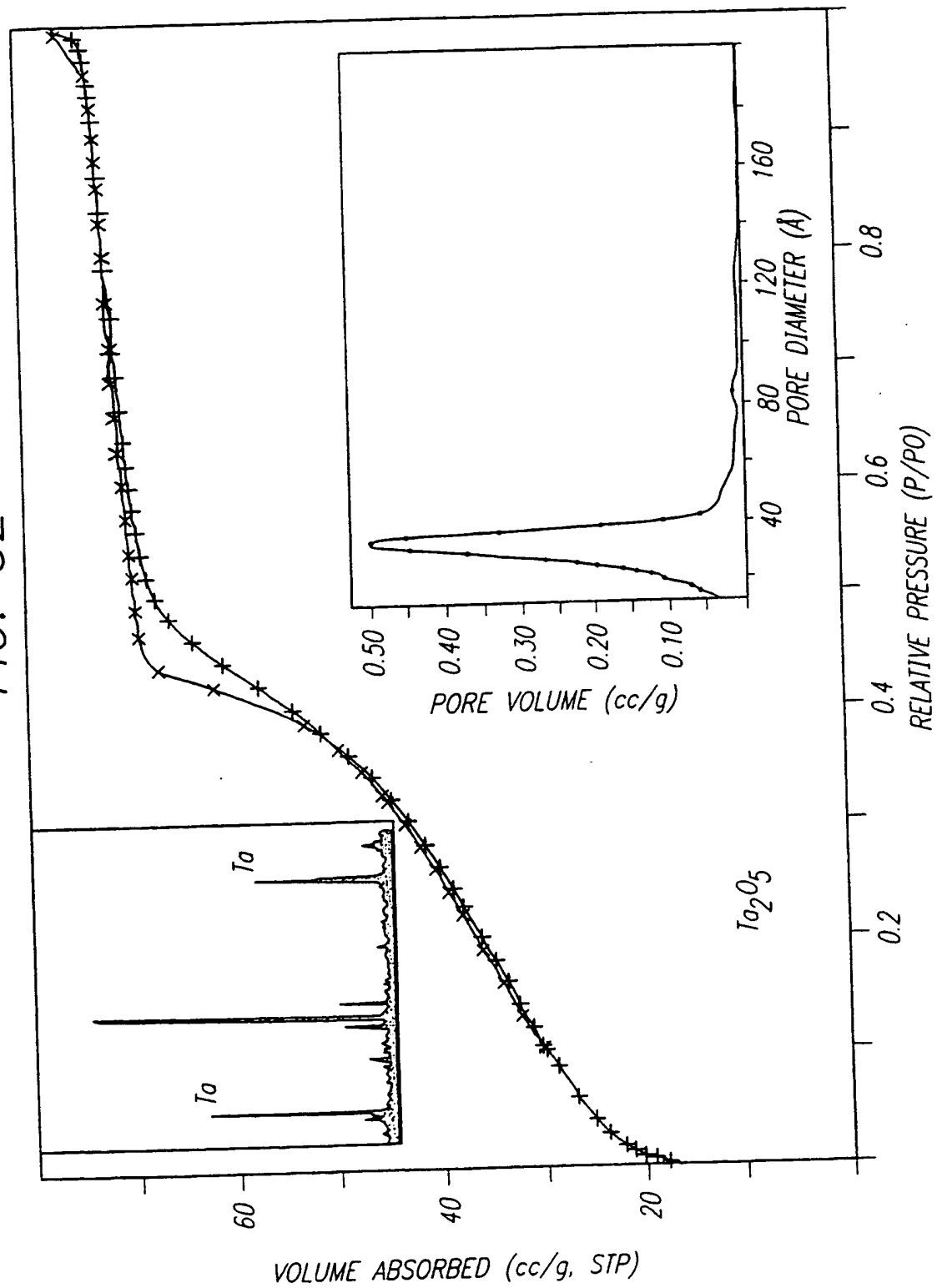
Ta
Ta
Ta_2O_5
VOLUME ABSORBED (cc/g, STP)
60
40
20
RELATIVE PRESSURE (P/PO)
0.2
0.4
0.6
0.8
PORE VOLUME (cc/g)
0.50
0.40
0.30
0.20
0.10
PORE DIAMETER (Å)
40
80
120
160

FIG. 33

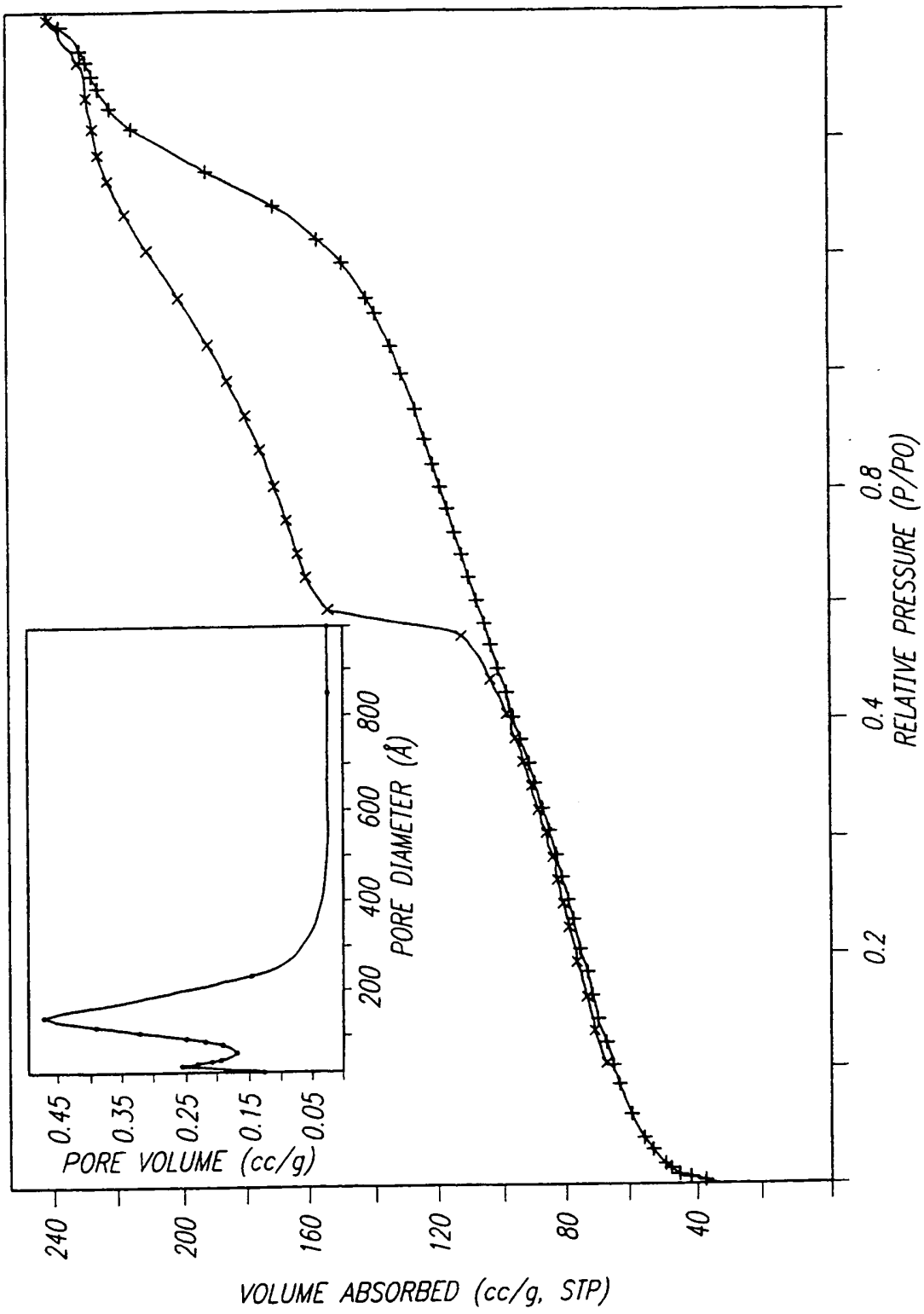

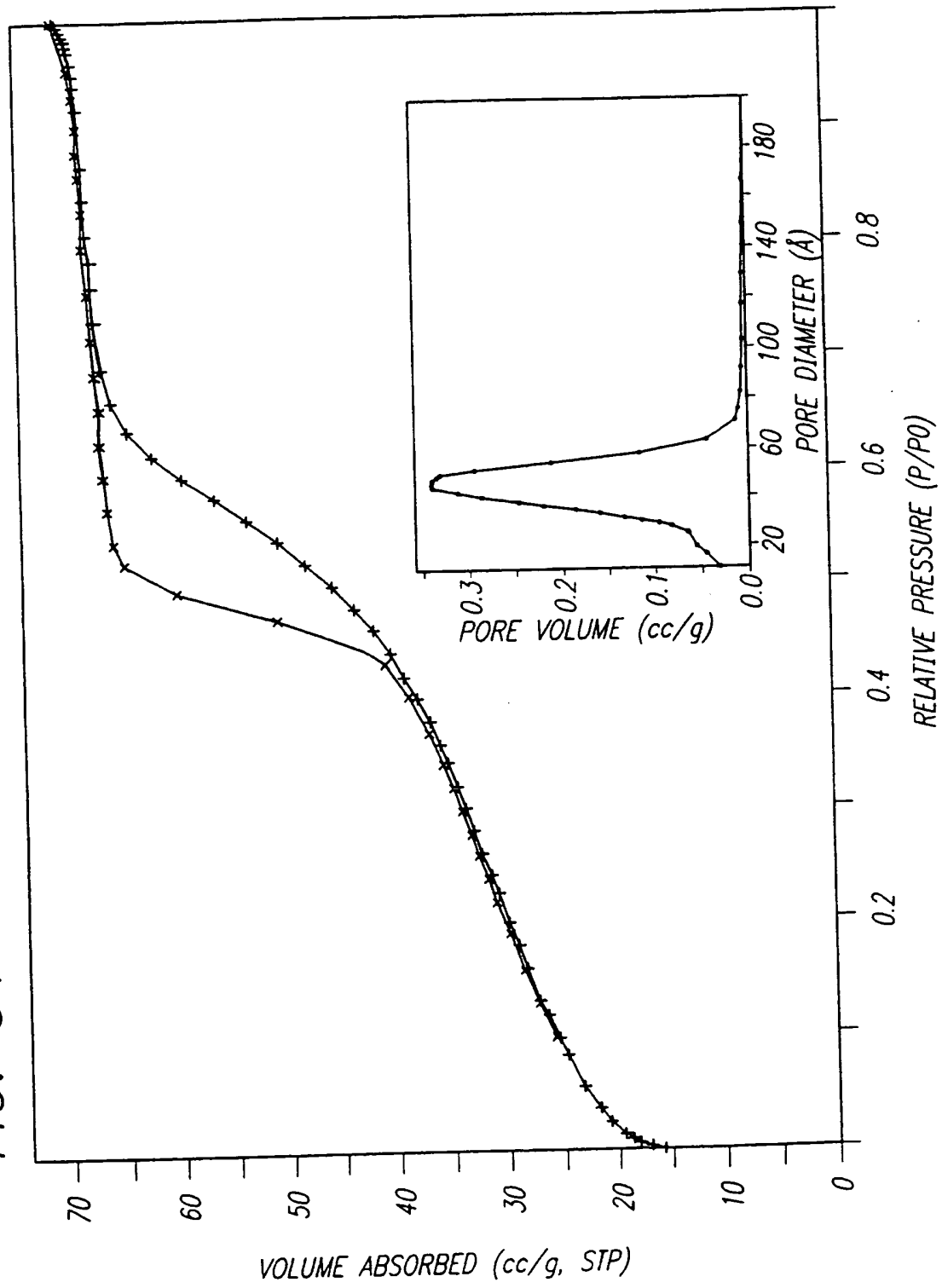
VOLUME ABSORBED (cc/g, STP)
0
10
20
30
40
50
60
70
RELATIVE PRESSURE (P/PO)
0.2
0.4
0.6
0.8
PORE VOLUME (cc/g)
0.0
0.1
0.2
0.3
PORE DIAMETER (Å)
20
60
100
140
180

FIG. 34

FIG. 35a

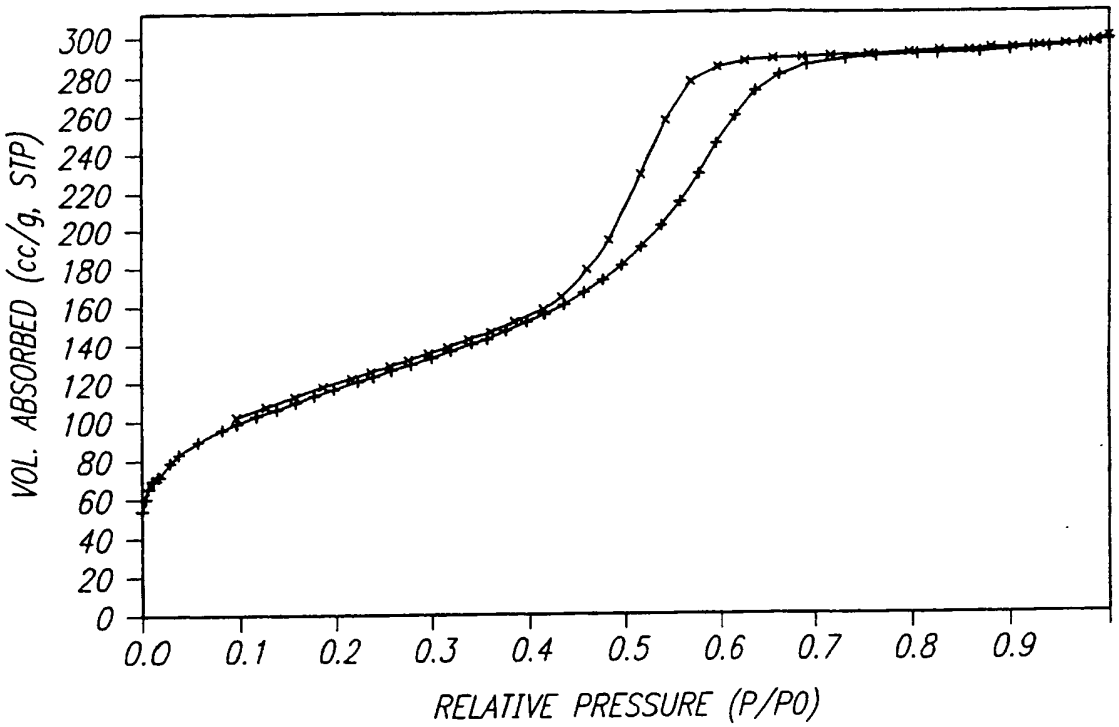

FIG. 35b

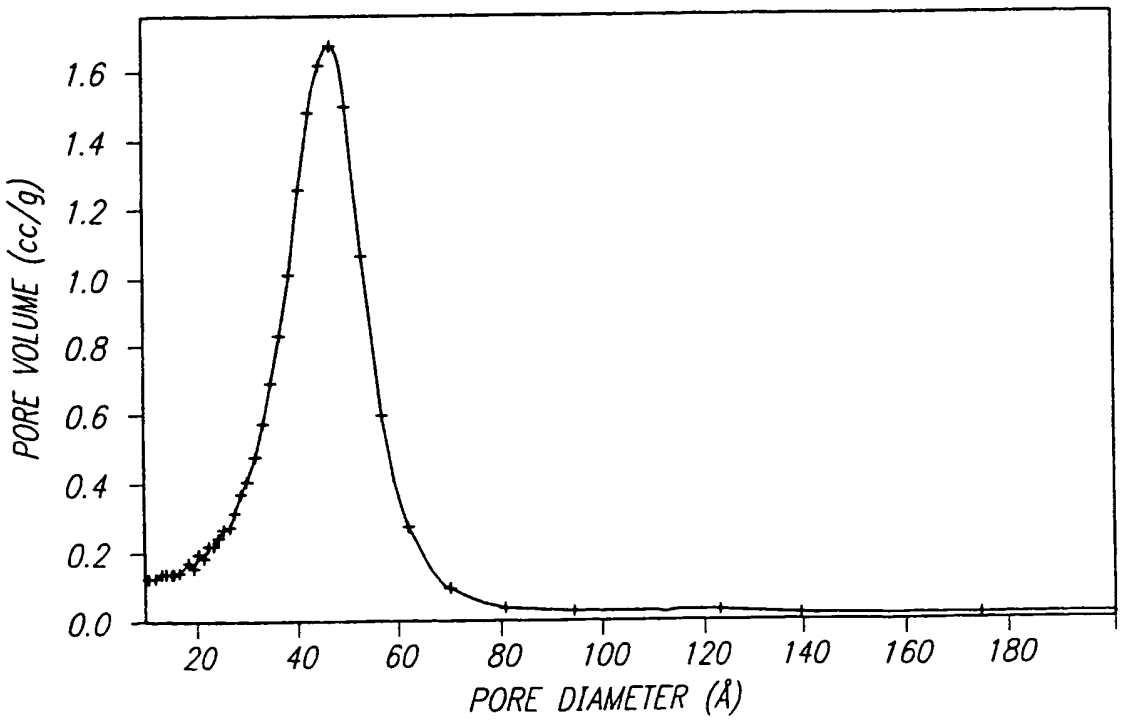

FIG. 36a

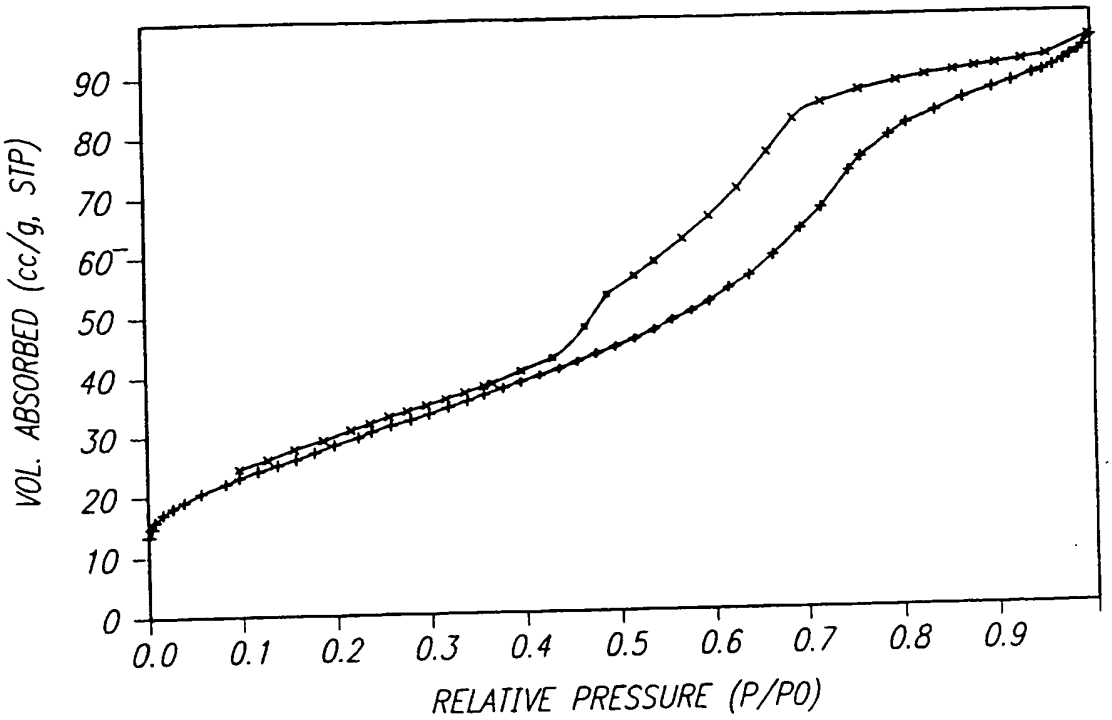

FIG. 36b

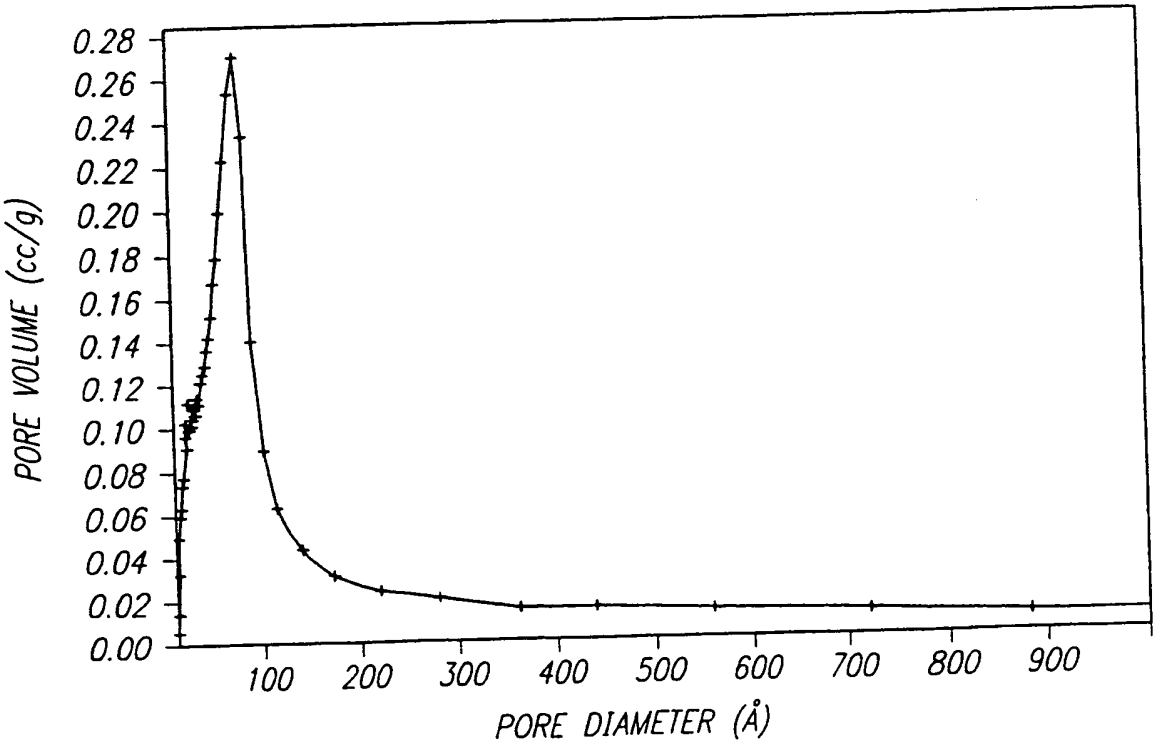

FIG. 37

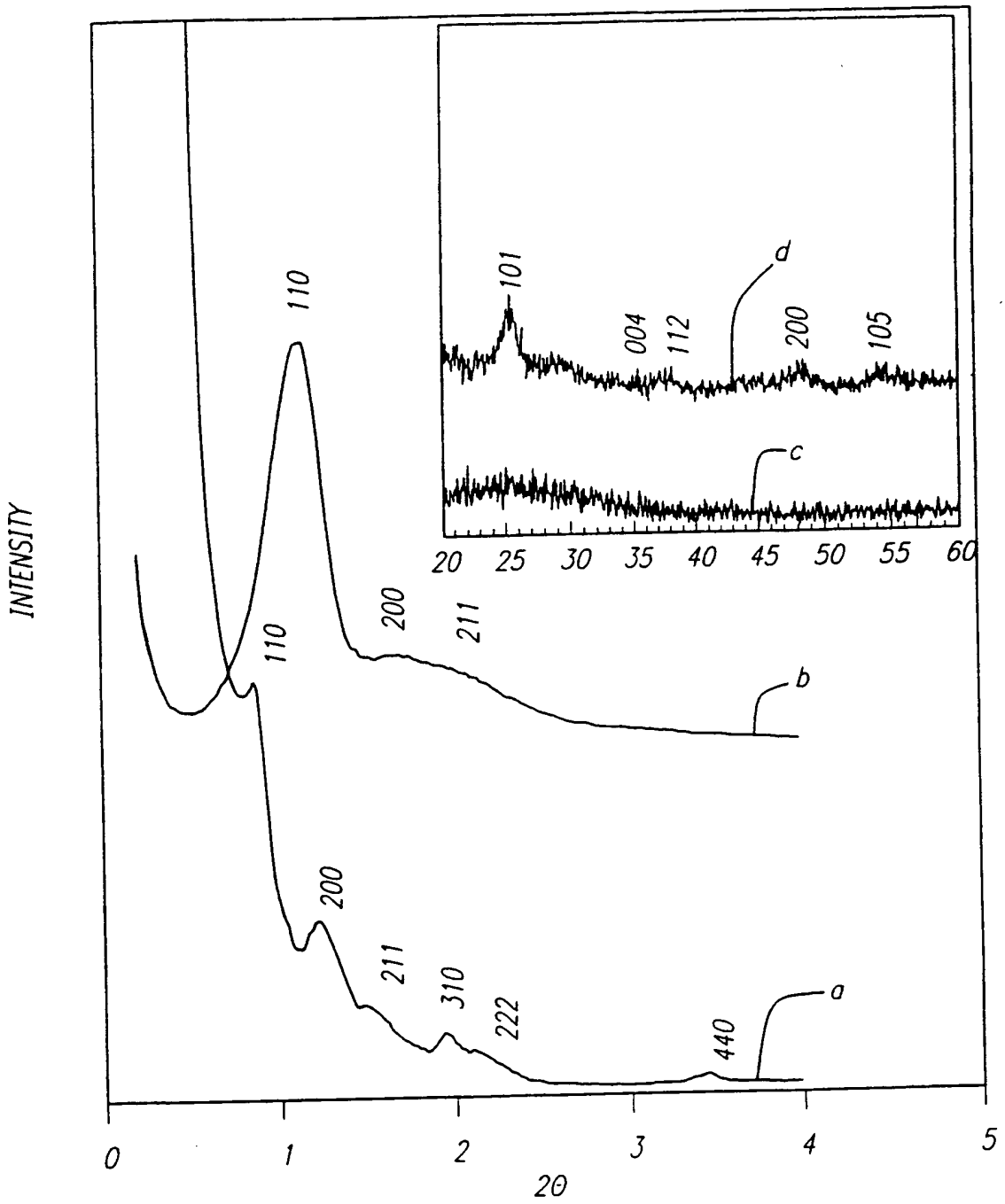

FIG. 38

20 nm

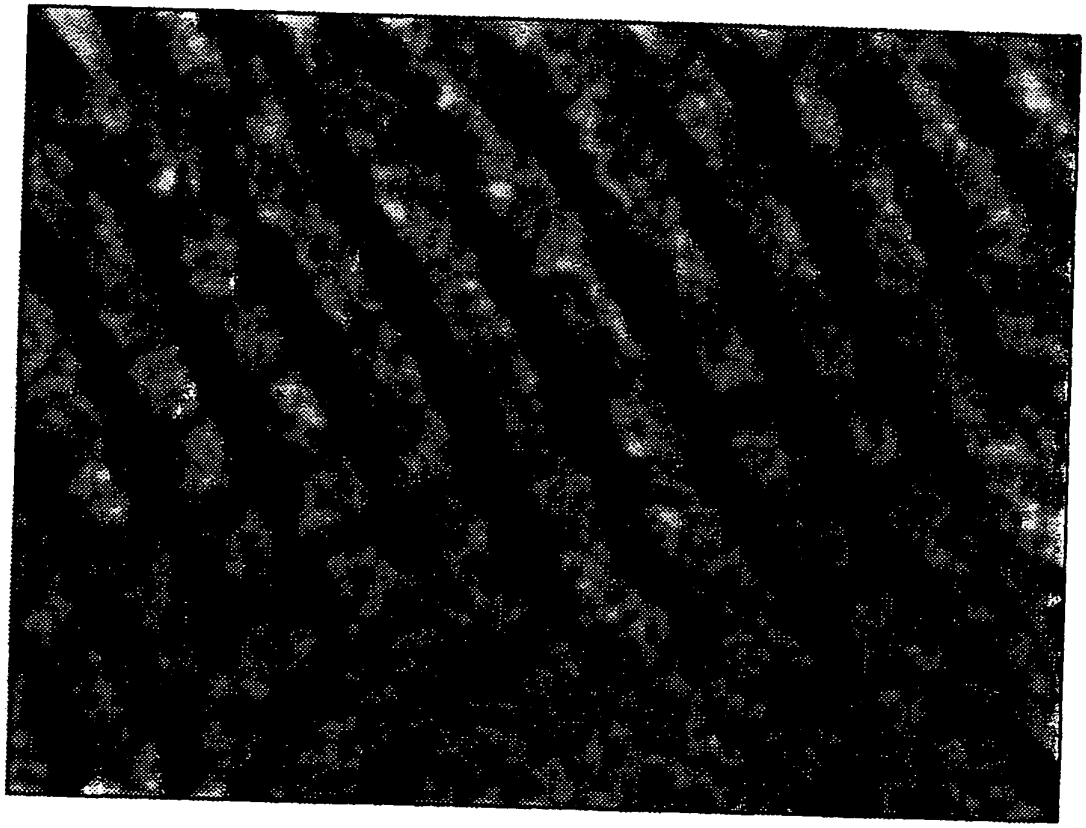

FIG. 39

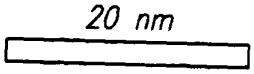

FIG. 40 10 μm

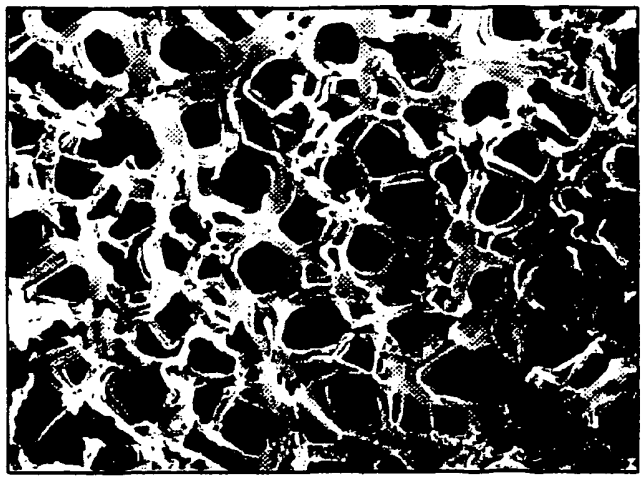

FIG. 41a

10 μm
0 kV X 3.000 12mm

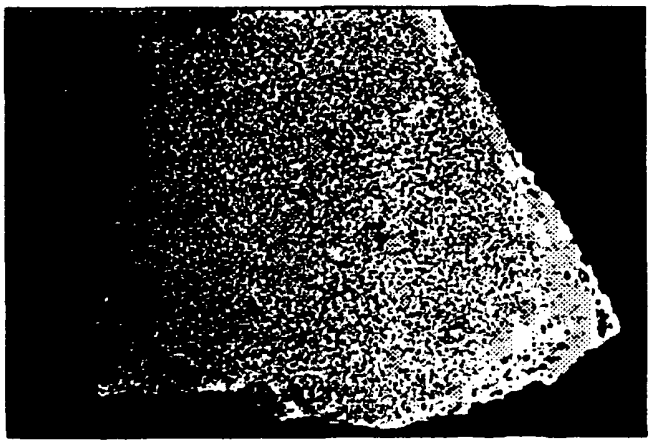

FIG. 41b

0.1 mm

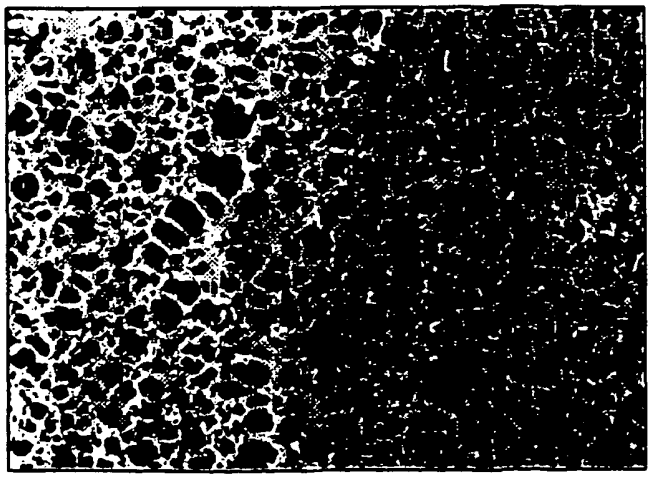

FIG. 41c

1 nm

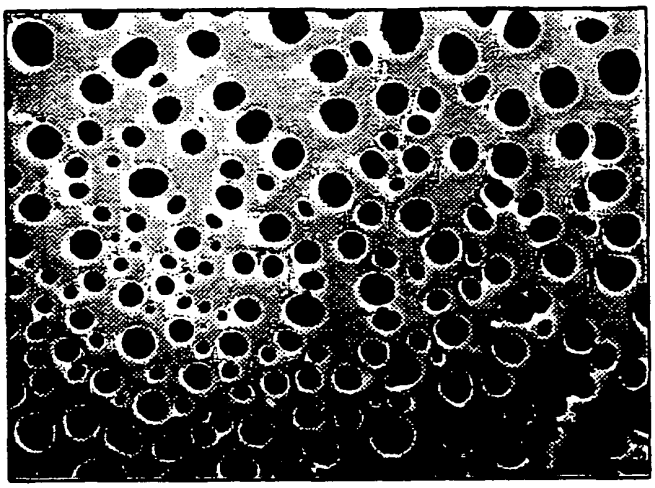

FIG. 41d

10 μm

3.0 kV x 1.300 10mm

FIG. 41e

10 μm

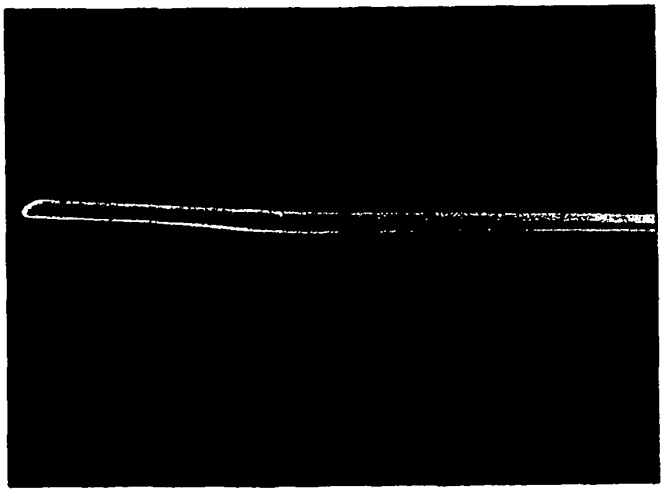

FIG. 41f

1 μm

3.0 kV x 5.500 11mm

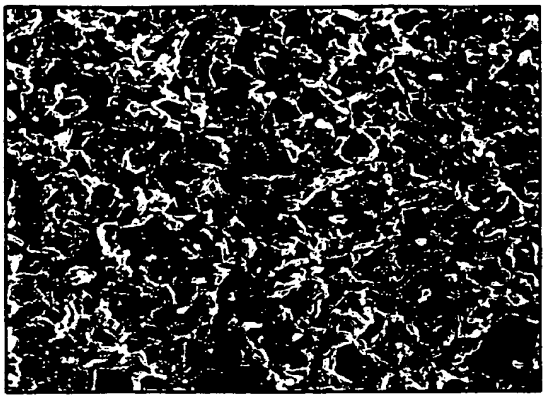

10 μm
JEOL 3.0 kV X 2.530 12mm

FIG. 42a

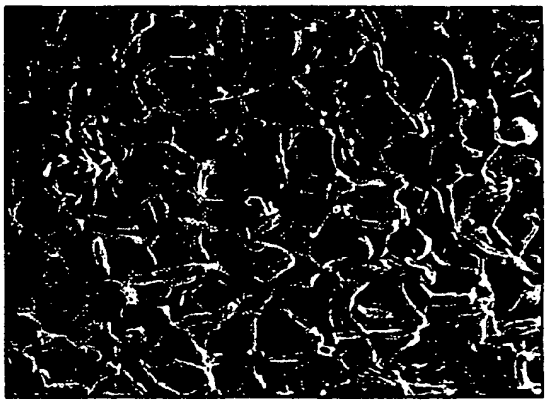

1 μm
3.0 kV X 5.000 12mm

FIG. 42b

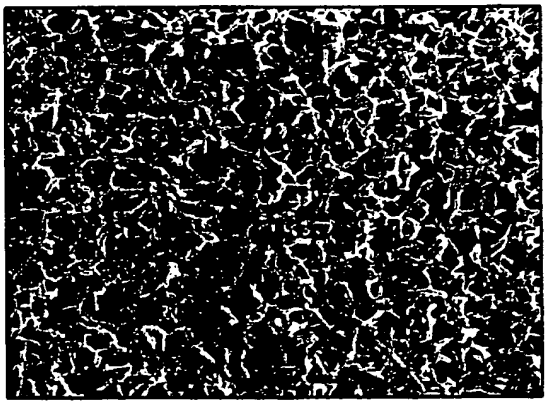

10 μm
3.0 kV X 2.700 11mm

FIG. 42c

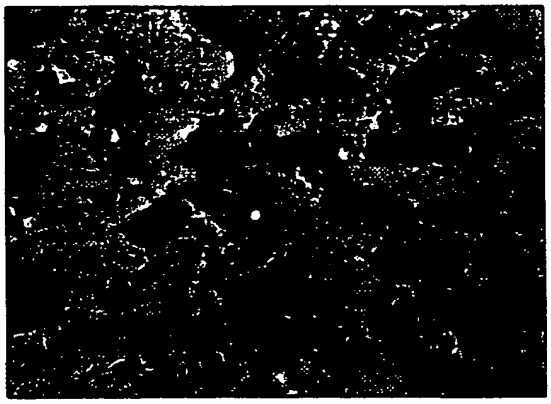

100 μm
JEOL 3.0 kV X 160 1.1mm

FIG. 42d

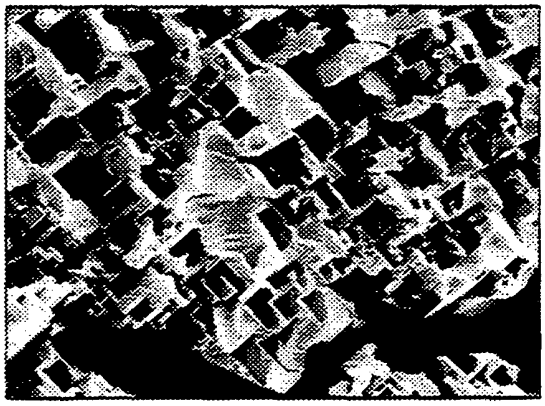

— 10 μm
3.0 kV X .550 12mm

FIG. 43a

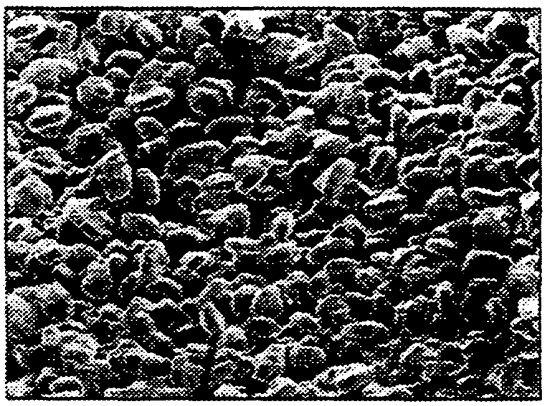

—— 10 μm
3.0 kV X 1.500 11mm

FIG. 43b

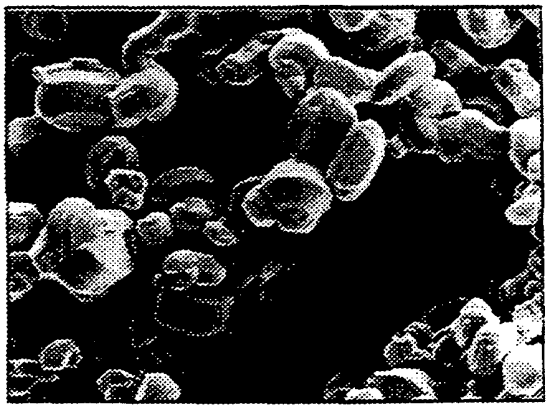

— 1 μm
3.0 kV X 5.000 12mm

FIG. 43c

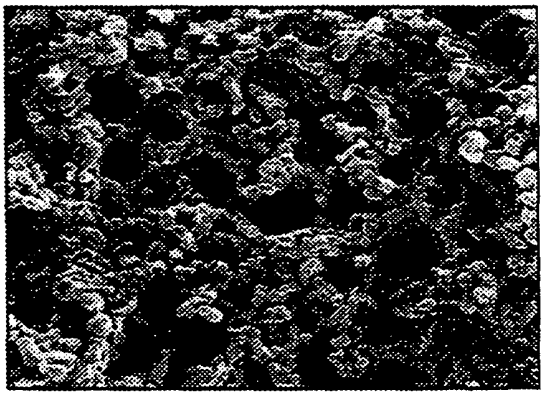

—— 10 μm
3.0 kV X 1.100 11mm

FIG. 43d

FIG. 44a

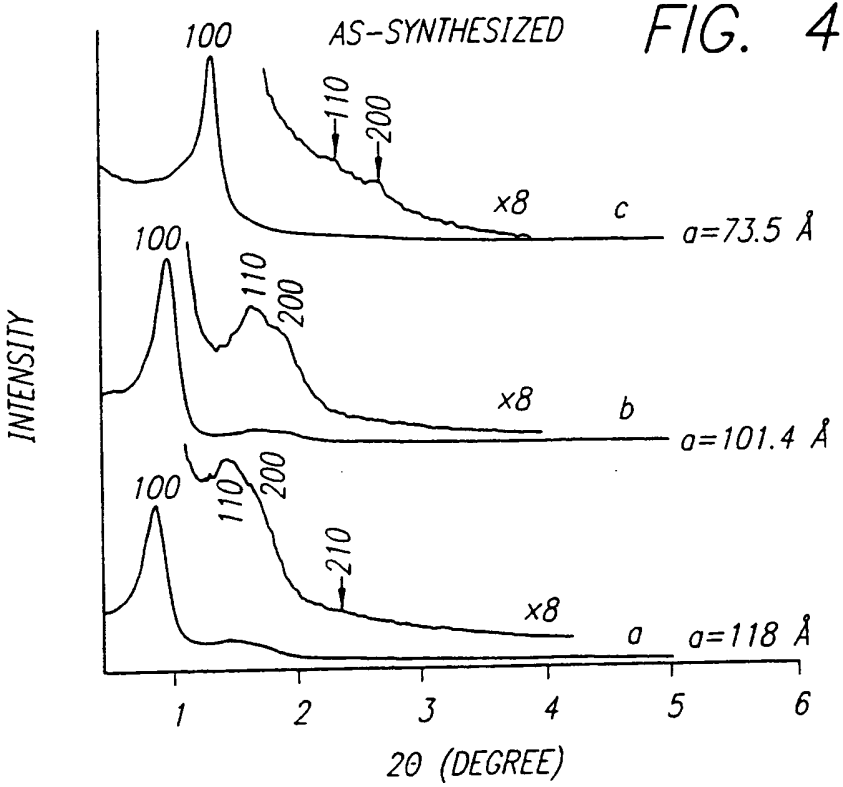

FIG. 44b

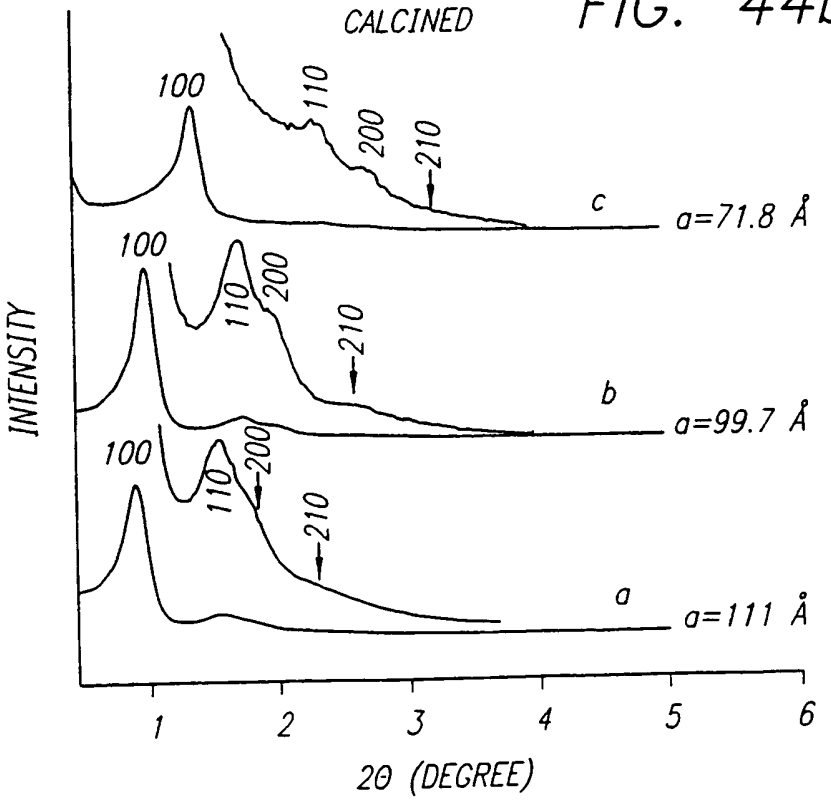

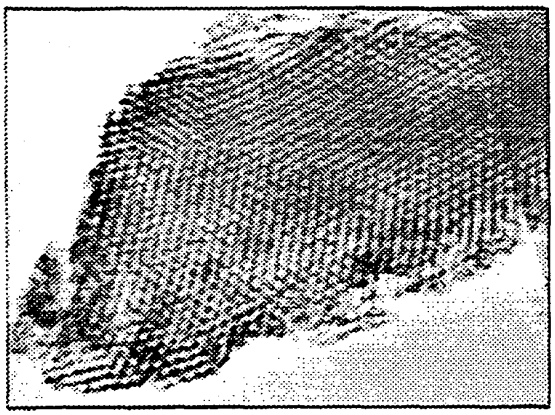

FIG. 45a

FIG. 45b

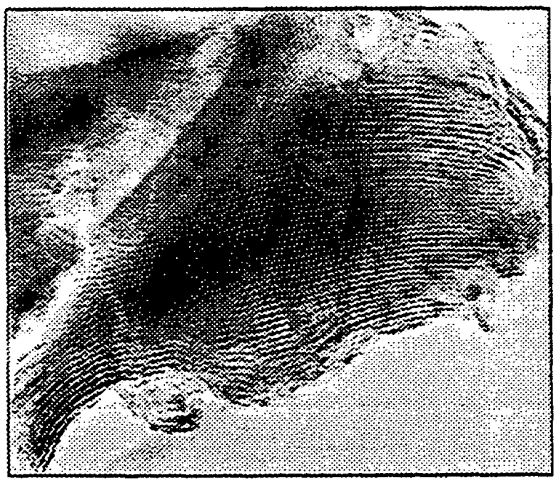

FIG. 45c

FIG. 45d

FIG. 46a

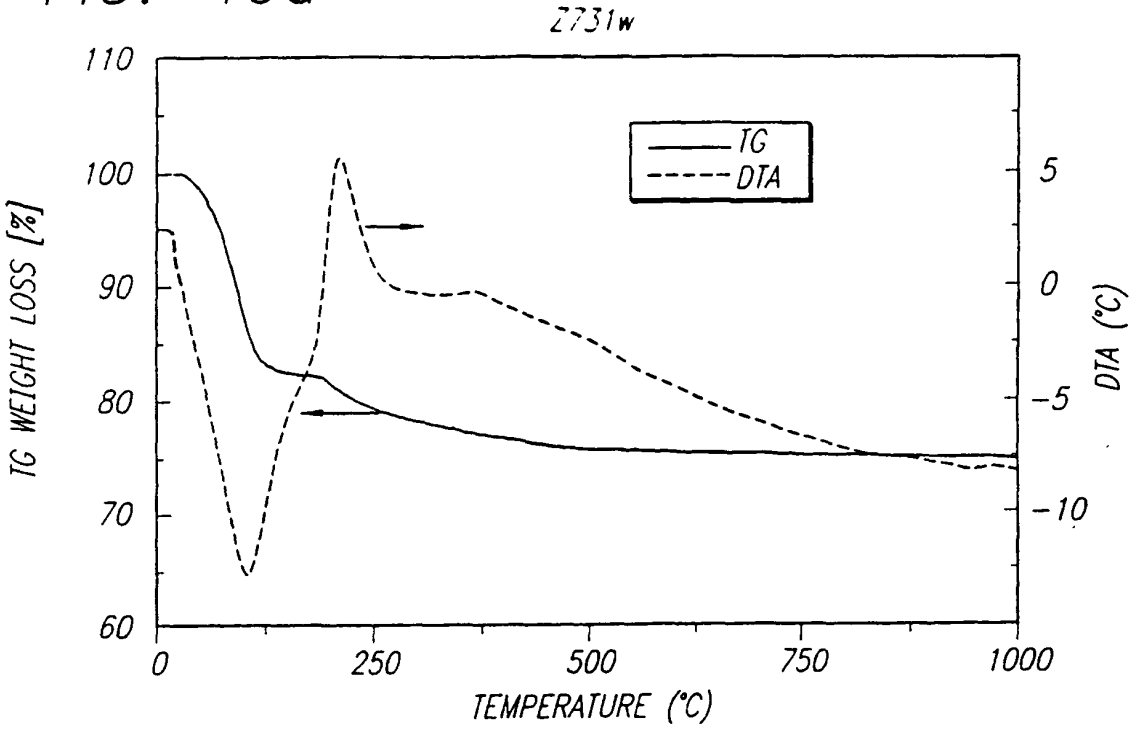

FIG. 46b

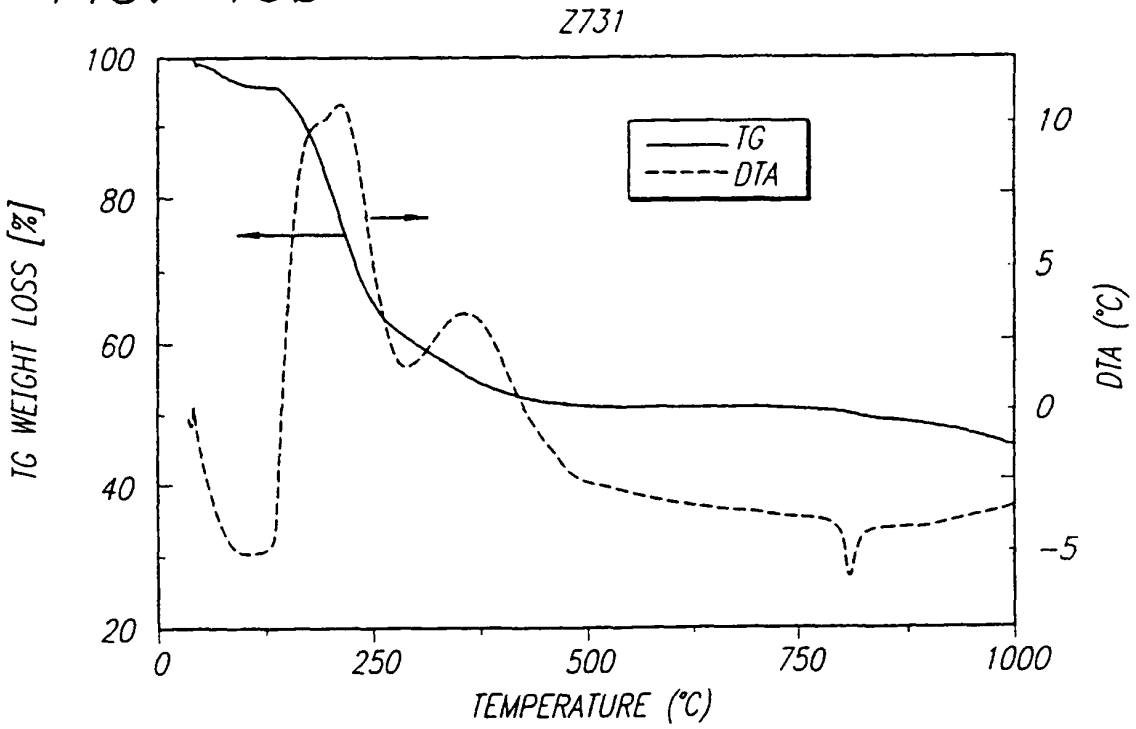

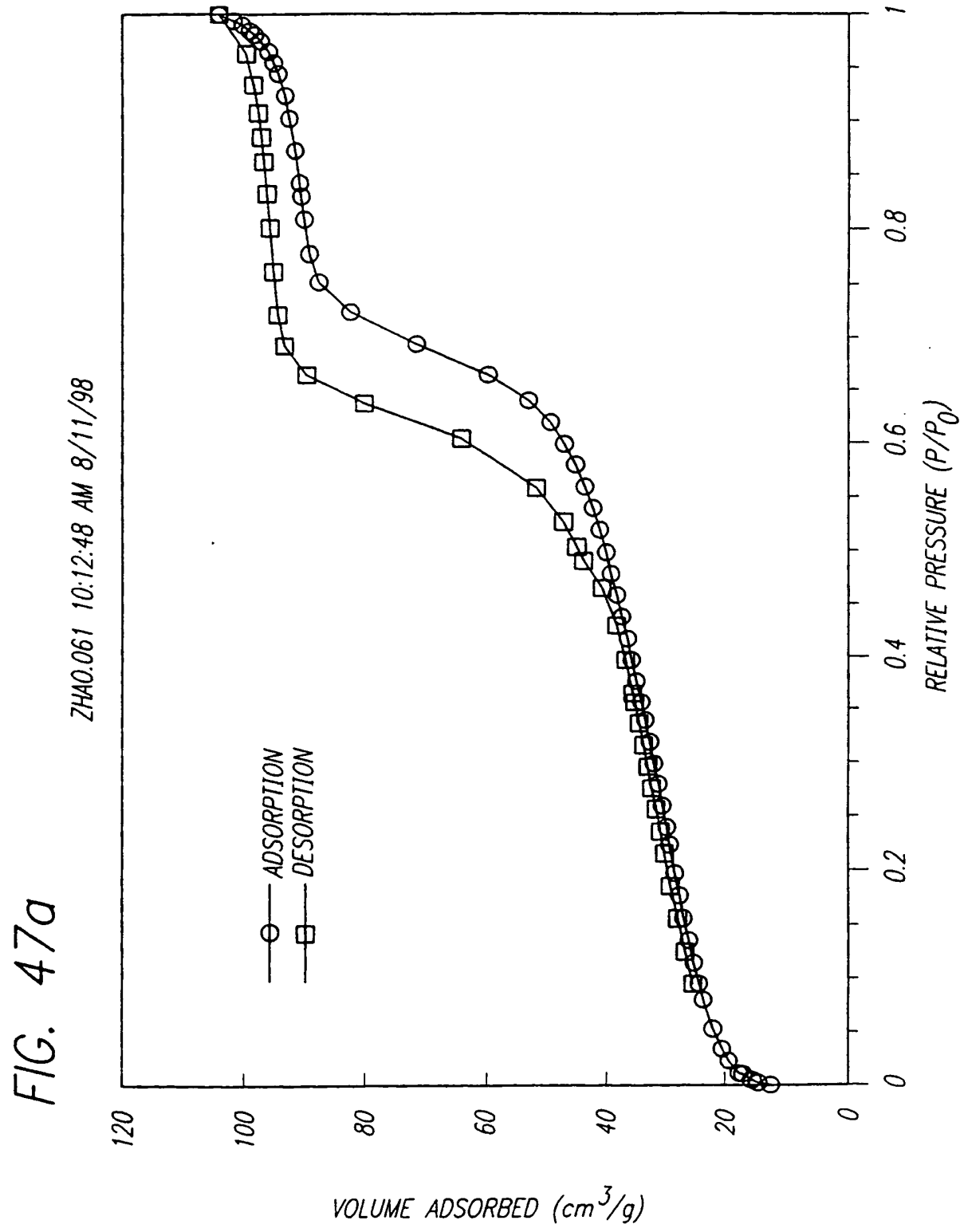

FIG. 47a

FIG. 47b

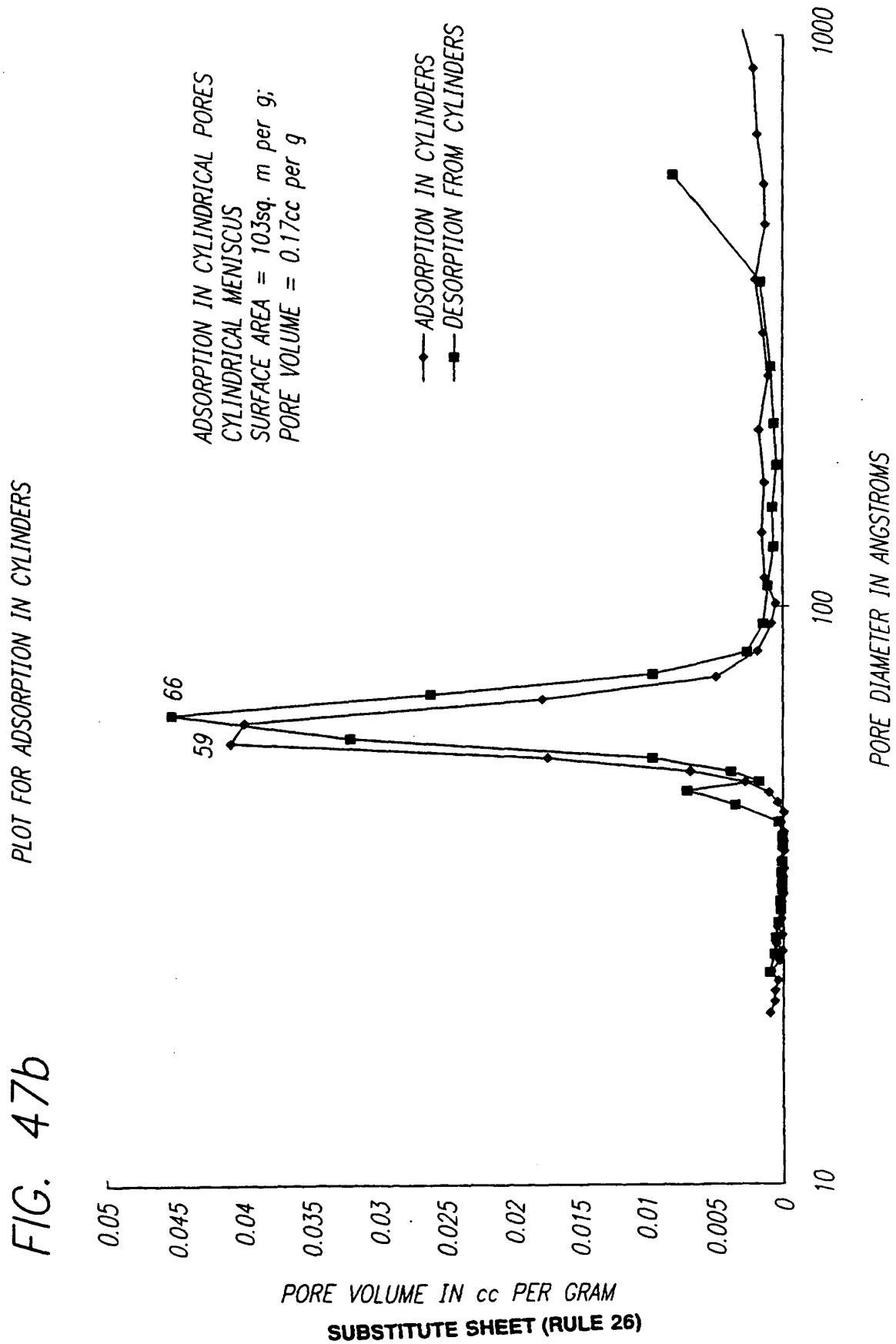

FIG. 48a

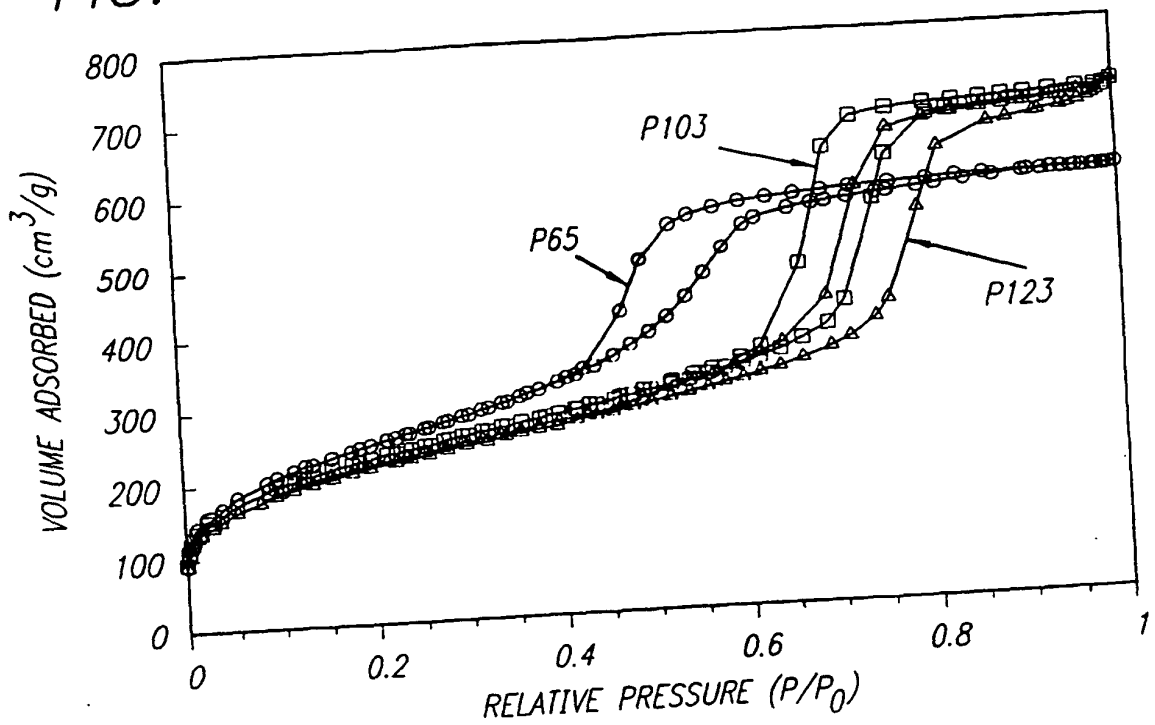

FIG. 48b

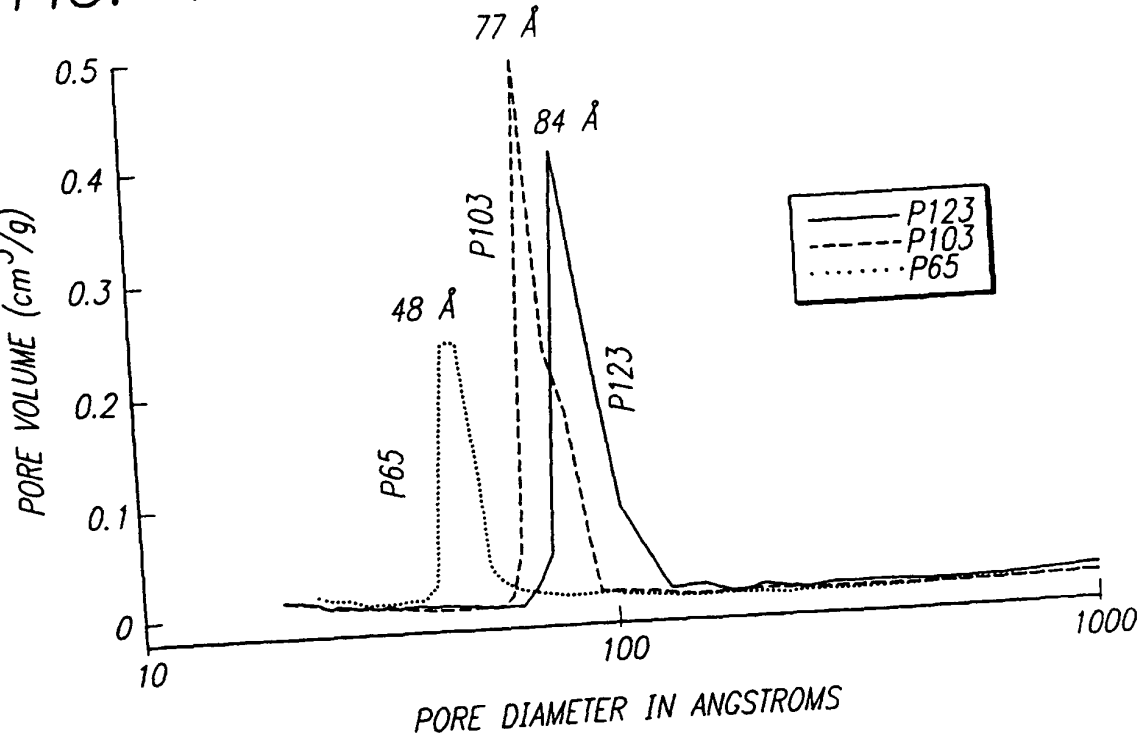

FIG. 49a

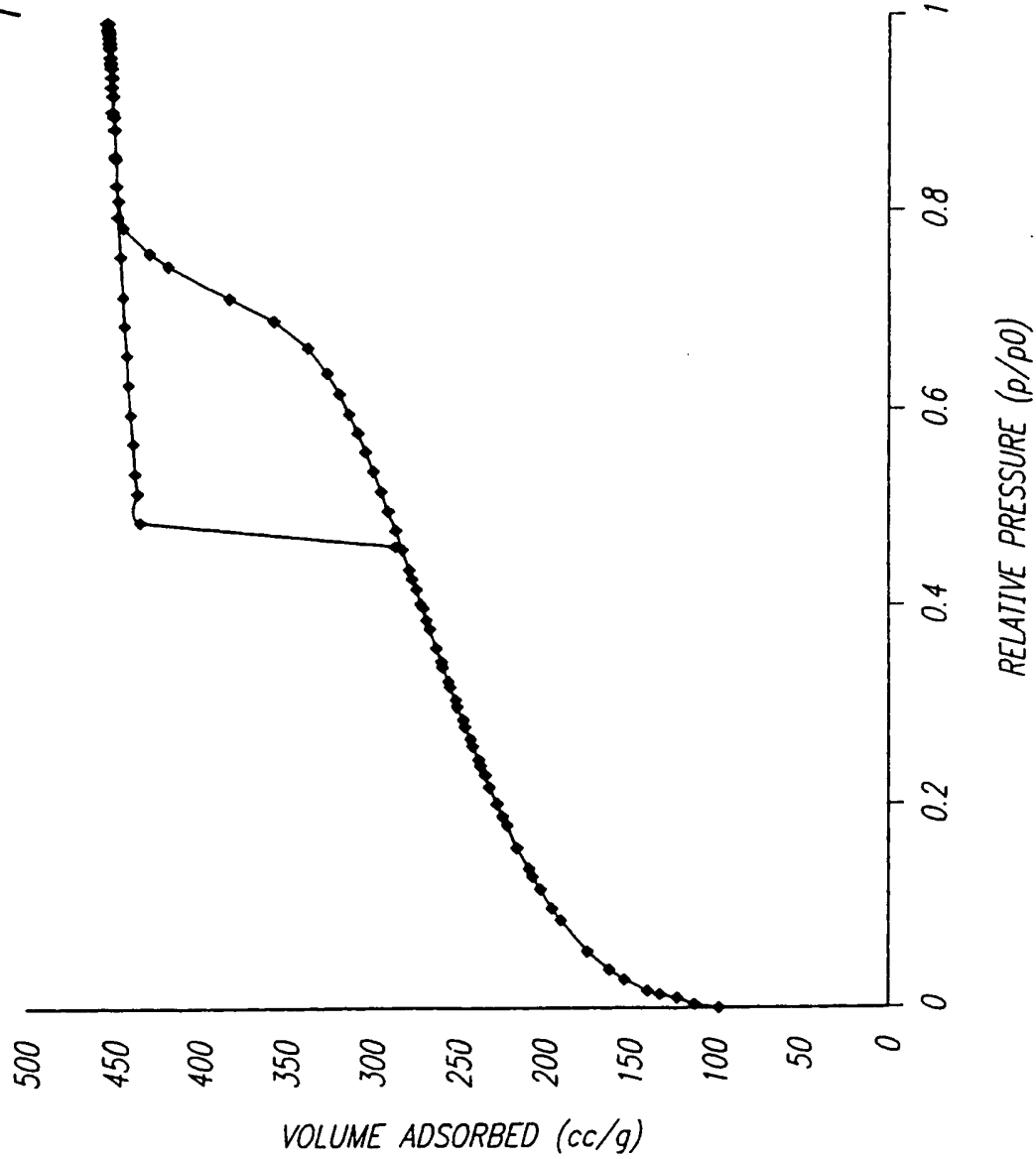

FIG. 49b

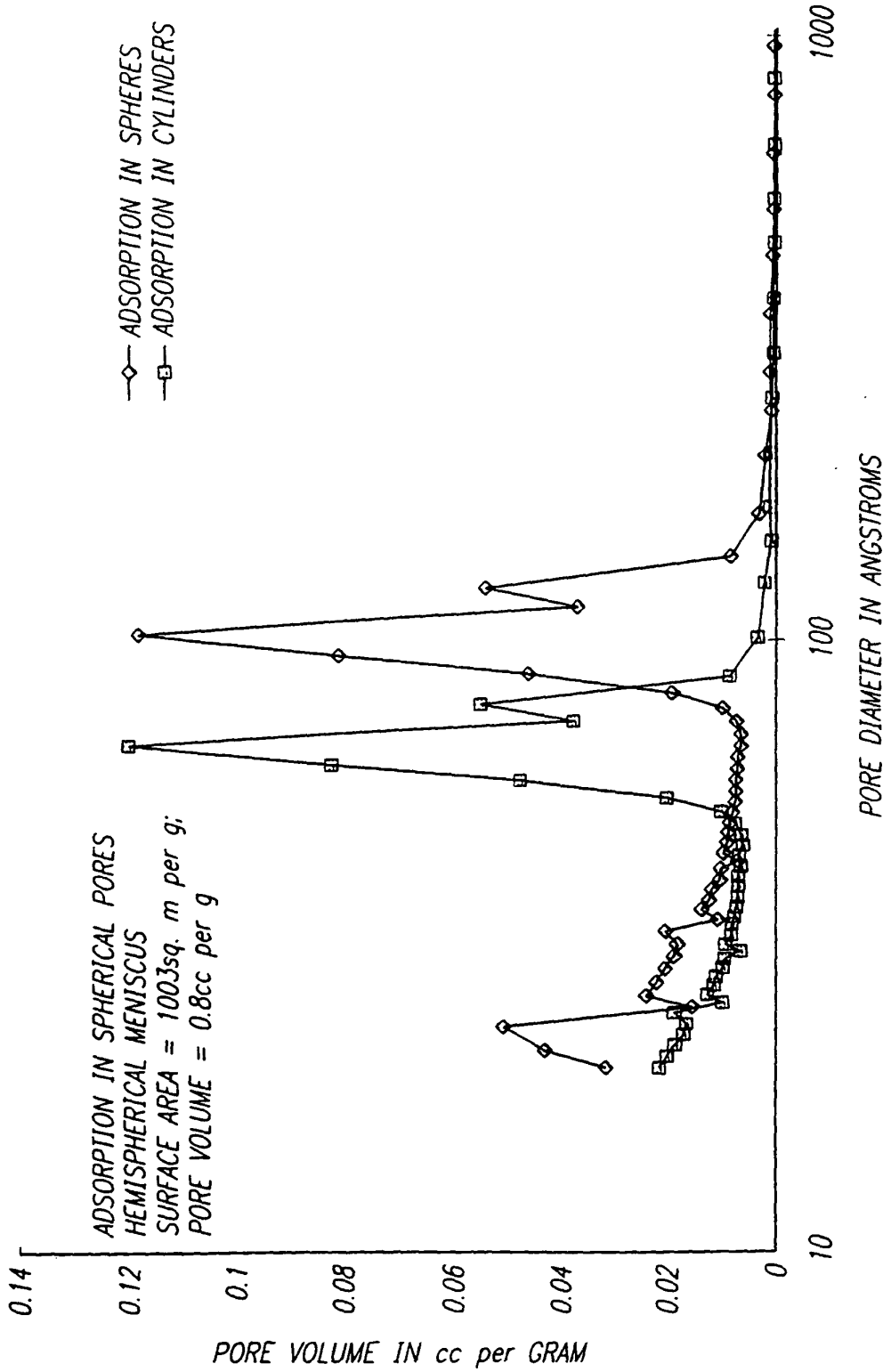

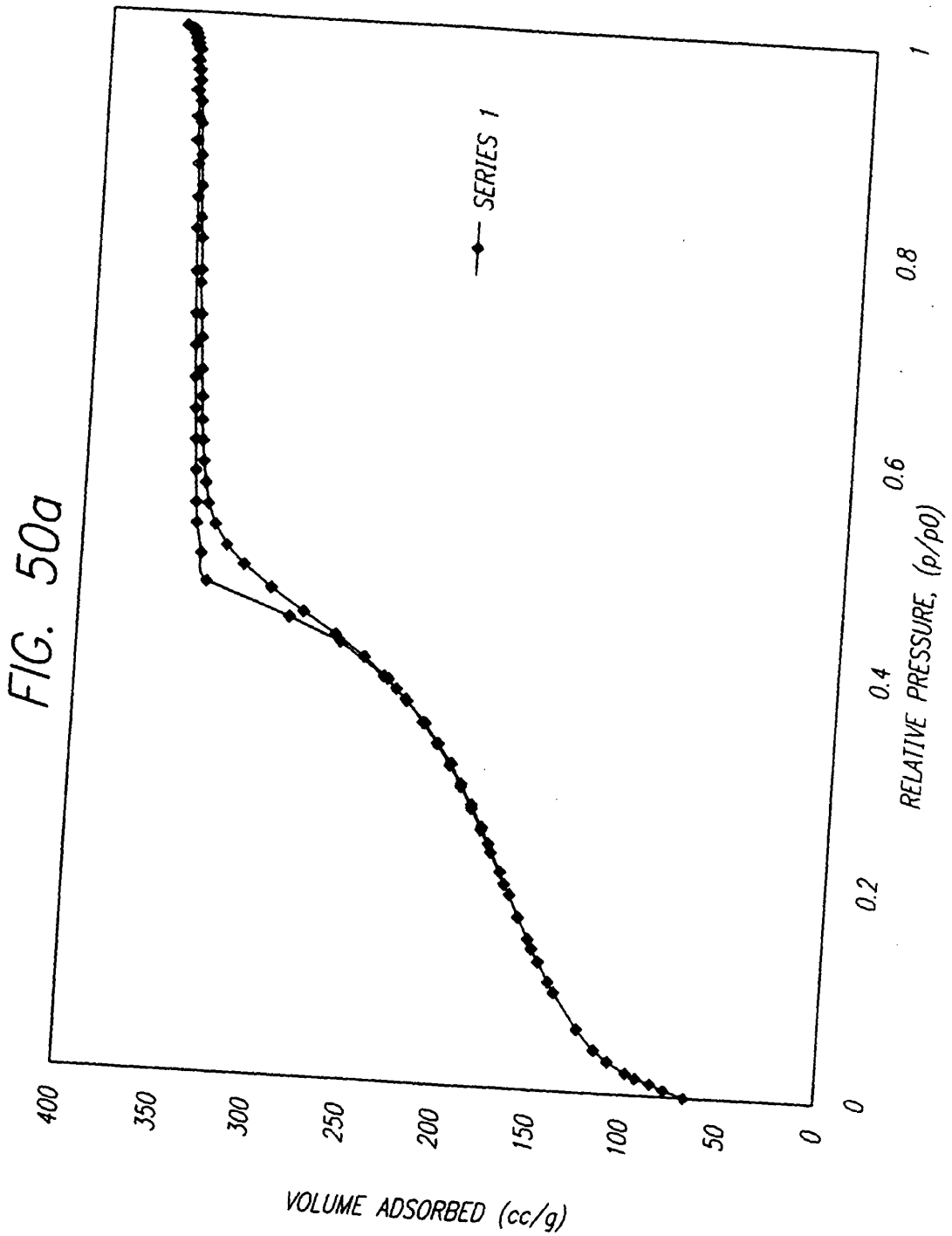
SERIES 1
VOLUME ADSORBED (cc/g)
400
350
300
250
200
150
100
50
0
0.2
0.4
0.6
0.8
1
RELATIVE PRESSURE, (p/pO)

FIG. 50a

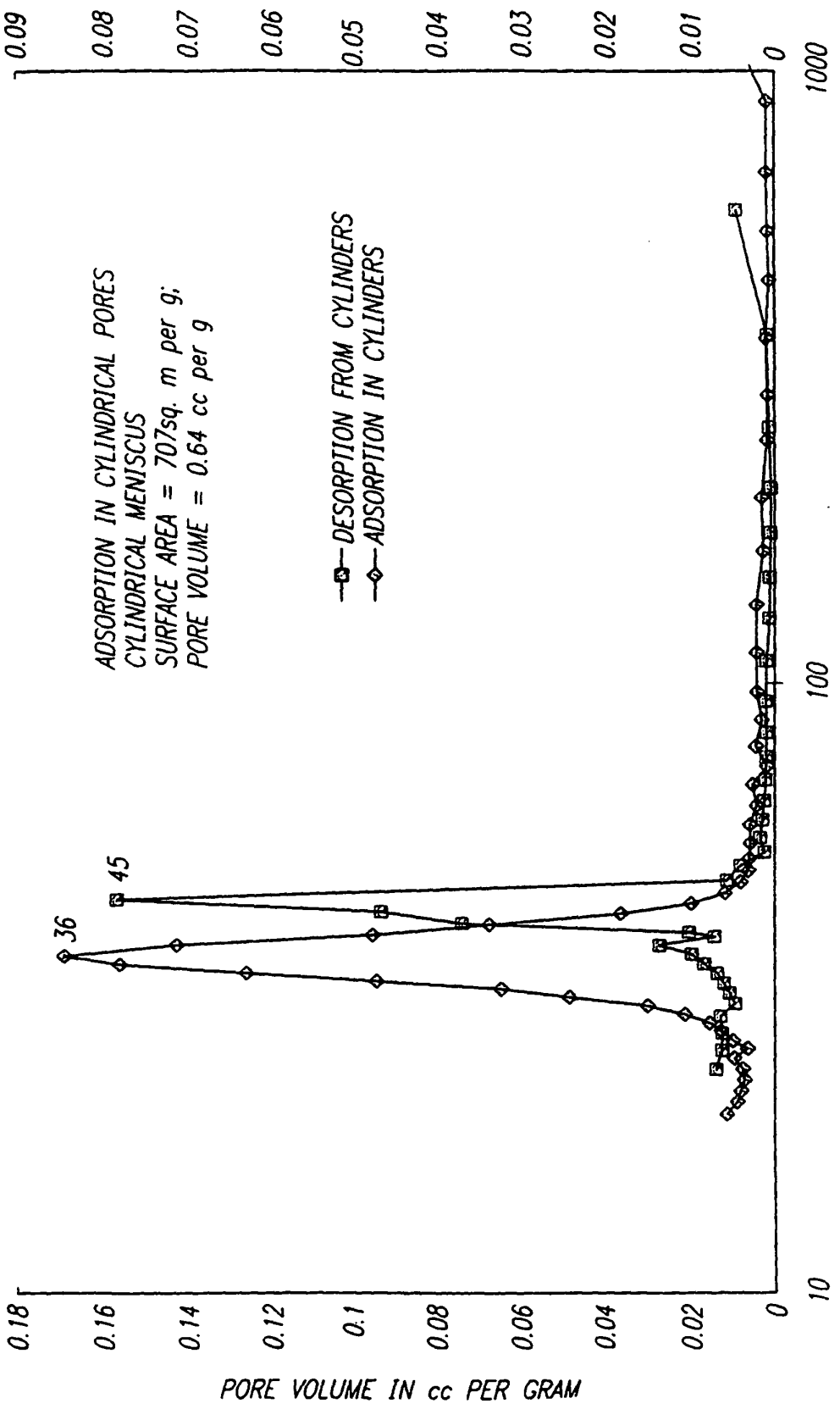

FIG. 50b

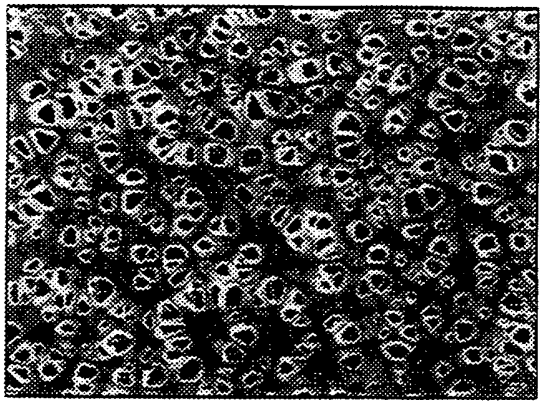

— 1 μm
3.0 kV X 4.000 12mm

FIG. 51a

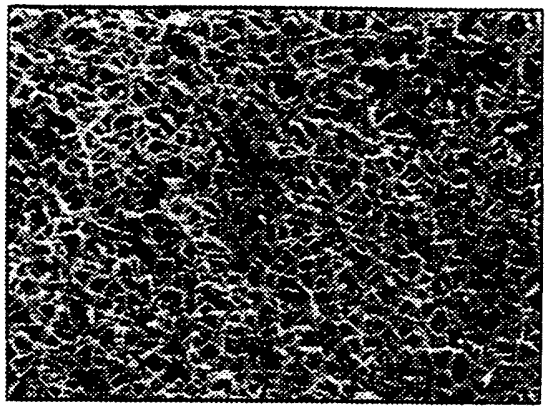

—— 10 μm
3.0 kV X 1.000 12mm

FIG. 51b

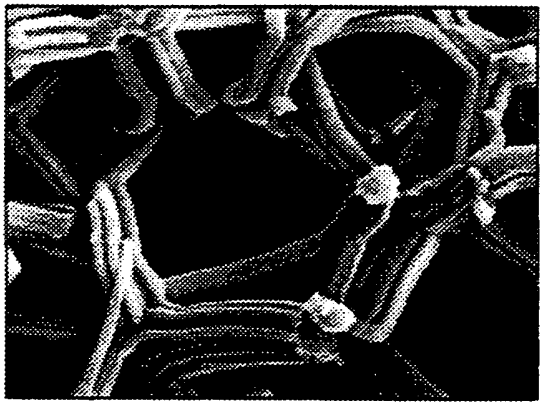

—— 1 μm
3.0 kV X 20.000 11mm

FIG. 51c

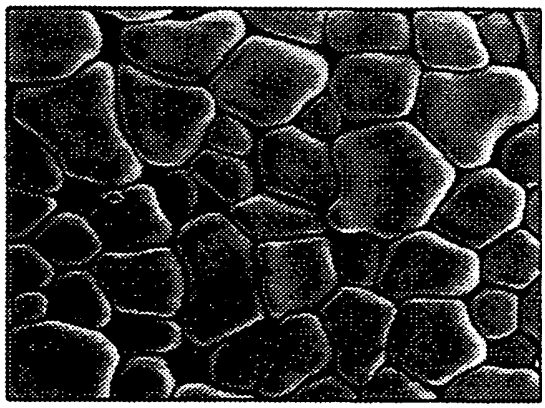

— 10 μm
3.0 kV X 500 11mm

FIG. 51d

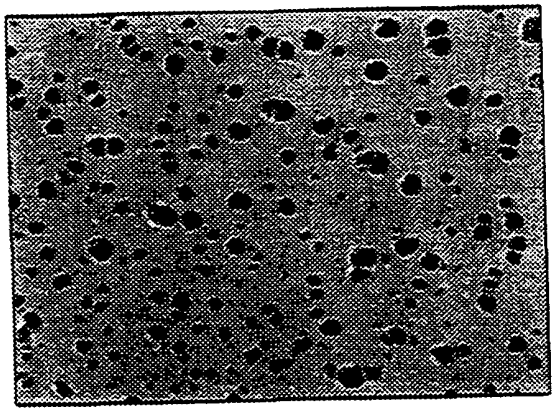

100 μm
3.00 kV X 250 12mm

FIG. 51e

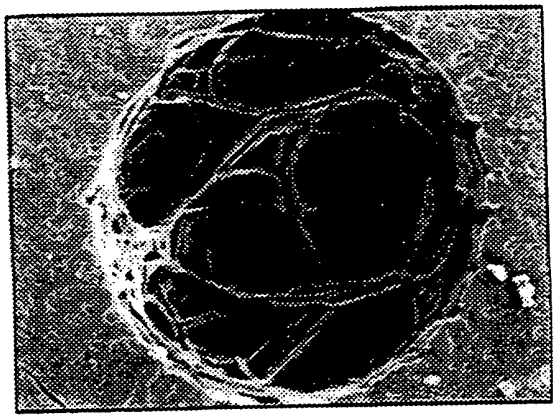

100 μm
3.00 kV X 250 12mm

FIG. 51f

10 μm
3.00 kV X 3.300 12mm

FIG. 51g

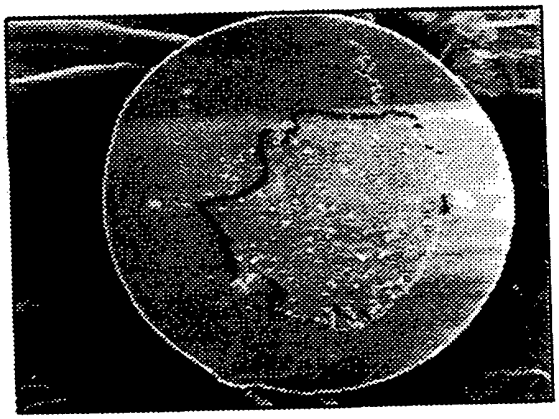

10 μm
3.00 kV X 3.300 12mm

FIG. 51h

FIG. 52

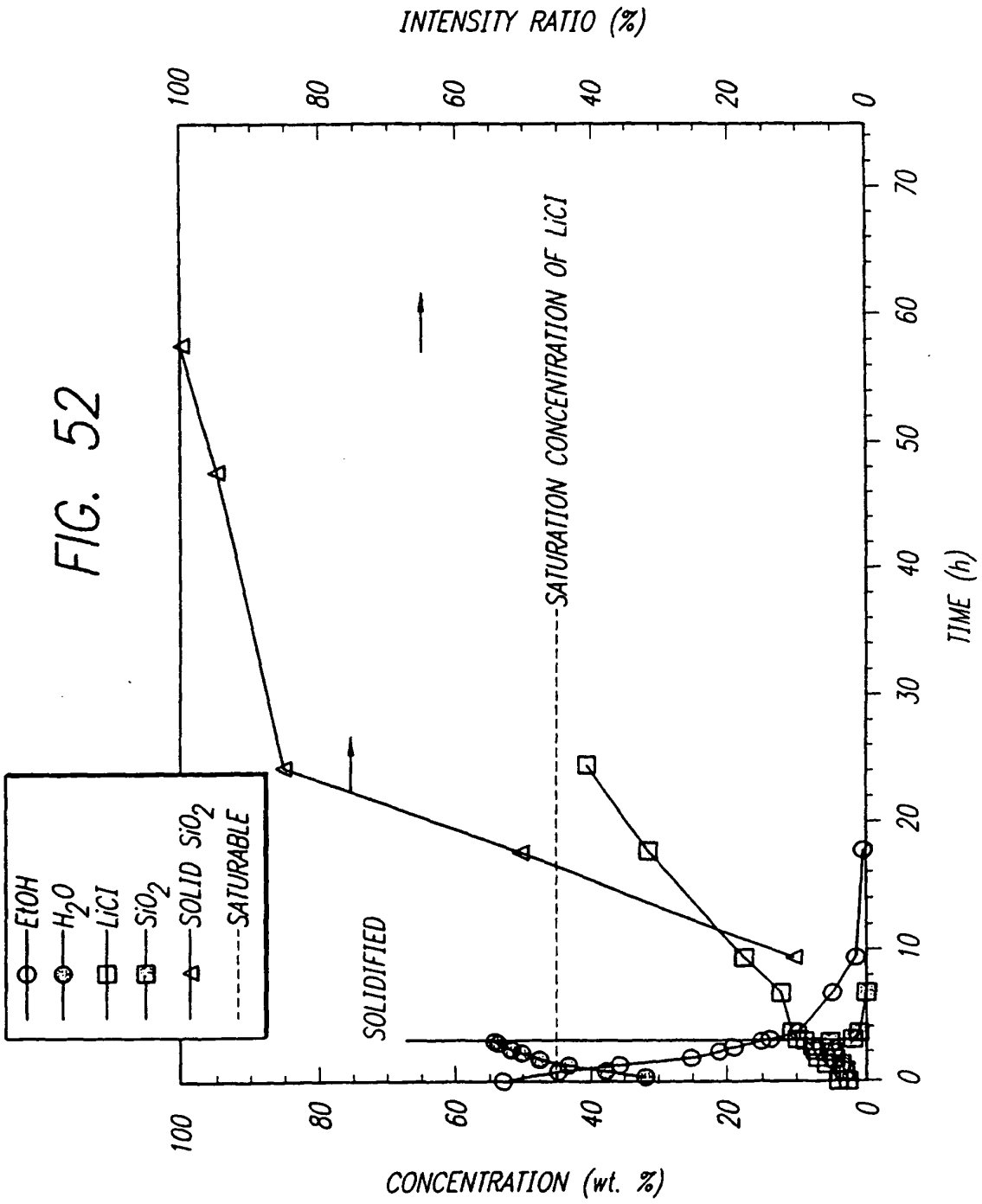

FIG. 53

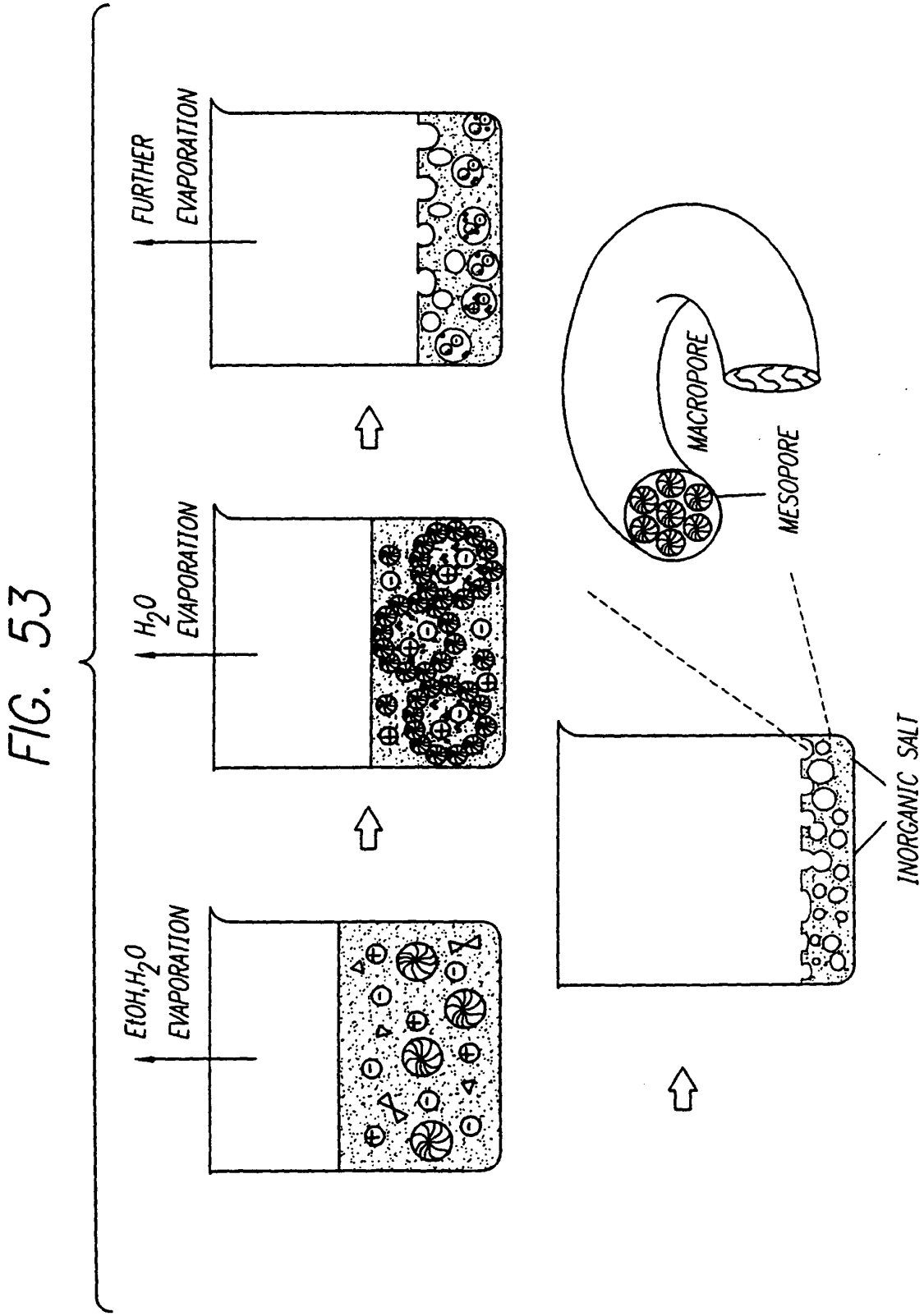
EtOH, H_2O EVAPORATION
H_2O EVAPORATION
FURTHER EVAPORATION
MACROPORE
MESOPORE
INORGANIC SALT

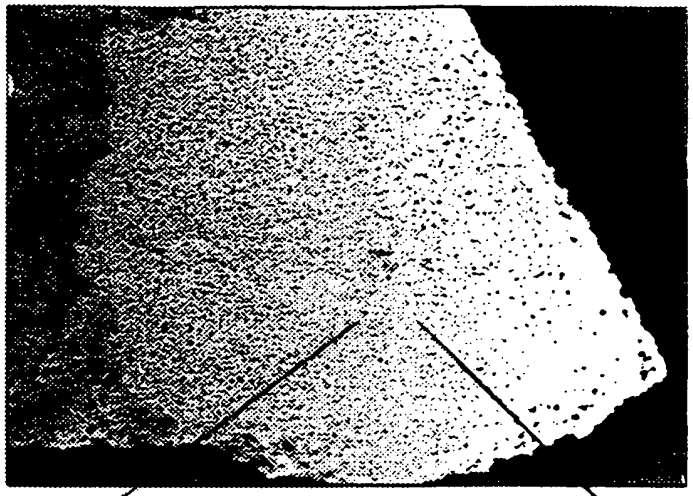

FIG. 54a

0.1 mm

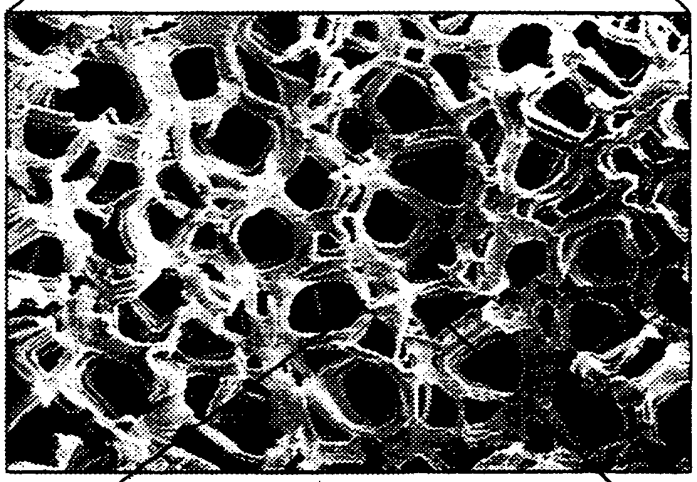

FIG. 54b

10 μm

3.0 kV X 3.000 12mm

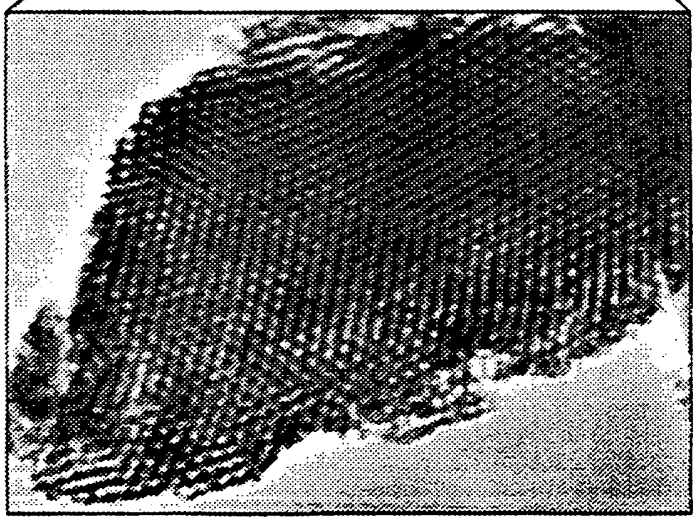

FIG. 54c

50 nm

INTERNATIONAL SEARCH REPORT

International application N .
PCT/US98/26201

A. CLASSIFICATION OF SUBJECT MATTER

IPC(6) :Pleas See Extra Sheet.
US CL :521/153, 134

According to International Patent Classification (IPC) or to both national classification and IPC

B. FIELDS SEARCHED

Minimum documentation searched (classification system followed by classification symbols)

U.S. : 521/153, 134

Documentation searched other than minimum documentation to the extent that such documents are included in the fields searched

Electronic data base consulted during the international search (name of data base and, where practicable, search terms used)

C. DOCUMENTS CONSIDERED TO BE RELEVANT

Category*	Citation of document, with indication, where appropriate, of the relevant passages	Relevant to claim No.
A	US 3,886,125 A (CHROMECEK) 27 May 1975, entire document	1-71
A	US 5,416,124 A (STRINGFIELD) 16 May 1995, entire document	1-71

☐ Further documents are listed in the continuation of Box C. ☐ See patent family annex.

*	Special categories of cited documents:	"T"	later document published after the international filing date or priority date and not in conflict with the application but cited to understand the principle or theory underlying the invention
"A"	document defining the general state of the art which is not considered to be of particular relevance	"X"	document of particular relevance; the claimed invention cannot be considered novel or cannot be considered to involve an inventive step when the document is taken alone
"E"	earlier document published on or after the international filing date	"Y"	document of particular relevance; the claimed invention cannot be considered to involve an inventive step when the document is combined with one or more other such documents, such combination being obvious to a person skilled in the art
"L"	document which may throw doubts on priority claim(s) or which is cited to establish the publication date of another citation or other special reason (as specified)	"&"	document member of the same patent family
"O"	document referring to an oral disclosure, use, exhibition or other means		
"P"	document published prior to the international filing date but later than the priority date claimed		

Date of the actual completion of the international search 10 JUNE 1999	Date of mailing f the international search report 07 JUL 1999
Nam and mailing address f the ISA/US Commissioner of Patents and Trademarks Box PCT Washington, D.C. 20231 Facsimile No. (703) 305-3230	Authorized office MORTON FOELAK Telephone No. (703) 308-1257

Form PCT/ISA/210 (second sheet)(July 1992)*

INTERNATIONAL SEARCH REPORT

International application No.
PCT/US98/26201

A. CLASSIFICATION OF SUBJECT MATTER:
IPC (6):

C08J 9/00; C08G 79/00,79/10,79/12